FACULTY OF ENGINEERING OF THE UNIVERSITY OF PORTO

Crashworthiness topology optimisation of a crash box to improve passive safety during a frontal impact

Christian Gutiérrez da Silva

Master in Mechanical Engineering

Supervisor: Doctor Pedro Miguel Guimarães Moreira

Co-Supervisor: Professor Marco Paulo Lages Parente

July 19, 2023

© Christian Gutiérrez da Silva, 2023

Crashworthiness topology optimisation of a crash box to improve passive safety during a frontal impact

Christian Gutiérrez da Silva

Master in Mechanical Engineering

July 19, 2023

Abstract

This research focuses on the application of topology optimisation algorithms for improving the crashworthiness of heavy passenger vehicles, particularly coaches (M3 Class III vehicle), in frontal impact conditions. The objective is to find the optimal arrangement of material to minimize compliance while meeting a volume constraint as to improve the structure of the vehicle for energy absorption.

The concept of crashworthiness design is crucial in the automotive industry, particularly in enhancing passenger safety. It aims to develop structures that can absorb maximum energy while minimizing intrusion, to maintain the driver's survival space. If so, crashworthiness design deals with conflicting objectives, and optimisation methods can be used to find a compromise between these parameters. Despite this potential, the application of topological optimisation in the context of vehicle structure crashworthiness is still limited. One of the main challenges is the non-linear nature of crash simulation that results in high computational costs, thus deeming the application of these kind of approaches impractical.

To account for said obstacle, this study performed the optimisation process on a single component, a crash box, employing optimisation algorithms built within a MATLAB code, that iteratively interfaces with Abaqus® where the crash simulation is performed. Afterwards, the optimised component was incorporated into the coach chassis baseline and tested using a finite element model on VPS/PamCrash®, simulating frontal impact conditions according to the ECE R29 regulation.

The application of this methodology demonstrated that evolutionary algorithms can effectively be applied for topology optimisation under crashworthiness conditions, generating an optimised crash box that improves the crashworthiness metrics of the coach baseline structure.

This research contributes to the limited existing literature on the topic of crashworthiness design of heavy passenger vehicles by recommending an optimised coach chassis with enhanced structural performance, coupled with an energy-absorbing component that improves the level of physical integrity of the driver. Additionally, it addresses the lack of regulations dedicated to frontal impact of coach structures by adapting a truck-based regulation, such as ECE R29, and applying it to determine the structural response of the dynamic explicit model.

Resumo

Esta pesquisa tem como foco a aplicação de algoritmos de otimização topológica para melhorar a *crashworthiness* de veículos pesados de passageiros, especificamente autocarros da Classe III M3, em condições de impacto frontal. O objetivo é o de encontrar a disposição ótima de material para minimizar a *compliance*, ao mesmo tempo em que atende a uma restrição de volume, a fim de melhorar a estrutura do veículo para absorção de energia.

O conceito de *crashworthiness* é crucial na indústria automóvel, especialmente para aumentar a segurança dos passageiros. O objetivo é desenvolver estruturas que possam absorver a máxima energia possível, ao mesmo tempo em que minimizam a intrusão, para manter o espaço de sobrevivência do condutor. Nesse sentido, o projeto em condições de *crashworthiness* lida com objetivos conflitantes, e métodos de otimização podem ser usados para encontrar um compromisso entre estes parâmetros. Apesar do seu potencial, a aplicação de otimização topológica no contexto de *crashworthiness* de estruturas de veículos ainda é limitada. Um dos principais desafios é a natureza não linear da simulação de impacto, que resulta em altos custos computacionais, tornando a aplicação desse tipo de abordagem impraticável.

Para contornar esse obstáculo, este estudo realizou o processo de otimização em um único componente, uma crash box que é um componente de absorção de impacto, empregando algoritmos de otimização incorporados em um código MATLAB, que interage iterativamente com o Abaqus®, onde a simulação de impacto é realizada. Posteriormente, o componente otimizado foi incorporado à estrutura básica do chassi do autocarro e testado usando um modelo de elementos finitos no VPS/PamCrash®, simulando condições de impacto frontal de acordo com a regulamentação ECE R29.

A aplicação desta metodologia demonstrou que algoritmos evolutivos podem ser efetivamente aplicados para a otimização topológica em condições de *crashworthiness*, gerando uma crash box otimizada que melhora os indicadores de resistência a impactos da estrutura do autocarro.

Esta pesquisa contribui para a escassa literatura existente sobre o tema *crashworthiness* de veículos pesados de passageiros, recomendando um chassi de autocarro otimizado com desempenho estrutural aprimorado, incluindo uma crash box que melhora os níveis de integridade física do condutor. Além disso, aborda a falta de regulamentações dedicadas ao impacto frontal de estruturas de autocarros, adaptando uma regulamentação baseada em camiões, como a ECE R29, e aplicando-a para determinar a resposta estrutural do modelo dinâmico explícito.

Acknowledgements

The accomplishment of this dissertation was possible with a great deal of external contribution and support. Starting with the companies and entities that supported this research, this dissertation work is a continuation of a research project developed in the scope of the project CRASH - Refª POCI-01-0247-FEDER-039711, funded by *"Programa Operacional Competitividade e Internacionalização"*. It was carried out at INEGI, specifically at UMAI, whose team I acknowledge for its good disposition during my internship. Also, I would like to express my gratitude to the teaching staff at the Department of Mechanical Engineering at FEUP, for their dedication and commitment in shaping the engineers of the future.

I would like to extend a special thanks to my supervisors at FEUP. To Doctor Pedro Moreira for his valuable input in the approach taken, and his feedback on the documents of this thesis, it was very much appreciated. To Professor Marco Parente for his guidance, theoretical support and for making available the Matlab interface used in this work. Also, I would like to thank him for being a reference to me among the teaching staff, and for challenging us students to live up to our best potential. Additionally, I would like to acknowledge Professor Francisco Queirós de Melo for his insights on the analysis of the results obtained.

I would like to thank my supervisors at INEGI, for their availability throughout these months, and guidance that putted me in the correct path to complete my dissertation. To Engineer Tiago Domingues for seeing potential in me, and helping me find a thesis proposal suited for my interests. To Engineer Rogério Lopes, for proposing this dissertation topic and for his constant support to face the challenges encountered during my research.

On a personal level, I want to thank my friends that were my emotional support throughout these years. My housemates and friends at RUF for the laughs and moments shared, specially this past year. To *Las Marías*, for the video chats, game nights and for always being excited for every new step I take in my life. Even from far away your support means a lot to me. Last but not least, to the amazing group of friends I built at FEUP during these five years. Companions of the days and nights. You have been like a family to me and I will cherish our friendship for life.

Finally, but most importantly, I want to thank my family. To my relatives in Madeira for welcoming with open arms when I started this adventure almost six years ago, and for always rooting for my success. To my family in Venezuela, thank you for your unconditional love and support. To my grandparents, that raised me and made me the man I am today. To my mother, who is the strongest woman I know and who works tirelessly for those she loves. Thank you for supporting all my dreams and giving me wings to fly, I dedicate this dissertation to you.

“What is meant for you will always gravitate towards you.
Trust the process, embrace the journey, and have faith in the timing.”

Sonia Ricotti

Contents

1 Introduction **1**

1.1 Problem Statement and Motivation 1
1.2 Objectives of the research 2
1.3 Methodology followed 3
1.4 Overview of the Dissertation Structure 3

2 Literature Review **5**

2.1 Crashworthiness Design Concept 6
  2.1.1 Crashworthiness Metrics 6
  2.1.2 Motivation for Coach Crashworthiness Improvement 7
  2.1.3 European Directives and Regulations 10
  2.1.4 Crash Simulation and difficulties 13
2.2 Structural Optimisation of Crashworthy Structures 15
  2.2.1 Multi-objective structural optimisation 15
  2.2.2 Fields of Structural optimisation 16
  2.2.3 Main Optimisation Methods for Crashworthiness Design 17
2.3 Topology Optimisation for Crashworthiness Design 20
  2.3.1 Overview of Topology Optimisation 20
  2.3.2 Application to Crashworthiness Optimisation 23
  2.3.3 Discussion of the Alternative Topology Optimisation Methods 28

3 2D Application **31**

3.1 2D Finite Element Model 31
  3.1.1 2D Model Definition 32
  3.1.2 2D Model Validation 34
3.2 ABAQUS-MATLAB Interface 36
  3.2.1 Application to Topology Optimisation 37
  3.2.2 Optimisation Problem Formulation 37
  3.2.3 Interface Implementation 38
3.3 ESO Method 42
  3.3.1 ESO Algorithm definition 43
  3.3.2 ESO Optimisation Results 43
3.4 BESO Method 45
  3.4.1 BESO Algorithm definition 46
  3.4.2 BESO Optimisation Results 46
3.5 Optimality Criteria Method 49
  3.5.1 Optimality Criteria Algorithm definition 49
  3.5.2 Optimality Criteria Optimisation Results 50

3.6 Discussion of the applied methods 52

4 3D Application **55**
4.1 3D Finite Element Model 56
4.1.1 3D Model Definition 56
4.1.2 3D Model Validation 56
4.2 ESO Method 60
4.3 BESO Method 64
4.4 Final Remarks of the 3D Application 67

5 Industrial Application **69**
5.1 Crash Box Development 69
5.2 Optimised Crash Box 72
5.3 Coach finite element model definition 76
5.3.1 Crash box assembly into the coach structure 79
5.4 Discussion of the Results 80
5.4.1 Impactor velocity results 80
5.4.2 Displacement results 81
5.4.3 Energy absorption results 84
5.4.4 Strain and acceleration results 85
5.5 Final Remarks of the results 89

6 Conclusions and Future Works **93**
6.1 Conclusions 93
6.2 Future Works 94

References **97**

A Deformation results in the coach structure **103**
A.1 Ceiling 104
A.2 Frontal structure (Left-hand side) 105
A.3 Rear structure 106
A.4 Internal frontal structure 107

List of Figures

2.1 Fatalities per million inhabitants in bus/coach crashes per country in the EU27 (2018-2020) [8]. 8
2.2 Share of fatalities in bus/coach crashes in the total number of fatalities, per country in the EU27 (2018-2020) [8]. 8
2.3 Annual number of fatalities in bus/coach crashes, and their share in the total number of fatalities in the EU27 (2011-2020) [8]. 9
2.4 Statistics by type of crash event (2018-2020) [11]. 9
2.5 Relevant geometric dimensions for the frontal impact test [13]. 11
2.6 Manikin used to verify the survival space [13]. 12
2.7 Fields of structural optimisation. a) Size optimisation, b) Shape optimisation and c) Topology optimisation [25]. 16
2.8 Force-displacement curves for an aluminium tube under axial load [31]. 19
2.9 Numerical instabilities of checkerboards and mesh dependency on a topology optimisation problem [36]. 22
2.10 Design domain of the beam problem [16]. 24
2.11 Internal energy density plots (Left) and maximum deformation (Right) of the topologies synthesized using the (a) linear, (b) non-linear, (c) and dynamic analyses. [16] (Modified) 25
2.12 Axial crushing of the topologically optimised sample (a) Experimental test; (b) Numerical simulation in ABAQUS [53]. 28

3.1 2D finite element axial crash model. 32
3.2 Boundary conditions applied on the 2D finite element axial crash model. 33
3.3 Force-Displacement curves. 34
3.4 Comparison of the Force-Displacement curves for 2D model validation. 35
3.5 Displacement results, in mm, obtained in the direction of axial crushing. 36
3.6 Matlab code to introduce geometric imperfections on the initial mesh. 40
3.7 Flowchart of the topology optimisation procedure on Matlab. 41
3.8 Von Mises Stress distribution, in MPa, obtained after running the 2D model. . . . 42
3.9 Element deletion with the ESO algorithm. 43
3.10 Verification of the ESO algorithm for the first iterations of the 2D model. 44
3.11 Evolution of the optimisation problem for the ESO method applied to the 2D model. 45
3.12 Resultant 2D Topologies obtained with the ESO method for a volume fraction of 50%. 45
3.13 Verification of the BESO algorithm for the first iterations. 47
3.14 Evolution of the optimisation problem for the BESO method applied to the 2D model. 47

3.15 Resultant Topologies obtained with the BESO method for a volume fraction of 50% (Mesh 1). 48
3.16 Resultant Topologies obtained with the BESO method for a volume fraction of 50% (Mesh 2). 48
3.17 Exponent update strategy implemented in Matlab. 49
3.18 Resultant Topologies obtained with the OC method (First run). 50
3.19 Areas with lower energy absorption, highlighted in black, for iteration 29. 51
3.20 Resultant Topologies obtained with the OC method (Second run). 52
3.21 Evolution of the objective function for the OC method applied to the 2D model. . 52

4.1 3D finite element axial crash model. 56
4.2 Displacement field, in mm, obtained for the 3D crash simulation. 57
4.3 Comparison of the Force-Displacement curves for 3D model validation [56]. . . . 57
4.4 Final geometry defined for the 3D crash model. 58
4.5 Displacement field, in mm, obtained for the 3D crash simulation with final geometry. 59
4.6 Displacement field, in mm, obtained with introduction of geometric imperfections on the mesh. 59
4.7 Von Mises Stress distribution, in MPa, obtained after running the 3D model. . . . 59
4.8 Verification of the BESO algorithm for the first iterations of the 3D model. 60
4.9 Evolution of the optimisation problem for the ESO method applied to the 3D model. 61
4.10 Resultant 3D topologies obtained with the ESO method for a volume fraction of 50%. 62
4.11 Resultant 3D topologies obtained with the ESO method for a volume fraction of 70%. 63
4.12 Evolution of the objective function for the ESO method applied to the 3D model (Mesh 3). 64
4.13 Evolution of the optimisation problem for the BESO method applied to the 3D model. 64
4.14 Resultant 3D topologies obtained with the BESO method for a volume fraction of 50%. 65
4.15 Resultant 3D topologies obtained with the BESO method for a volume fraction of 70%. 66

5.1 Crushing force (KN) and distance (mm) responses of single-cell, double-cell and triple-cell columns [65]. 70
5.2 Final Geometry chosen for the crash box component. 70
5.3 Area of application assumed for the crash box component. 72
5.4 Evolution of the optimisation problem for the BESO method applied to the final model. 73
5.5 Final Geometries obtained with the optimisation algorithm. 74
5.6 Force-Displacement curves for the crash box component with different volume fractions. 75
5.7 Comparison of the component contour before and after manual smoothing. 76
5.8 Selected section and its corresponding prototype that was tested according to ECE R-29 [68]. 77
5.9 Finite element coach model simulated in [68]. 78
5.10 Simplified coach structure in the FE model used in this research. 79
5.11 Position of the crash box component, highlighted in red, in the coach structure. . 80
5.12 Impactor translational velocity curves (m/s) for all cases under study. 81

5.13 Location of nodes for displacement results. 82
5.14 Displacement, in mm and *X* direction, of selected nodes for all cases under study. 82
5.15 Point created on the steering wheel to monitor its displacement. 83
5.16 Intrusion of a point on the steering wheel, in mm, for all cases under study. . . . 83
5.17 Trajectory of a point on the steering wheel on the *XY* plane for all cases under study. 84
5.18 Internal Energy absorbed by the structure, in KJ, for all cases under study. 84
5.19 Acceleration results obtained (in g). 85
5.20 Location of some strain gauges on the coach structure [68]. 86
5.21 Deformation results measured in the A-pillars. 87
5.22 Deformation results measured in the right-hand side of the frontal structure. . . . 88
5.23 Deformation in the driver's door for the studied structures. 89

A.1 Location of strain gauges in the ceiling of the coach structure [68]. 104
A.2 Deformation results measured in the ceiling of the coach structure. 104
A.3 Deformation results measured in the left-hand side of the frontal structure. 105
A.4 Location of strain gauges in the left-hand side of the coach structure [68]. 105
A.5 Deformation results measured in the rear of the coach structure. 106
A.6 Location of strain gauges in the rear of the coach structure [68]. 107
A.7 Location of strain gauges in the internal frontal structure of the coach [68]. 107
A.8 Deformation results measured in the internal frontal structure of the coach. 107

List of Tables

2.1 European directives and regulations related to bus and coaches [9]. 10

3.1 Density and elastic properties for mild steel [56]. 33
3.2 True stress-plastic strain data points to define plasticity properties of mild steel [56]. 33
3.3 Summary of the finite element model for the 2D crash simulation. 34
3.4 Parameter comparison between reference and applied 3D finite element model. . 35
3.5 Geometric parameters of the two meshes used on the optimisation process for the 2D model (element type CPS4R). 42

4.1 Parameter comparison between reference and applied 3D finite element model. . 58
4.2 Geometric parameters of the meshes used on the optimisation process for the 3D model (element type S4R). 60

5.1 Density and elastic properties for aluminium [67]. 71
5.2 True stress-plastic strain data points to define plasticity properties of aluminium [67]. 71
5.3 Summary of the final crash box finite element model. 72
5.4 Reduction achieved in the strain energy for the optimised geometries. 73
5.5 Energy Absorption for the crash box component with different volume fractions. 75
5.6 Mass of the full crash box considering the volume of active elements and the density of Aluminium. 76
5.7 Nomenclature given to the strain gauges used on the experimental procedure [68]. 78
5.8 Peak energy absorption values for all structures under study. 85

Abbreviations and Symbols

Abbreviations

ALLIE	All Internal Energy
AR	Addition Ratio
BESO	Bi-directional Evolutionary Structural Optimisation
CA	Cellular Automaton
CAD	Computer-Aided Design
CAE	Computer-Aided Engineering
CFE	Crash Load Efficiency
CP	Crash Pulse
DIC	Digital Image Correlation
EA	Energy Absorption
ECBOS	European Coach and Bus Occupant Safety
ECE	Economic Commission for Europe
ESL	Equivalent Static Loads
ESO	Evolutionary Structural Optimisation
EPDDEN	Plastic energy density dissipated in the element
EU	European Union
FEA	Finite Element Analysis
FEM	Finite Element Method
GSA	Ground Structure Approach
HCA	Hybrid Cellular Automata
INEGI	Instituto de Ciência e Inovação em Engnharia Mecânica e Engenharia Industrial
Intr	Magnitude of Intrusion
MMA	Method of Moving Asymptotes
LU	Load Uniformity
OC	Optimality Criteria
RR	Rejection Ratio
SEA	Specific Energy Absorption
SED	Strain Energy Density
SIMP	Solid Isotropic Material with Penalization
SQP	Sequential Quadratic Programming
UMAI	Unidade de Monitorização Avançada e Integridade Estrutural
UNECE	United Nations Economic Commission for Europe
UR	Usage Ratio
VF	Volume Fraction

Symbols

a_{max}	Peak Acceleration
C	Damping Matrix
d	Displacement
E	Elastic Modulus
E_k	Kinetic Energy
F	External Force
F_{max}	Peak Crash Force
K	Stiffness Matrix
kg	Kilogram
KJ	Kilo Joule
M	Mass
mm	Millimetre
MPa	Mega Pascal
m/s	Meter per second
N	Newton
p	Penalization Parameter
R	Residual
v	Elemental volume
V	Volume
x_i	Design Variable
λ	Lagrange Multiplier
ρ	Material Density
ε_p	Plastic Strain
ν	Poisson's Ratio
σ_t	Yield Stress

Chapter 1

Introduction

The purpose of this chapter is to provide the reader with an overview of the dissertation document, including a concise summary of the topic to establish its significance and motivation. The relevant institutions where this project was carried out are acknowledged. In this case, the dissertation was conducted at INEGI - Institute of Science and Innovation in Mechanical and Industrial Engineering, specifically at the Advanced Monitoring and Structural Integrity Unit (UMAI).

Futhermore, the overall aim of the research project is outlined, along with the specific objectives that were pursued to achieve it. Lastly, the methodology followed and the structure of the dissertation document are described. It is worth mentioning that the research developed in this dissertation was presented orally at the 5th Doctoral Congress in Engineering (DCE) at FEUP, and an abstract was submitted to the 5th International Conference on Structural Integrity (ICSI2023).

1.1 Problem Statement and Motivation

The unavoidable nature of vehicle accidents represents a great risk to the safety of drivers and passengers. For the case of heavy passenger vehicles like buses and coaches, the risks are aggravated, since the quantity of people involved increases.

Having these risks in mind justifies the importance of including passive safety systems in vehicle structures to mitigate the effects in the event of a crash, aiming to reduce its consequences, specially in terms of injury levels. Among this type of systems, deformations zones and components are of outermost importance to reduce the amounts of crash energy that are transferred to the occupants of the vehicle. This type of measures are already extensively implemented by manufacturers in the automotive industry.

However, the current structure of large vehicles often lacks proper passive safety measures, which poses significant risks to the vehicle driver and its passengers, specially in the case of frontal impact. In such cases, a significant portion of the impact energy is transferred to the frontal structure, increasing the risk for injuries in drivers, potentially leading to casualties.

If so, enhancing vehicle structures for energy absorption should be a priority. In this regard, the application of topology optimisation techniques emerges as a promising approach to derive new geometries optimised for the intended purposes, and at a reduced mass.

The topic of topology optimisation has been around since the 1980's, and nowadays is extensively used by engineers, specially in the first stages of the design process. It has also been integrated within the environment of many commercial FEM software packages. These techniques have been significantly researched and developed, establishing their applicability in scenarios where assumptions of material elasticity and small deformations are valid. On the contrary, in a crash event, the structures undergo large deformations and exhibit non-linear behaviour, which interrupts the application of the more established topology optimisation techniques. Indeed, the number of researches in this field is limited, compared to static applications, particularly for the specific case of heavy passenger vehicle structures.

Still, approaches can be found on theory that bypass the challenges inherent to crash simulation and tackle topology optimisation for crashworthiness objectives. Alternative methods have been devised that show promising results for the application of topology optimisation in this context. Some are based on relaxation of the non-linear phenomena of crash simulation while others simplify the problem by applying the techniques at a component level. This research contributes by further extending the number of investigations aiming to enhance the structural performance of vehicles, in order to fill the existent theoretical gap in this field of topology optimisation.

1.2 Objectives of the research

The overall aim of the research project is to improve the crashworthiness of a coach structure by incorporating an energy-absorbing component optimised by means of topology optimisation techniques for conditions of frontal impact. The following objectives were established and pursued to aid in the accomplishment of this aim.

- Evaluate the capabilities of different topology optimisation algorithms in generating geometries for crashworthiness conditions;
- Determine the best performing algorithm and employ it to synthesize an optimised crash box component;
- Integrate the optimised component into a numerical model of a coach and simulate a frontal impact scenario, under the guidelines of regulation ECE R-29;
- Analyse the crashworthiness performance of the structure coupled with the optimised component, and discuss its implications by assessing a series of crash parameters.

1.3 Methodology followed

The first two objectives proposed in this dissertation were accomplished by implementing an interface between Matlab and Abaqus, to perform topology optimisation, with algorithms that gather data from iterative explicit dynamic simulations. A sequential approach was followed, testing CAE models with increased complexity being representative of axial crashes, to evaluate the performance of the studied algorithms. Ultimately, reaching an optimised geometry proposal that can be added to the frontal structure of a coach.

As for the remaining two objectives, the software VPS/PamCrash® was used to simulate a frontal impact test of a coach finite element model, whose structure was updated by addition of the optimised crash box. Also, the software was used to retrieve the crash parameters for data analysis.

1.4 Overview of the Dissertation Structure

The structure of this dissertation work is comprised of several chapters, starting with a literature review, methodology application, and ending with an analysis and discussion of the obtained results, followed by some final remarks and the references that were consulted throughout this work.

Chapter 2 lays the theoretical background needed. It starts by presenting the notion of crashworthiness design and the motivation behind the improvement of vehicle structures for passive safety reasons. Subsequently, a brief picture of the existing European legislation for large vehicles is presented, giving special emphasis to regulation ECE R-29. Additionally, an overview of topology optimisation is provided together with its application to crashworthy structures.

Chapter 3 outlines the details behind the implementation of the Abaqus-Matlab interface and its application to a two-dimensional crash model. Afterwards, Chapters 4 and 5 apply this approach to three-dimensional geometries. Moreover in Chapter 5, the final optimised crash box is obtained and the results of the frontal impact simulation are presented and discussed.

Finally, Chapter 6 concludes this research with some final remarks about the impact of the optimisation procedure in the crashworthiness of the structure, and provides insights into possible further studies that can be conducted.

Chapter 2

Literature Review

This chapter presents the theoretical foundation that supports the arguments presented in this dissertation work. Prior to delving into the central theme of the dissertation, which is the topology optimisation of crashworthy structures, some relevant notions need to be introduced. The fundamental concept of crashworthiness design was reviewed, as well as some indicators to assess the performance of a vehicle structure in terms of crashworthiness.

This research work aims to optimise the structure of a coach at a component level and for conditions of frontal impact. Therefore, it is relevant to address the motivation for improving these types of vehicle structures. This was accomplished by providing relevant facts and statistics related to coach accidents, with the purpose of shedding light on the significance of improving the current design of buses and coaches, aiming to enhance the passive safety of both drivers and passengers, especially in the event of frontal collision.

To replicate the conditions of a frontal impact, the research will adhere to the guidelines of regulation ECE R-29. Hence, a more dedicated review of its details will be provided, along with an overview of other European regulations related to buses and coaches. This will provide a more thorough legislative perspective on the subject. Numerical simulation will be the tool used to recreate said conditions. If so, the intricacies and difficulties of crash simulation will also be addressed.

In a subsequent section, a theoretical examination of structural optimisation is provided, covering the general formulation and main fields, which include topology optimisation. This is followed by a review of the primary optimisation methods and algorithms and their applications within the field of crashworthiness design.

After establishing the initial theoretical groundwork, an introduction to topology optimisation for crashworthiness design is in order. The main theoretical aspects provided include the classic topology optimisation methods, as well as the numerical instabilities associated with these approaches, that impulsed the appearance of alternative methods. Then, the focus is regained towards the application of the methodology to optimise crash structures. Different state-of-the-art methods are introduced, and examples of practical applications found in the literature are given. Finally, some advantages and drawbacks of said methods are discussed.

2.1 Crashworthiness Design Concept

Crashworthiness design plays a crucial role in the automotive industry when it comes to ensuring passenger safety. It involves analysing and designing a vehicle to effectively handle crash events, aiming to maximize energy absorption while minimizing the loads transmitted to occupants. The ultimate goal is to enhance passenger safety [1].

From a crashworthiness point of view, a well-designed vehicle should ensure that the accelerations experienced by passengers remain below injury thresholds, while also limiting the intrusion into the passenger compartment to minimize the risk of lower extremity or chest/head injuries. However, achieving these two objectives poses a conflicting problem. While low accelerations require compliance and flexibility in the structure to absorb energy, the constraint on the penetration requires rigidity. If so, striking the right balance between these conflicting objectives is a key challenge in crashworthiness design, and by applying structural optimisation methods a compromise can be found, and the current design of public transport vehicles can be improved [2].

As defined in the scope for this work, the attention is targeted towards optimisation of coach structures under conditions of frontal impact. In a frontal crash, most of the energy is absorbed by the frontal structure of the vehicle which, in consequence, deforms plastically and intrudes into the driver's operating area [3]. The objective is to enhance passive safety by ensuring that, in the aftermath of the impact, there is no contact between the driver and non-resilient parts of the vehicle's structure, in other words, the survival space has to be maintained [4].

As part of the concept of crashworthiness design, it is important to define specific crashworthiness metrics that are used to evaluate the level of safety of a structure and determine if improvements are needed. Additionally, statistical evidence is provided to justify the motivation behind investing in the upgrade of public transport vehicles are presented. These topics will be addressed in the following sections.

2.1.1 Crashworthiness Metrics

Fang et al. in [5], present a classification of crashworthiness metrics into two groups depending on the criteria they are based on. These groups are injury-based metrics and energy-based metrics. The first group measures the safety of vehicle occupants during a crash by utilizing human dummies as simulation tools. Injury-based metrics can be defined from a biomechanics point of view, to measure the response of the occupants in the event of a crash, or as indices that are direct consequences of structural crashworthiness, such as the vehicle crash pulse (CP) or the magnitude of intrusion ($Intr$). Also, the peak acceleration (a_{max}) and peak crash force (F_{max}) are extensively employed as design criteria, since high accelerations imply large impact forces transmitted to the passengers which translates into a higher risk of injury.

As for the energy-based metrics, this group focuses on the amount of energy absorbed by the structure as to minimize the kinetic energy transmitted to the occupants. In particular, the energy absorption (EA) metric has gained significant attention from researchers, it is evaluated by analysing the collapsed components after the crash in the absence of a dummy. Its formulation can be seen in Equation 2.1, where *F(s)* represents the instantaneous impact force at the crash distance *s*, and *d* represents the total crash displacement. The energy absorption can also be determined by computing the area under the force-displacement curve [1].

$$EA(d) = \int_0^d F(s) \cdot ds \tag{2.1}$$

The energy absorption can also be defined by considering the efficiency in utilizing the mass of the structure (*M*). The energy absorption is then transformed into a specific metric by computing it per unit mass (Refer to Eq. 2.2). Other criteria related to energy absorption include the crash load efficiency (*CFE*), its reciprocal the load uniformity (*LU*), and the usage ratio (*UR*).

$$SEA(d) = \frac{EA(d)}{M} \tag{2.2}$$

Fang et al. in [5] also summarize the most commonly used metrics in literature, for both types of crashworthiness criteria. Additionally, Horstemeyer et al. in [6], compared the two different groups of criteria for the design of vehicular components under side impact. The authors concluded that injury-based design approaches could result in significantly safer structures and that it is a more judicious approach since the ultimate goal of crashworthiness optimisation is to ensure passenger safety. A drawback, however, is the complexity of modelling the damage of the dummy on crash simulations.

2.1.2 Motivation for Coach Crashworthiness Improvement

For the particular situation of coaches, collisions not only pose a risk to the driver's safety but also endanger more people compared to collisions involving other vehicles [7]. Figure 2.1 depicts the number of road fatalities in bus/coach crashes per million inhabitants and per country in the EU27 during the 2018-2020 period. As it can be seen, the European landscape is varied, presenting a higher mortality rate in the eastern part of the EU.

The mortality rate is a significant measure of road safety; however, to provide a comprehensive understanding of the situation, it is important to compare these numbers with those from crashes involving other types of vehicles. This comparison helps to contextualize the data and assess the relative safety performance of different vehicle types. The following figures show the proportion of mortal bus crashes within the total number of road fatalities per country (Figure 2.2), and the total number of accidents per year in the EU27, together with the share relative to all road fatalities (Figure 2.3). According to this data, it can be concluded that the number of accidents accounts for a small share of the overall scenario. As a matter of example, in 2020, bus/coach crashes accounted for 2% of all road fatalities in the EU, and this trend has decreased slightly since the year 2011.

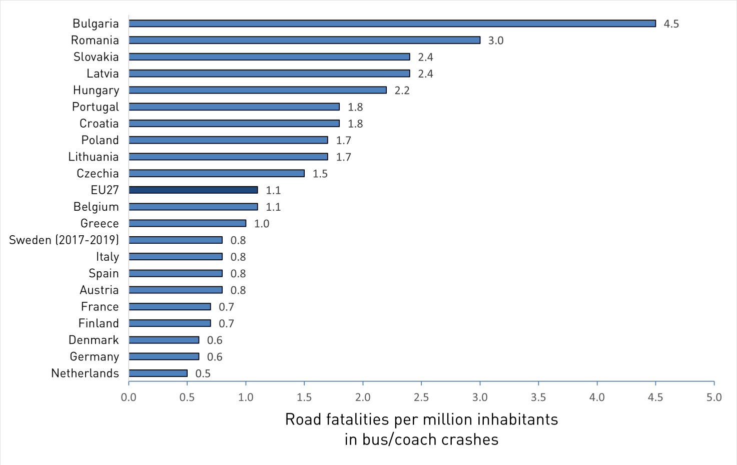

Figure 2.1: Fatalities per million inhabitants in bus/coach crashes per country in the EU27 (2018-2020) [8].

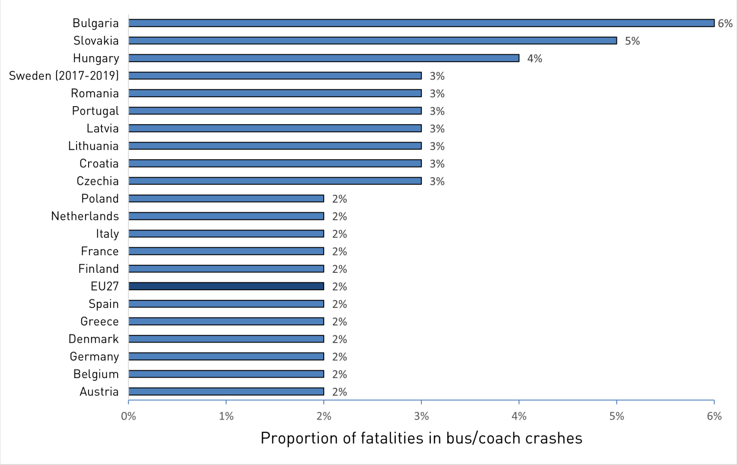

Figure 2.2: Share of fatalities in bus/coach crashes in the total number of fatalities, per country in the EU27 (2018-2020) [8].

Although the previous accident statistics present a pattern that indicates that transport by bus and coach can be considered the safest mode of road transportation [9], it can also be argued that the small percentage of bus accidents does not pertain to the fact that they can be considered safer, but rather to their small ratio relative to other road vehicles [7]. In any case, a consensus can be reached in the perspective that, still, further improvements can be made to increase the safety standards of these types of vehicles. One approach is to incorporate structural components that have been successfully implemented in other forms of transportation and have demonstrated their effectiveness in enhancing crashworthiness [9].

Recentering the focus towards the specific case of frontal impact, some more detailed statistics can be analysed. Despite being less serious in terms of injury than other types of crashes, they occur more frequently, making up a significant portion of casualties in vehicle accidents [9]. Generally, frontal collisions tend to be the most common, followed by side and rear impacts [10].

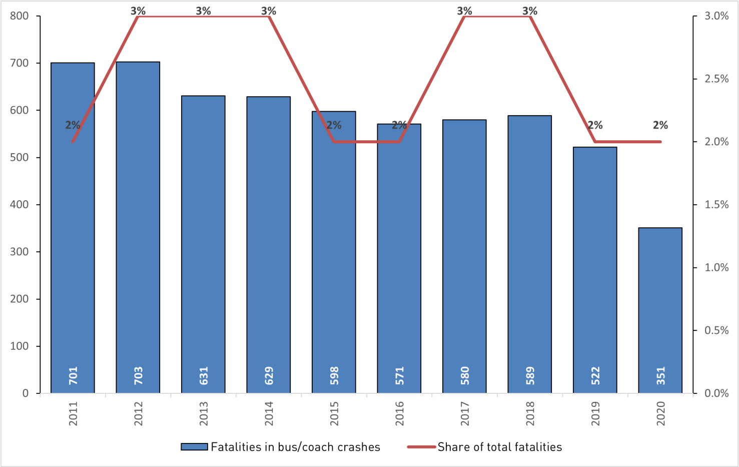

Figure 2.3: Annual number of fatalities in bus/coach crashes, and their share in the total number of fatalities in the EU27 (2011-2020) [8].

Detailed statistical data for vehicle accidents disaggregated by crash event is not readily available. According to some authors, two versions of frontal collision can be distinguished: simple and combined frontal collision, where the latter involves additional events such as side crashes or rollovers triggered by an initial frontal impact [7]. This complexity in categorizing different crash events may explain the lack of detailed crash figures. Still, data is available for certain countries in the report "Statistics of Road Traffic Accidents In Europe and North America" by the United Nations Economic Commission for Europe (UNECE) [11]. As an example, figures depicting the number of accidents between vehicles (Figure 2.4a) and the number of people killed (Figure 2.4b) categorized by crash event type are presented. These figures show that, during the 2018-2020 period, frontal impact accounted for a significant proportion of accidents in the selected country.

It is important to note that the availability and specific data may vary across countries and regions. However, the provided figures serve as an illustration of the contribution of frontal impact in overall crash statistics.

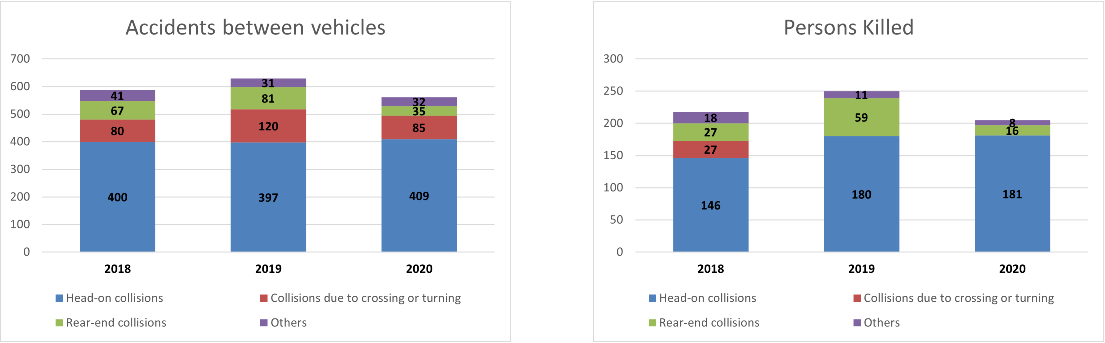

(a) Accidents between vehicles

(b) Persons killed

Figure 2.4: Statistics by type of crash event (2018-2020) [11].

Having the above-stated reasons in mind explains the motivation to optimise vehicle structures to, subsequently, increase the safety of the driver and passengers. However, the existent literature regarding suggestions on improvement of crashworthiness for passenger vehicles is limited [12]. Additionally, it can be verified a lack of regulations dedicated to frontal impact of coach structures, the next section discusses the available European directives and regulations that can be related to the case of study.

2.1.3 European Directives and Regulations

According to the European Coach and Bus Occupant Safety (ECBOS) project, there are seven regulations with their respective five directives that concern the structural and seat design of buses and coaches. These regulations are elaborated by the European Economic Commission (ECE) and Table 2.1 presents them according to their area of application [9].

Table 2.1: European directives and regulations related to bus and coaches [9].

		European Directive	**ECE Regulation**
Obligatory use of seat belts		91/671 - 2003/20/EC	
Seat belts anchorages		76/115 - 96/38/EC	14 R05
Seats, seat's anchorages and head restraint		74/408 - 96/37/EC	80 R01
Safety belts and restrain systems		77/541 - 2000/3/EC	16 R04
General construction of large passenger vehicles	>22 + 1	2001/85/EC	36 R03
	<22 + 1		52 R01
	Double-deck		107 R00
Rollover resistance			66 R00

Among the available regulations for buses and coaches, it can be seen that they pertain, mainly, to the general requirements for the certification of these vehicles. Such is the case of regulations ECE R-36, R-52 and R-107, which outline the general characteristics for the construction of large passenger vehicles. In terms of simulating rollover impacts, regulation R-66 is commonly referenced in the literature [9].

However, for the specific case of frontal impact, there is not a dedicated regulation that specifically addresses the structural requirements for buses and coaches. The only regulation that can be considered as an exception is regulation R-80, as discussed by Mayrhofer et al. [9], because it indirectly addresses frontal collisions by presenting the requirements and test methods for the strength of passenger seats and their anchorage.

This highlights a gap in the regulatory framework when it comes to addressing the specific needs and challenges associated with frontal collisions in these types of vehicles. In this study, this shortcoming will be surpassed by applying another European regulation, namely ECE regulation R-29 [13].

2.1.3.1 ECE Regulation Nº 29

It can be verified that, out of the existing regulation for passenger vehicles, there is not one dedicated to evaluating the resistance in a frontal impact accident. Still, the regulation ECE-

R29 can be adapted to the case of interest. Indeed, various authors have relied on the guidelines provided by this regulation for conducting their analyses of coach frontal impacts, for instance in [12, 4, 14]. This regulation is standardized for heavy vehicles with a separated cab, such as trucks, and in addition to certifying the vehicle structure for frontal impact conditions, it also encompasses tests to evaluate the resistance of the A-pillars and roof in a rollover accident.

- **Test A:** Frontal impact test, intended to evaluate the resistance of a cab in frontal impact accident.
- **Test B:** Impact test to the A-pillars of the cab intended to evaluate the resistance of a cab in a 90° rollover accident with subsequent impact.
- **Test C:** Cab roof strength test intended to evaluate the resistance of a cab in a 180° rollover accident.

As for the scope of this work, the interest is concentrated towards the test procedure for frontal impact, namely Test A, its description will be briefly presented in this section, according to the information available in the regulation [13]. The test consists of an impactor constructed from steel with a minimum and evenly distributed mass of 1,500 kg. Additionally, regulation R29 specifies the geometrical characteristics of the impactor, Figure 2.5 depicts all relevant dimensions for the test. The impactor is rigidly suspended by two beams separated by not less than 1,000 mm and at a minimum distance of 3,500 mm from the axis of suspension to the geometric centre of the impactor (dimensions f and L on Figure 2.5, respectively). Said geometric center must be at a distance "c" below the R point of the driver's seat, as shown in Figure 2.5. Finally, the impactor has a rectangular and flat striking surface that shall measure 2,500 x 800 mm with round edges having a radius of curvature of 10 mm ± 5 mm.

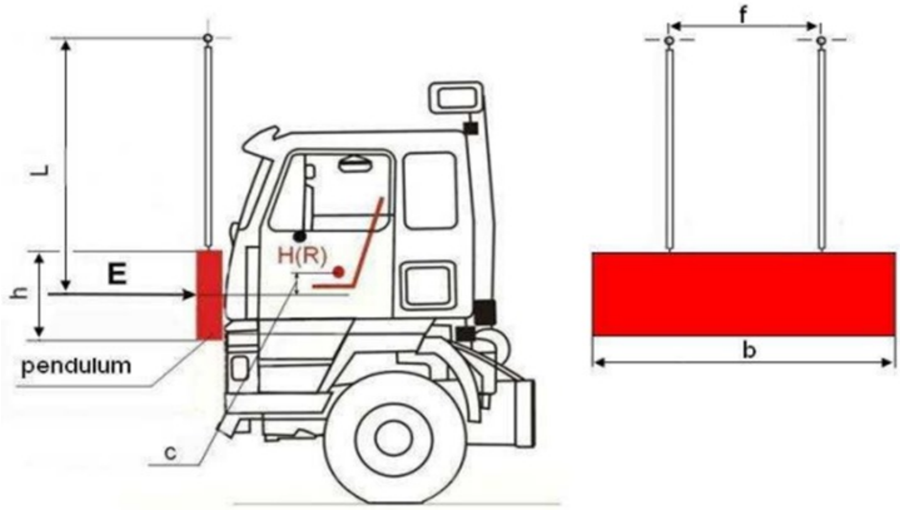

Figure 2.5: Relevant geometric dimensions for the frontal impact test [13].

Depending on the vehicle's classification, the impactor must strike its frontal structure with a certain amount of energy. For vehicles of categories N1, and N2 with a gross vehicle mass not exceeding 7.5 tonnes, the energy shall be 29.4 KJ, while the value increases to 55 KJ in the case of vehicles of categories N3, and N2 with a gross vehicle mass exceeding 7.5 tonnes. For the case of study, which is a passenger vehicle of category M3, the energy value adopted for the impactor will be 55 KJ.

In order for the vehicle structure to comply with the guidelines of the regulation, the driver's survival space shall be maintained after the impact tests are performed, meaning that the cab will not undergo large deformations that would translate into material penetration into said survival space. To confirm this, a human manikin, as defined in Figure 2.6, needs to be accommodated in the cab with the seat in its median position and, after impact, no contact should be verified between the test manikin and non-resilient parts, which are parts of the structure with a Shore-Hardness of 50 or more. Additionally, non-resilient components that can be removed by employing a force of less than 100 N without the use of any tools are not to be taken into consideration.

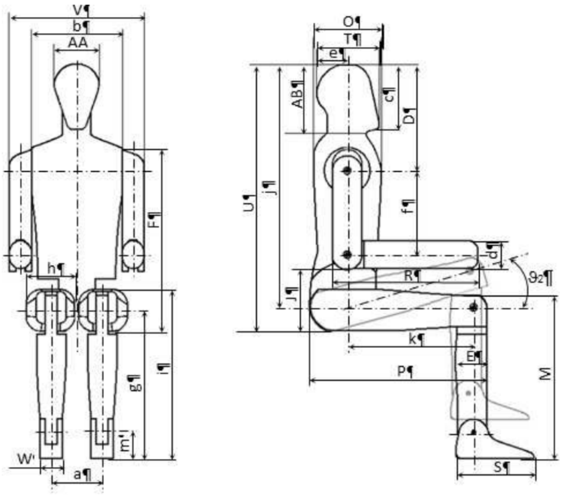

Figure 2.6: Manikin used to verify the survival space [13].

Many authors have decided to follow the guidelines of the European directives and regulations to perform experimental and numerical studies with the aim of determining the crashworthiness performance of a vehicle. For instance, the authors of [3] and [12] examined a coach front body's ability to absorb energy during a frontal collision while taking into account the ECE R-29 regulation. The experimental setup was used to validate the accuracy of the numerical model, using camera images or more complex monitoring technologies like Digital Image Correlation (DIC). By doing so, it is possible to keep track of the evolution of parameters like strain, accelerations and displacements during the crash test and compare them to the values obtained in the simulation. The objective is to ascertain whether the requirements of the regulation are met by the baseline models.

Some other strategies found in literature only apply the numerical approach to simulate the conditions of the crash test. As a matter of example, S. Rooppakhun et al. [15] used a numerical pendulum, as described in the regulation, to predict the response of a high-decker bus body to frontal impact.

2.1.4 Crash Simulation and difficulties

In the past, crashworthiness design relied heavily on trial-and-error testing methods due to the limited computational power available. However, with the progress in computer-aided engineering (CAE), numerical simulations have become the predominant approach for crashworthiness design [16]. Ideally, and due to its expensive nature for crash conditions, full-scale experimental testing should only be used to validate the results of numerical models [17]. Once the design is simulated and refined using CAE, it can be validated through actual crash testing to ensure its performance and safety. However, and due to the complex nature of a crash event, its simulation is not as straightforward and presents challenges, which are highlighted in this section. All in all, a vehicle crashworthiness simulation has a higher degree of complexity when compared to a linear analysis, that assumes perfect elastic behaviour of the structures. This approximation is no longer valid in crash simulation, in which non-linear interactions among material non-linearities, geometry and transient nature of boundary conditions need to be considered [18].

2.1.4.1 Material modelling

During a crash event, structures experience large deformations, which invalidates the elastic material assumptions that are characteristic of the simpler linear simulation approach. Therefore, due to the dynamic nature of crashworthiness simulation, the constitutive material models need to incorporate both elastic and plastic behaviour to accurately capture the material response.

An additional factor to take into account is the fact that different materials need to be considered to accurately represent the real-world conditions of a vehicle structure. This implies incorporating various material models of varying complexity within the same finite element model.

Finally, regarding the topic of topology optimisation, which will be presented and explored later in this thesis, material modelling plays a crucial role. Many of the methods and algorithms used to obtain the optimal geometries pretended in topology optimisation are based on interpolations of the material properties. This constitutes a challenge because of the appearance of elements with non-physical material properties, which can lead to unstable simulations, particularly when solving for large, non-linear deformations [17, 16].

2.1.4.2 Contact

Due to the significant deformations that occur during a crash, different parts of the structure come into contact with each other. Thus, the contact algorithm is essential to accurately model this phenomenon in a crash simulation. There are various methods available for modelling contact, but the penalty method is the most widely used in crash applications [17].

2.1.4.3 Integration scheme

Additionally, a crash simulation is best described as a dynamic problem, in which time-dependent entities such as acceleration and velocity must be taken into account, thus, a dynamic explicit model representative of such conditions is needed. The dynamic response of such model can be expressed by a state equation, refer to Eq. (2.3), in which M, C and K are the mass, damping and stiffness matrices respectively. On the other side of the equation, F is the external force and R is the residual [1].

$$M\ddot{d}(t) + C\dot{d}(t) + Kd(t) = F(t) - R(d,t) \tag{2.3}$$

Another aspect to be considered for a dynamic analysis, is the type of integration scheme to solve the equations of motion in Eq. (2.3), namely by implicit or explicit method. An implicit solver is more accurate since it evaluates the displacement d at each time step, signifying, in exchange, a higher computational burden. By contrast, the explicit method uses direct numerical integration of the equation of motion to gather the displacement information, making it the quickest solver out of the two and the most adequate for crashworthiness simulation which deals with large deformations and varying material properties [1, 19].

For that reason, the explicit integration scheme is implemented in this study. First, the explicit solver of Abaqus® is used to simulate the crash event at a component level in order to, iteratively, obtain the structural optimisation intended. Afterwards, VPS/PamCrash® serves as the software to perform the final frontal impact simulation with the optimised component integrated into the baseline structure of the coach.

2.1.4.4 Difficulties of numerical crash simulation

In order to be representative of the real-world conditions intended, crash simulation models are characterized by their large size. In contrast, the size of the elements needs to be small to avoid accuracy issues, as a result, a complete model after mesh generation can reach a number of elements in the order of millions, and since computation time is directly related to the number of elements, this translates into a large computational effort. To reduce computation time, parallel computing can be used.

Another specificity of these types of models is the need to simulate a mix of different materials and joining elements that are typical of vehicle assemblies, and that can be modelled following different strategies with varying levels of accuracy and complexity. If so, the real challenge is to accurately represent the conditions of the vehicle crash in a simulation achieved with reasonable computational effort.

2.2 Structural Optimisation of Crashworthy Structures

Structural design optimisation has gained attention in the automobile field during the past decades since it has revealed itself as an interesting tool to synthesize a lightweight and crashworthy structure [5]. In general, when a mechanical structure fails to meet its desired performance, structural optimisation can be applied to improve its performance based on a defined parameter or objective, for structural optimisation said parameter is often the stiffness/mass ratio [20].

Formally, an optimisation problem with a single objective is defined by a set of design variables, X, which are usually defined between a lower and upper bound, and are used to minimize or maximize an objective function, F, subjected to a number n of G constraints, refer to Eq. 2.4 [21].

$$\begin{gathered} Find\ X\ that: \\ Minimizes\ F \\ Subject\ to:\ G_j \leq\ 0 \\ where,\ X_L \leq\ X\ \leq\ X_U \end{gathered} \tag{2.4}$$

Among the pioneers in this field, L. Schmidt [22] stands out with his review on the evolution of structural optimisation, which in the 60's was known as structural synthesis. In this work, the author presents the basic definitions and fundamental concepts of structural synthesis, among them, the objective function and design variables are defined. The latter being the defining quantities of a structural system that are changed during the redesign process, and that constitute the objective function used as criteria to choose between different acceptable designs.

2.2.1 Multi-objective structural optimisation

The formulation presented above is characteristic of a single objective optimisation. Nonetheless, if all the load cases representative of the different types of crash events are considered, crashworthiness design becomes a multi-load case optimisation problem in which an analysis must be performed for each load case. The traditional approach of linear-static problems is to solve such multi-load cases by representing the final value as a weighted sum of the compliance or strain energy from each load case for each element [16, 23].

Multi-load optimisation is relevant for industrial applications in the automotive industry since a particular vehicle component can be influential for several test cases. As a matter of example, the authors of [24] applied multi-objective optimisation algorithms to the problem of frontal crash safety of a full-scale vehicle, having full and 40% offset frontal crashes as multi-load conditions.

Indeed, the multi-objective formulation is appropriate to represent the real conditions of crash events. However, there is a clear increase in complexity when applying this approach. An opportunity for simplification is to employ the strategy of optimising a particular vehicle component independently, specifically, optimising the most influential part depending on the load case of interest. Following the idea, this study proposes a single-objective optimisation approach for a specific component, namely a crash box, under frontal impact conditions.

2.2.2 Fields of Structural optimisation

Three different techniques can be used to optimise the structural performance of a particular structure subjected to a set of boundary and loading conditions, namely size, shape and topology optimisation (Figure 2.7). Said categories differ on the type of design variable involved, and thus in the type of algorithm used to solve the optimisation problem.

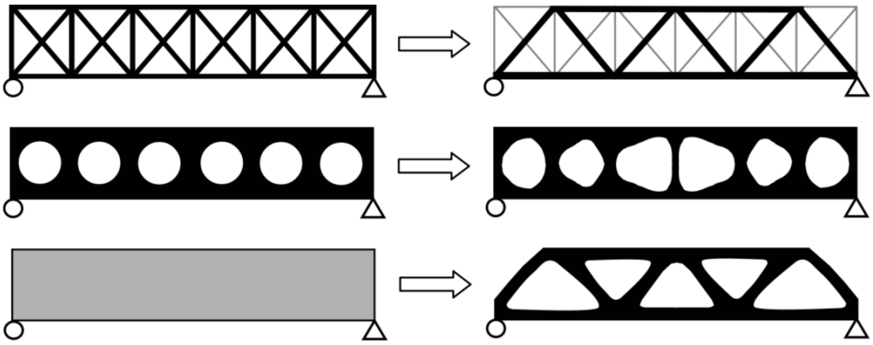

Figure 2.7: Fields of structural optimisation. a) Size optimisation, b) Shape optimisation and c) Topology optimisation [25].

Size optimisation is the simplest type of structural optimisation, using design variables such as plate thicknesses and bar cross-sectional areas [26]. The aforementioned simplicity of this type of approach comes from the fact that the domain of the design model and state variables is known *a priori*, and is fixed throughout the process. In other words, there is no need to modify the finite element model, only being necessary to update the thickness values. Moreover, size optimisation problems can often be solved with standard optimisation algorithms [25].

Still, for many problems, shape design outperforms sizing design. In shape optimisation, the design variables control the geometry of the structure and change the Finite Element Method (FEM) model as the optimisation undergoes, the goal is to find the optimum shape of the geometry of the part, which is now the design variable. It constitutes an evolution relative to the sizing optimisation problem, thus entailing an increase in complexity and representing the progression of structural analysis and optimisation tools in order to tackle more difficult problems in structural optimisation [25, 26].

Lastly, focusing on the structural optimisation method employed in this work, topology optimisation is an iterative process aimed at finding the optimal arrangement of structural material within a limited volume. The objective is to achieve the best possible mechanical performance for the design concept [1]. In a topology optimisation problem, the known variables are the applied loads, support conditions, structure volume, and potentially some additional design constraints [25], making it the preferred approach to generate efficient design concepts at early design stages, while sizing and shape optimisation are usually combined into a single process and applied at a later stage [27].

Regarding the typical formulation for a topology optimisation problem (Refer to Eq. 2.5), it follows the pattern of a general structural optimisation problem. The design variables are the densities of the elements in the FEM model (ρ_i), which means that it involves many more design variables in contrast with sizing and shape optimisation. Its objective is that of minimizing a global structural response, represented by an objective function (f). The optimisation problem is typically constrained on the mass or volume of the design space. Specifically, the volume of the optimised structure, computed by considering the elemental volumes (v_i), shall be equal to or lower than the objective volume defined (V) [1].

$$\begin{aligned} &minimize\ f(\rho) \\ &subject\ to\ \sum_{i=1}^{N} \rho_i v_i \ \leq \ V \\ &\qquad\qquad \rho_{min} \ \leq \ \rho_i \leq \ \rho_{max} \end{aligned} \tag{2.5}$$

2.2.3 Main Optimisation Methods for Crashworthiness Design

Before diving with more detail into the theoretical aspects of topology optimisation and its application to crashworthiness design, a brief review of the existent methods, or algorithms, used for optimisation of crash structures will be presented. However, this is not a straightforward task since there are different ways of classifying the methods, and a particular method can fit the description of more than one classification.

One of the most spread classifications is between gradient and non-gradient-based methods, as presented by Sigmund in [28]. This classification is quite straightforward, as it categorizes the methods based on whether sensitivity information is computed or not to perform the optimisation. One of the drawbacks of this kind of classification is that it fails to differentiate optimisation methods that use hybrid approaches. In any case, the classification of gradient-based optimisation techniques encompasses the homogenization and density approaches, the level-set approach, among others. While the non-gradient-based techniques include the classic implementation of methods like genetic algorithms, artificial immune algorithms, ant colonies, particle swarms, differential evolution schemes, and others.

Le Riche and Haftka in [29] present a review of methods following a classification between local and global optimisation algorithms. Said algorithms may or may not use gradient information and according to the classification, the latter prevents getting stuck at local, suboptimal points, thus being able to converge to better solutions than local algorithms.

In [17], Hunkeler defined an alternative classification based on the type of structural information used by the optimisation method to move forward in the iteration process. The first group is comprised by the optimisation methods using the variations in the nodes or elements of the model to calculate the sensitivities. On the contrary, the second group uses only the objective and constraint functions to go from one iteration to the other, this category includes, for example, the evolutionary algorithms and response surface methods. The main difference between both types of algorithms is the level of understanding of the physical phenomenon, the first group considers the influence of each element in the model while the second is more of a black-box approach. If so, the first category of algorithms demonstrates a stronger comprehension of the underlying physical phenomenon. In exchange, it is more difficult to apply and requires more iterations than the second one, making the latter more popular to implement for crashworthiness applications.

Another possible classification is to distinguish between individual and population-based methods, or heuristic and non-heuristic methods.

2.2.3.1 Application to Crashworthiness Design

Despite the many possible classifications presented above, one general conclusion can be reached regarding the usage of algorithms in the context of optimisation of crashworthy structures. As mentioned in a previous section, crash simulation carries a high computational weight due to its size and general non-linear nature. In consequence, applying gradient-based methods becomes challenging since the crash computation needed to retrieve gradient information becomes unrealistic for the number of elements present in the model. Hence, derivative-free methods based on objective and constraint functions are more commonly used when it comes to crashworthiness design. Although these methods do not guarantee optimal solutions, they enable the improvement of the objective function with a limited number of iterations, which is deemed satisfactory in this field.

When it comes to the preferred structural optimisation field for crashworthiness design, the literature predominantly focuses on size and shape optimisation approaches, as mentioned in [17]. As for topology optimisation, its exploration is still relatively limited, even though the number of publications on the topic has seen an increase in the past decade. A recurring approach found in literature is to identify and optimise the weaker regions of a structure by adding a reinforced profile, or increasing the thickness of the existing one, and incorporating energy-absorbing elements [3].

These type of energy-absorbing structures have also been the topic of researches that aim to seek an optimal design for crashworthiness applications [30]. For the case of frontal impact, deformable, yet stiff front structures are required to absorb the kinetic energy, thereby minimizing the transmission of crash energy to the occupants [5]. Among the configurations that show potential for these conditions, thin-walled tubes have received significant attention due to their collapse in a controlled progressive folding pattern under axial crushing [4]. A typical energy absorption of an aluminium thin-walled structure is shown in Figure 2.8.

Particular focus has been given to the influence of different geometric sections on their energy absorption capabilities. In fact, it has been concluded that the number of corners on a cross-section largely determines its performance in terms of energy absorption. For that reason, thin-walled tubes with multiple cells and internal webs are also regarded as efficient configurations and have been the subject of crashworthiness optimisation [5].

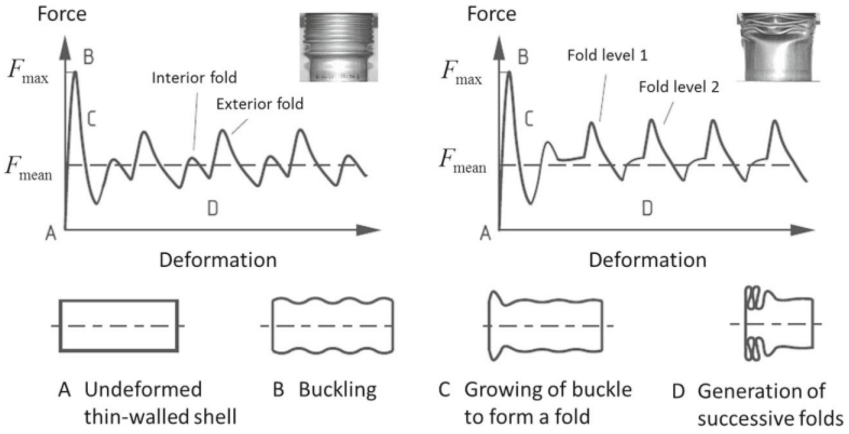
Force
F_{max}
F_{mean}
A
B
C
D
Interior fold
Exterior fold
Deformation
Force
F_{max}
F_{mean}
A
B
C
D
Fold level 1
Fold level 2
Deformation
A Undeformed thin-walled shell
B Buckling
C Growing of buckle to form a fold
D Generation of successive folds

Figure 2.8: Force-displacement curves for an aluminium tube under axial load [31].

Crashworthiness optimisation has also been applied to specific automotive components such as longitudinal rails, side pillar structures, bumper systems and crash boxes. Application examples can be found in [5].

For the specific case of bus structures, researchers have adopted the approach of analysing the baseline structure to subsequently propose a redesigned bus structure with increased energy absorption capacity due to the addition of energy absorbers. For instance, Güler et al, in [3], proposed an optimisation of the crashworthiness performance of an intercity coach under frontal impact by adding energy-absorbing geometries, designed to increase the driver survival space. Most specifically, the energy absorption characteristics of conical energy absorbers with a circular cross-section and of an accordion geometry were tested under the conditions of regulation ECE R-29. Similar investigations have been performed by Cerit et al. and Rooppakhun et al. in [14, 15], respectively.

P. Jongpradist et al. [4] investigated the strength of a bus structure under frontal impact and recommended crashworthiness improvements by adding a crumple zone, made from thin-walled members, and a rigid compartment zone. The influence of the number of energy absorbers and their material was studied, as well as the effect on stiffness and rigidity of the compartment zone achieved by modifying the cross-sectional profiles of the A-pillars.

One final insight that can be retrieved from these applications in the context of optimisation of large vehicle structures is that a simplified numerical model is often used for the simulation. If so, it can be argued that parts of the vehicle body that have no significant effect on the output of the simulation can be subtracted from the model, hence diminishing the computational resources needed.

2.3 Topology Optimisation for Crashworthiness Design

Topology optimisation has gained significant popularity in industrial applications, leading to its incorporation into various FEM codes [27]. Nevertheless, as it became clear from the information presented in the previous section, applications of topology optimisation in the context of crashworthiness are still limited despite its potential, even more for the specific case of bus and coach structures.

In this section, an overview of topology optimisation is presented, starting with the classic optimisation methods that are well-established for static problems and that evolved into alternative methods with improved capabilities to tackle more complicated problems such as crashworthiness design. Having this background, a review of the practical applications found in the literature is presented, specifically in the context of interest. Finally, a discussion of the methods is presented, with the intention of highlighting their advantages and drawbacks.

2.3.1 Overview of Topology Optimisation

The goal of topology optimisation is to find the shape of a structure with the maximum utility of the material available in the design space while maximizing or minimizing a specified objective and satisfying a set of constraints, that range from design to volume constraints.

In the early stages, topology optimisation primarily focused on tackling straightforward problems with elastic material properties, linear deformations, and static loading conditions [16]. Theoretical exploration of these aspects began in the 1980s, with authors such as Bendsøe and Kikuchi leading the way [32]. Their contributions introduced topology optimisation as an alternative approach to shape optimisation, which had already been extensively studied and refined over a period of more than fifteen years. This pioneering work also marked the emergence of topology optimisation as a computational tool.

Decades later, books like the one published by Bendsøe and Sigmund [25] reviewed in depth the theory, methods and applications of the classic topology optimisation techniques applied to continuum stiff structures. In summary, the traditional approach to topology optimisation is to assume an elastic behaviour with small deformation of the structures. For that reason, nowadays, this structural optimisation technique is well-established for linear static problems that satisfy these assumptions [16].

2.3.1.1 Classic Topology Optimisation Methods

The classic topology optimisation methods as described by Bendsøe et al. in [25] and [32] used an approach labelled as the Optimality Criteria (OC) method to derive an optimal design for minimum compliance, tackling the topology optimisation as a material distribution problem. To do so, material modelling or material parametrization is necessary. Topology optimisation can be performed using discrete or continuous discretizations, and the choice of discretization method determines the appropriate material parametrization to be employed in the material model.

For instance, the simplest material parametrization is the discrete material model, in which each element is represented by its density as design variable (x_i) which takes a value of either zero or one, meaning that the element is void or has material, respectively. This material model can be represented by Eq. 2.6.

$$\chi(x_i) = \begin{cases} 0 & \longrightarrow \text{no material} \\ 1 & \longrightarrow \text{material} \end{cases} \tag{2.6}$$

On the other hand, for continuum structures, the material parametrization model allows the design variables to assume any value between zero and one. The pioneer methods used two strategies for computing effective material properties for values that lie between said range, namely, the homogenization and density approaches.

The homogenization method is a technique first presented by Bendsøe and Kikuchi in [32] where two material constituents are considered, substance and void, and it functions as an interpolation model for void and full material, with the goal of finding the optimal void distribution. In this method, the domain is divided into elements, and each element contains a microstructure composed of numerous small holes that are periodically distributed within the base material [33]. This method belongs to the initial numerical methods for topology design of continuum structures that were based on using composite materials as the foundation for describing the intermediate material properties that can result from the interpolation technique [25].

As for the density method, a single design variable is assigned to each material element. Said design variable connects the relative density of an element to its elastic modulus, through the use of an interpolation scheme. According to [16], one of the most commonly used interpolation techniques is the Solid Isotropic Material with Penalization (SIMP) model, having been used in early works in the field, such as [34], following an expression as depicted in Eq. 2.7, where p is the penalization parameter and E_0 is the elastic modulus of the base isotropic material.

$$E_i(x_i) \;=\; x_i^p E_0 \tag{2.7}$$

The power parameter p, ($p \geq 1$), is employed to guide the elemental densities within the design domain towards either full density (x=1) or no density (x=0). By doing so, it is intended to avoid intermediate material properties that are typically not isotropic and cannot be represented within the original design description of only isotropic material [25]. According to Bendsøe and Sigmund [25], in order to obtain a true black-and-white configuration, $p > 3$ is usually required. The density approach can be used with both gradient and non-gradient methods to distribute material continuously throughout the iterations, allowing the smooth and efficient evolution of the topology during the optimisation process [16].

2.3.1.2 Numerical Instabilities

When applying topology optimisation methods, especially based on the material distribution procedure, the optimisation results are prone to be affected by numerical instabilities. These instabilities often manifest in the form of checkerboards, mesh dependencies, and local minima. The reference book by Bendsøe and Sigmund [25] provides a comprehensive review on this topic, and the main insights are presented below.

The checkerboarding phenomenon refers to the formation of regions of alternating solid and void elements arranged in a checkerboard-like pattern. Its appearance is due to the discretization of the original continuous problem that overestimates the stiffness of the checkerboards in the finite element analysis since these types of material layouts have an artificially high stiffness. Consequently, it is not surprising to encounter them being generated by the optimisation process, despite being non-physical.

Mesh dependencies, in its turn, refer to the phenomenon where different mesh sizes or discretizations yield qualitatively distinct optimal solutions. In other words, the choice of mesh can significantly influence the outcome of the optimisation process, leading to variations in the final design solution.

Lastly, the local minima instability arises from the non-convex nature of most topology design problems. This implies that multiple local minima can exist, resulting in different solutions for the same discretized problem depending on the choice of initial solutions and algorithm parameters.

Figure 2.9 depicts the appearance of the checkerboard pattern (Figure 2.9 b) and the influence of the mesh size (Figure 2.9 c and d), for the benchmark topology problem of an MBB beam, i.e., a simply supported structural domain to which a central point load is applied [35].

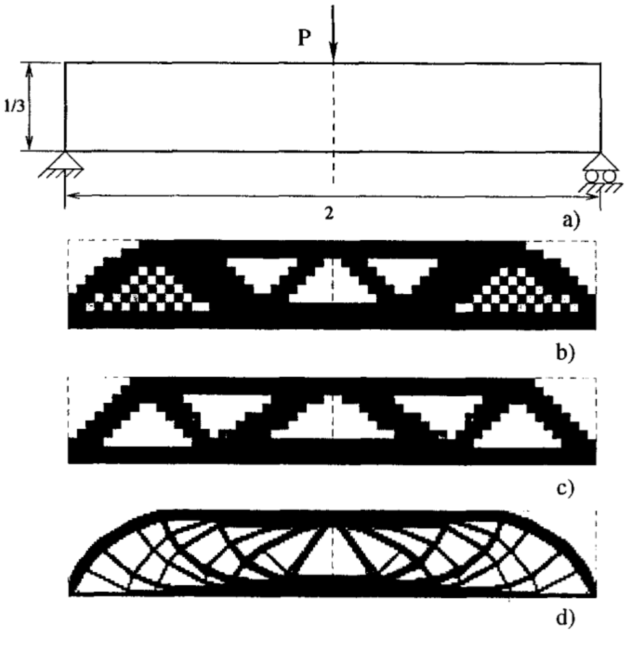

Figure 2.9: Numerical instabilities of checkerboards and mesh dependency on a topology optimisation problem [36].

To address these issues, the use of regularization techniques is recommended. According to Sigmund and Petersson [36], perimeter control and mesh-independent filtering have shown promise in mitigating the aforementioned numerical instabilities. Among these techniques, filtering methods are the most straightforward to implement. They involve adjusting the design sensitivity of each element based on a weighted average that includes the element itself and its eight immediate neighbours. This approach is commonly used for alleviating both checkerboarding and mesh dependency problems [16].

2.3.2 Application to Crashworthiness Optimisation

In dynamic problems such as crashworthiness optimisation, the objective is to maximize the energy absorbed by the structure during a crash event while maintaining a certain level of safety at a minimal cost. Safety considerations are typically assessed based on the accelerations and forces experienced during the crash, while cost factors are primarily determined by the amount of material needed for component manufacturing and the fabrication process involved [16].

The first approaches to the application of topology optimisation in crashworthiness design started in 1996 with the work of Mayer et al. [37], the authors developed a methodology to handle topology optimisation for elastic-plastic materials at a component level, namely for an automotive rear rail. The goal was to maximize energy absorption for a given volume, applying the homogenization technique and an optimality criteria algorithm.

Similarly, Pedersen in [38] applied the technique to obtain a desired energy absorption history for a crushed structure, used to improve the crashworthiness of transportation vehicles. In his approach, a quasi-static finite element analysis is used and the optimisation problem is solved by the Method of Moving Asymptotes (MMA).

Both of the previous approaches share a common characteristic in that they rely on several assumptions that relax many of the non-linear phenomena typically associated with a crash event. The explicit consideration of displacement and accelerations is not present in the work of Mayer et al. [37], and Pedersen [38] assumes low accelerations for the crushing of the structure and no contact between elements.

The classic topology optimisation methods resort to the use of sensitivity information to perform the optimisation, which is practically infeasible for crashworthiness simulations due to the intensive computational cost associated with it. Therefore, the above simplifications are made to avoid discontinuities that cause numerical difficulties in the convergence of a solution. Still, classical methods, despite being efficient for static problems, lack sufficient capabilities to satisfy the demand for crashworthiness topology optimisation [18].

In consequence, alternative methods have been developed in theory and will be explored next. Mainly, these methods can be divided into two groups. The first group consists of non-linear topology optimisation techniques developed to be applied in the context of crashworthiness design. The second group involves simplifications of the non-linear problem into a static loading problem based on the displacements information, allowing to perform the topology synthesis with the well-established linear methods [19].

2.3.2.1 Hybrid Cellular Automata (HCA) Method

The method of Hybrid Cellular Automata applied for topology optimisation was devised by Tovar et al. in [33], as a methodology inspired by the process of structural adaptation in bones, with the purpose of driving the overall structure to an optimal configuration. It is a non-gradient method, labelled as hybrid because it combines elements of the Cellular Automaton (CA) paradigm with Finite Element Analysis (FEA).

Most specifically, it performs the structural analysis using the finite element method and the design domain is discretized into a regular lattice of cellular automata (CAs). Each CA in the design domain senses the strain energy density (SED) within its vicinity and decides, based on the SED level, to modify the surrounding structure until only relevant cells are kept.

Among the convenient aspects of this method, the fact that no gradient information is required in the design process can be highlighted, which is of special benefit for crashworthiness applications. Furthermore, the HCA algorithm is applicable to both 2D and 3D models, and it can produce convergent solutions that are less susceptible to numerical instabilities while maintaining a reduced number of iterations.

Regarding the application of HCA to the synthesis of topologies in crashworthiness design, the work done by Patel [16] stands out in the field. The author developed a methodology based on the HCA method to synthesize structures under non-linear transient loading and deformation, with considerations of material plasticity. The idea is to ensure that all elements within the structure contribute to energy absorption through plastic deformation.

To demonstrate the methodology, the author applied the algorithm to an aluminium beam design problem subjected to an impact from a rigid pole. Static and dynamic finite element analyses were conducted to study the influence in the final topology obtained. The static problem was modelled by applying a distributed static load with a magnitude that produces, approximately, the same displacement as the pole impact, whereas the dynamic problem allows for elastic-plastic deformations in the material. The design domain for both cases studied by the author is shown in Figure 2.10.

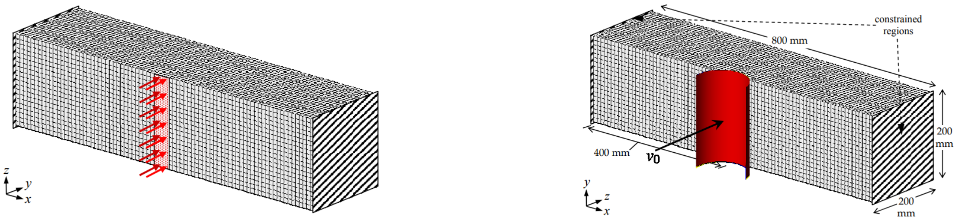

(a) Static approach

(b) Dynamic approach

Figure 2.10: Design domain of the beam problem [16].

Moreover, for the static approach, both linear and non-linear elastic material behaviour were considered. This allowed to compare three final topologies, as depicted in Figure 2.11, and conclude that the internal energy density distribution in the topologies synthesized using dynamic analysis (Figure 2.11 c) was found to be more uniform as compared to the structure generated using the conventional approach of modelling the structure as an elastic-static problem (Figures 2.11 a and b).

This result highlights the importance of considering the dynamic nature of crash events when optimizing structures for crashworthiness. Finally, in his work [16], Patel also extended the application of the HCA algorithm to the multiple load case.

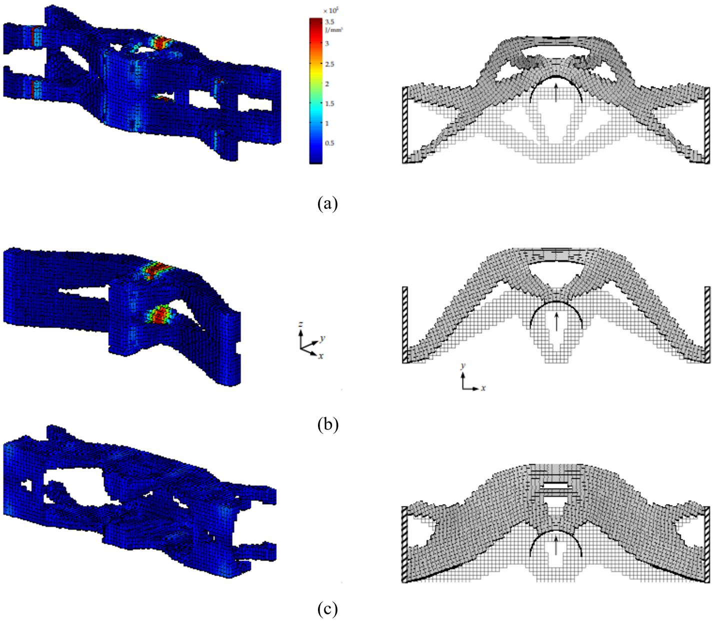
(a)
(b)
(c)

Figure 2.11: Internal energy density plots (Left) and maximum deformation (Right) of the topologies synthesized using the (a) linear, (b) non-linear, (c) and dynamic analyses. [16] (Modified)

Another interesting practical application of this method is that it has been incorporated into the commercial software *LS-DYNA*, on an environment to perform topology optimisation known as *LS-OPT/Topology* [39]. The work done by Müllerschön et al. [40] marked the initial experience of utilizing this software to solve industrial problems, namely, it applied the HCA method to determine a suitable geometry for a bumper.

To conclude, we can discuss the extension of the HCA method to be applied to thin-walled structures. Considered as an improvement, the HCA algorithm is modified so that it can be applied to these types of structures, which are extensively used in current vehicle structures taking advantage of their special energy absorption behaviour. Applications to crashworthiness design can be found on the study by Duddeck et al. [31] and further studies were conducted by Hunkeler in his PhD thesis [17]. The geometries were produced using shell elements, and the authors conducted evaluations based on fully non-linear crash simulations.

2.3.2.2 Equivalent Static Loads (ESL) Method

As it has been stated throughout this theoretical review, one of the primary obstacles in utilizing topological optimisation in crashworthiness design is effectively handling the non-linearities of the crash dynamic process. For this reason, alternative methods have been developed to simplify such dynamic problem through an equivalent static counterpart, the Equivalent Static Loads (ESL) approach belongs to this alternative group [5].

The methodology revolves around the concept of substituting a fully dynamic non-linear crash simulation by a series of consecutive linear simulations, having Park et al. [41] among the first works to propose this idea. These linear simulations utilize equivalent static loads, that generate deformation effects equivalent to those produced by the dynamic load. By adopting this approach and replacing the computationally intensive explicit simulations with linear simulations, the overall computational burden is significantly reduced, leading to faster analysis and optimisation processes [17].

According to Hunkeler [17], the application of this method to topology optimisation has been materialized through two different forms, which differ in the definition of static loads. One possibility is to work with global ESL that, in the context of crashworthiness design, represents the overall effect of the external forces and constraints acting on the vehicle structure or component during a crash scenario. This allows to apply the method to large-scale practical problems, examples of that are applications by authors like Cavazzuti et al. [42], that performed a topology optimisation of a full vehicle structure under different load cases.

Alternatively, the static loads can be defined at the finite element level by applying artificial forces to each node of the model. This approach is known as nodal-based ESL and allows for finer control of the model deformation but, in exchange, the effort to extract the loads is higher.

In recent years, this approach has been used to derive equivalent static loads for the case of thin-walled structures, similar to what was presented previously for the HCA method. Such was the case of the works presented by Davoudi & Kim [43] and Ren et al. [44]. The researchers applied the methodology at a component level, specifically for an automotive crash box, being able to synthesize topologies that successfully predict the location of plastic hinges in the structures, which are the main areas to enhance their energy absorption.

2.3.2.3 Evolutionary Methods

Besides the non-linear optimisers and the method of equivalent static load, there are other unique topology optimisation approaches to enhance structural performance, such is the case of the evolutionary methods.

Evolutionary Structural Optimisation (ESO) was initially proposed in the 1990's by Xie and Steven in [45]. The objective of ESO was to emulate the evolutionary mechanism found in biological structures in order to achieve similar structural shapes through the application of finite element analysis. The authors proposed a so-called, simple evolutionary procedure based on the empirical concept that a structure evolves towards an optimum by slowly removing inefficient material. In this process known as hard-kill method, material that is deemed ineffective according to a predetermined rejection criterion is identified and subsequently removed.

After its introduction, ESO was further developed by Querin et al., who in [46] presented the Bi-directional Evolutionary Structural Optimisation (BESO) method as a natural corollary of ESO. The BESO method implements a bidirectional algorithm which enabled the simultaneous addition of efficient material to the structure while removing inefficient material. The evolutionary methods have been used to solve a variety of size, shape and topology optimisation problems, using binary design variables to do so [47, 48].

However, like all novel techniques, the first versions of the evolutionary methods suffered from deficiencies that required further research. One such limitation was that it overlooked relevant details of structural optimisation like the need to account for numerical instabilities. Indeed, evolutionary methods continued to undergo further advancements to address the aforementioned issues and improve their algorithms. Researchers of this field implemented tactics that were efficiently applied during the same decade for other optimisation methods. Investigations like the one developed by Li et al. in [49] focused on the checkerboard problem, while others constituted efforts to mitigate mesh-dependency, adopting strategies of perimeter control [50] and filtering [47]. This last work, carried out by Huang and Xie, is considered one of the major development for this type of method, it proposes a sensitivity filter and a stabilization scheme using history information to materialize a convergent and mesh-independent BESO.

All of the previous contributions resulted in a BESO algorithm with improved robustness compared to traditional ESO [51]. According to Huang et al., the majority of research on ESO/BESO focused, initially, on optimising structures with linear material properties and small deformations, but in light of the improvements, evolutionary methods started to be applied to more complex problems. Said authors modified the method to be extended to the more demanding task of topology design of energy absorption structures, which involve non-linear material and large deformation [52].

More crashworthiness applications have been developed in recent years. As a matter of example, the authors of [53] performed an optimisation of a thin-walled square tube, made out of mild steel, subject to an axial crushing load. The BESO algorithm was modified to be compatible with shell elements, that better represent the geometrical non-linearities of axial crushing in energy-absorbing members. By applying the methodology, the geometry of the thin-walled structure was optimised by obtaining patterns of material and void, most specifically on the tube sidewalls. The authors reported that the energy absorption was maintained at a reasonable level despite the weight reduction achieved through the optimisation. The results were verified experimentally and compared to those obtained numerically in terms of crushing and crashworthiness responses, a comparison of the axial crushing behaviour of the optimised geometry can be seen in Figure 2.12.

Some last methods that can be mentioned are the Ground Structure Approach (GSA) and the Graph and heuristic-based methods. First, the Ground Structure Approach consists in filling the design space with elementary macro-elements that have a simplified crash behaviour, and are

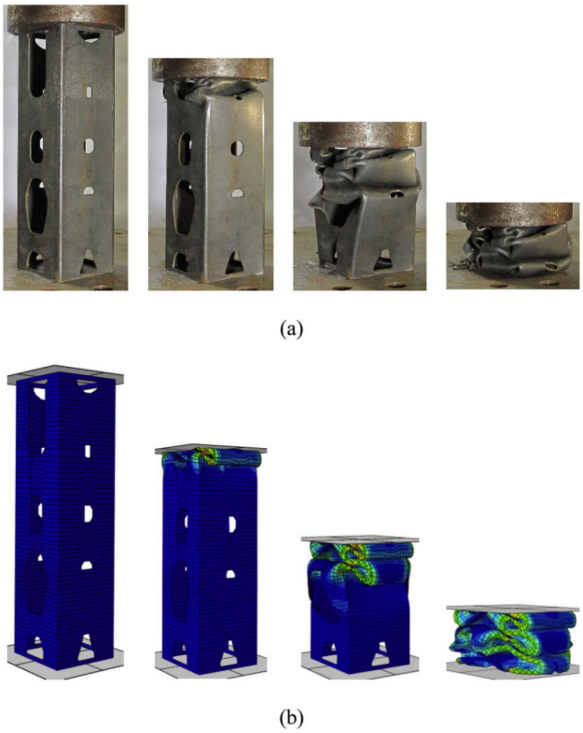

(a)

(b)

Figure 2.12: Axial crushing of the topologically optimised sample (a) Experimental test; (b) Numerical simulation in ABAQUS [53].

modified to reach an optimum design [17]. As for the graph and heuristic method, it can only solve problems with a 2D design space, hence the technique has been applied for the design of profile cross-sections of crashing structures [5]. A thorough review, as well as some relevant applications examples, can be found in the works of Soto et al. [54], and Ortmann and Schumacher [55].

2.3.3 Discussion of the Alternative Topology Optimisation Methods

In the last section, a review of the applications of various topology optimisation methods in the context of crashworthiness design was presented. Starting with the pioneer approaches that adapted the classic optimisation methods by including linear assumptions to bypass the challenges imposed by the non-linearities inherent to crash simulation. Still, it was noted that these methods are limited in capturing all the relevant aspects of a fully non-linear, transient dynamic crash simulation.

Despite all the shortcomings, these first attempts served as a foundation for the development of more advanced approaches. From the literature review, it was possible to deduce that these last methods can be considered the state-of-the-art in the field of topology optimisation for crashworthy structures. Most specifically HCA, ESL and evolutionary methods are the subject of many research papers highlighting their prominence and relevance in the field. Such is the case of the comparative study presented by Chuang and Yang in [18], where the main concerns in the application of the

ESL and HCA methods are presented, together with a comparison of the results obtained to the example of a vehicle structure subjected to a full frontal impact.

In the case of ESL, the primary issue revolves around the accuracy of the equivalent static load in depicting the response field in crashworthiness analysis. This question of whether the ESL method provides a sufficiently precise representation of the complexity of crash events also arose in [43]. Additionally, the authors discussed the significant modelling and correlation efforts that result from the two different finite element codes required in the ESL method. From an industry application perspective, this represents an extra burden due to the need for pre and post-processing of the model to fully meet crashworthiness design requirements.

In contrast, by opting for the HCA method, no model conversion is required, ensuring that the data accuracy is not compromised between the optimisation and simulation runs. However, the authors also reported some issues and limitations for this method, being the primary concern the accuracy and robustness of the algorithm, which normally implies a higher number of iterations to achieve better optimisation results. This could result in computational inefficiency, particularly when dealing with large-scale industrial applications.

Another comparative research was presented in [23], this time focusing on the contrast between gradient-free techniques, such as HCA, and the more established topology optimisation methods, like the optimality criteria method (OC) and the method of moving asymptotes (MMA). To highlight the differences between the methods, three linear-static design problems were proposed, and the results indicated that the HCA method was the most efficient in terms of the number of required iterations to generate a result.

As for the evolutionary methods, those have also been compared with mathematical programming methods, such as MMA, and OC methods in regard to an important distinction that pertains the definition of the design variables in each approach. Instead of using continuous design variables, evolutionary approaches tackle the optimisation problem using discrete representations as design variables [16]. This was deemed as one of the attractive features of ESO/BESO methods by Huang and Xie in [47], since a discrete approach is very easy to implement and results on a clear optimal topology with no grey area, i.e., no intermediate densities. The authors also address the main deficiencies of the evolutionary methods, which include its propensity to numerical instabilities as a drawback of its simplicity. Also, as it was discussed in a dedicated section, evolutionary approaches can derive mesh-dependent and/or non-convergent solutions.

Chapter 3

2D Application

Having established the theoretical background, this chapter proceeds with the practical application developed in this research. The objective is to apply topology optimisation techniques to derive an optimal design for a crash box that can be integrated into the frontal structure of a coach. The crash box is intended to enhance energy absorption capabilities and ultimately improve the passive safety levels for the driver.

In order to materialize this application, the chosen approach is to utilize the capabilities of an ABAQUS-MATLAB interface for conducting topology optimisation and explicit simulation of a finite element model. To assess the potential of the interface, a sequential approach is adopted in this work. Instead of initially optimising a full vehicle component, the focus is on a 2D approach that simulates an axial crash scenario. This allows for a gradual transition to more complex three-dimensional models. The objective is to evaluate the results obtained from applying different optimisation methods and identify the most effective approach for synthesizing an optimal topology that meets the specified conditions.

The practical application in this study involves the evaluation of several algorithms, including evolutionary methods (ESO and BESO), and an Optimality Criteria approach. Detailed information about the Matlab implementation of these algorithms and the development of the interface is provided in a dedicated section.

The chapter also presents the 2D finite element model, along with the obtained topologies using the different applied methods. A thorough discussion of the results is provided, leading to a conclusion regarding the best-performing methods. Said methods will be further tested and evaluated in a 3D implementation.

3.1 2D Finite Element Model

As an initial approach to test the optimisation procedure, a two-dimensional axial crash simulation was conducted. In this simulation, the crash box is simplified as a rectangular plate that is impacted by a rigid body. The choice of a two-dimensional approach is motivated by the fact that the Matlab interface made available for this work was built for optimisation of two-dimensional models. With that in mind, the objective is to evaluate the capabilities of the interface using a simplified approach that aligns with the initial configuration of the code. Once the performance of the interface is assessed in the two-dimensional context, further updates and modifications will be made to enable its application to three-dimensional models that can better capture the dynamics of an axial impact and provide a more comprehensive representation of the real-world scenario.

3.1.1 2D Model Definition

Figure 3.1 represents the finite element model for the 2D axial crash. It depicts both intervening bodies, the crash box and the impactor. The 2D crash box was modelled as a planar shell with a length of 300 mm and a width of 50 mm. Regarding the impactor, it is simulated with a 2D analytical rigid body, having a mass of 90 kg and an impacting speed of 15 m/s on the X direction. The properties of the impactor were defined on a reference point that was conveniently created for this purpose. It is relevant to point out that all the parameters were defined according to those used by Nagel and Thambiratnam in their study about straight energy absorbers [56]. This step was carried out for subsequent validation purposes.

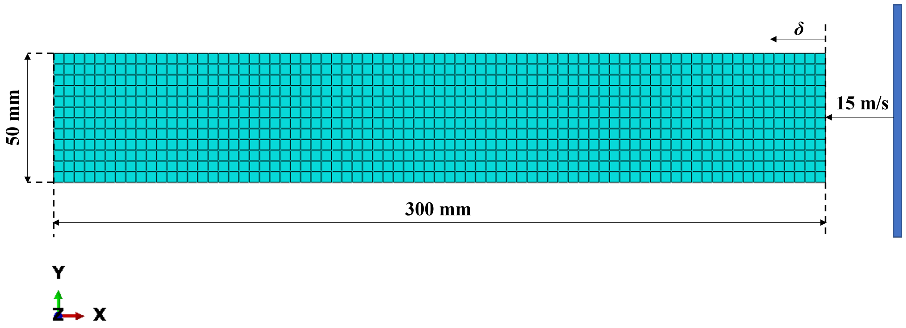

Figure 3.1: 2D finite element axial crash model.

Since the impactor was modelled as a rigid part, there was no need to define material properties for it. Nevertheless, definition of material properties for the crash box is of uttermost importance. The selected material was a mild steel, with properties according to [56]. Table 3.1 shows the density and elastic properties, and Table 3.2 contains approximated true stress-plastic strain data points that were used to define the plasticity properties of steel in the finite element model. The material properties are assigned to the part by creating a solid, homogeneous section.

It is relevant to point out that the above-defined material properties were obtained by the authors using a standard tensile test. However, the component to be simulated in this numerical approach is to be subjected to compressive loads. Still, simulating for the tensile material properties can be considered a valid approximation for this type of ductile material, as it was done on the reference study to investigate the energy absorption response of rectangular tubes under axial impact loading.

In a subsequent step, the boundary conditions for the problem were defined. To simulate impact loading, the 2D crash box was fully fixed on one side, while the opposite side was impacted

Table 3.1: Density and elastic properties for mild steel [56].

Density (ρ) [Ton/mm^3]	**Young's Modulus (E) [MPa]**	**Poisson's Ratio (ν)**
7.80E-09	210,000	0.3

Table 3.2: True stress-plastic strain data points to define plasticity properties of mild steel [56].

Yield Stress (σ_t) [MPa]	304.6	344.19	385.51	424.88	450.39	470.28
Plastic Strain (ε_p)	0	0.0244	0.0485	0.0951	0.1384	0.191

by the rigid body that represents the impactor. This body was constrained to advance only in the direction of axial crushing, which for this model is the X direction. Similarly, the same type of displacement restriction was set for the nodes that interface with the rigid body surface. Figure 3.2 shows the constraints applied to the intended nodes.

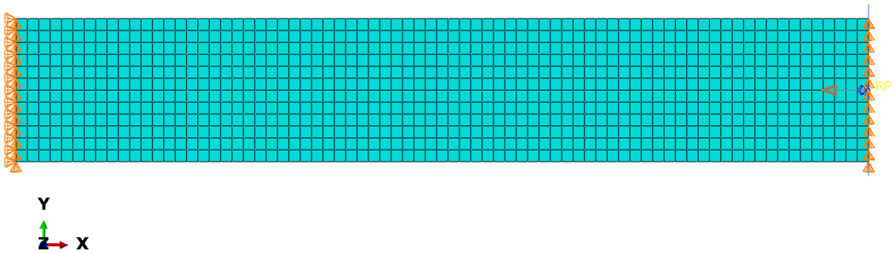

Figure 3.2: Boundary conditions applied on the 2D finite element axial crash model.

Once the individual components and their properties were established, it was possible to move forward with the assembly. During this stage, the focus was to properly define the interactions between the bodies, namely the contact non-linearities inherent in the crash event. This involved modelling the interactions between the crash box and the rigid wall to ensure realistic collision behaviour. First, a general contact formulation was utilized to account for the self-contact of the crash box part. This formulation is well-suited for capturing the effects of large and rapid deformations that commonly occur in crash analyses. Additionally, a surface-to-surface contact was established between the rigid body and the contacting nodes located at the right-hand end of the crash box. The above contact properties were defined using a friction coefficient of 0.2 and penalty friction formulation.

This dissertation work follows an explicit approach to the formulation of the crash simulation. As such, the model is defined with an according step procedure of the dynamic, explicit type with a time step t = 0.02 s. The crash box length and the speed of the impactor were used as the parameters to calculate the time step necessary to consider the crash simulation completed. After the simulation is submitted this assumption can be verified, by certifying that the impactor reaches a null velocity within the time given for the simulation.

Before submitting the simulation to run, it was necessary to mesh the part. Among the available element types for the solid section defined, plane stress elements of the type CPS4R were selected for the mesh. These elements are interpreted as quadrilateral, bilinear elements with reduced integration and hourglass control [57]. The part was seeded with a size of 4 mm, thus resulting in a total number of 988 nodes and 900 elements for a first iteration.

Table 3.3 constitutes a summary of the most important dimensions generated for the 2D axial crash simulation.

Table 3.3: Summary of the finite element model for the 2D crash simulation.

Nodes	Solid Elements	Parts	Contacts	Boundary Conditions
988	900	2	2	3

3.1.2 2D Model Validation

In order to validate the constructed two-dimensional model, the conditions applied in [56] were replicated to the possible extent, considering that the authors validated the performance of a 3D crash box. The intention is to see if the results obtained with the presented numerical model are a good fit with those obtained in [56] that will be taken as reference values. The force-displacement curve obtained from the reference study is shown in Figure 3.3a, while the corresponding curve for the 2D model is plotted in Figure 3.3b.

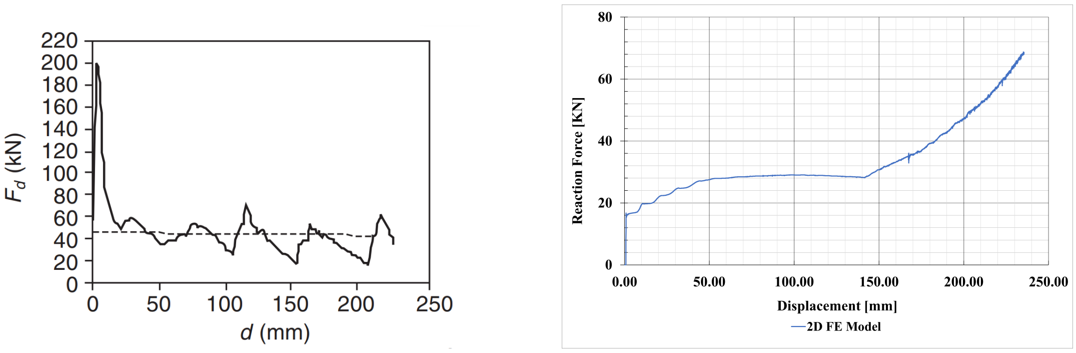

(a) From reference study [56].

(b) From defined 2D model.

Figure 3.3: Force-Displacement curves.

Using a data acquisition algorithm, the approximate points of the reference curve were obtained, allowing for a more detailed comparison with the curve obtained from the simulation using the 2D model, both curves are plotted on the same graph that is shown in Figure 3.4. The plotted data represents the displacement of the impactor's reference point and the cumulative effect of the reaction forces experienced by the fixed nodes, both in the axial direction. Despite the fact that the curve corresponding to the 2D model displays a different behaviour, its results are on the same order of magnitude. So, it can be argued that the definition of the model was correctly done, considering the fact that the values taken as reference come from a model with higher dimensionality.

In a subsequent chapter, a three-dimensional implementation will be studied with a finite element model that can better replicate the conditions of the studies found in literature. It is expected that the results obtained for that case constitute a better approximation.

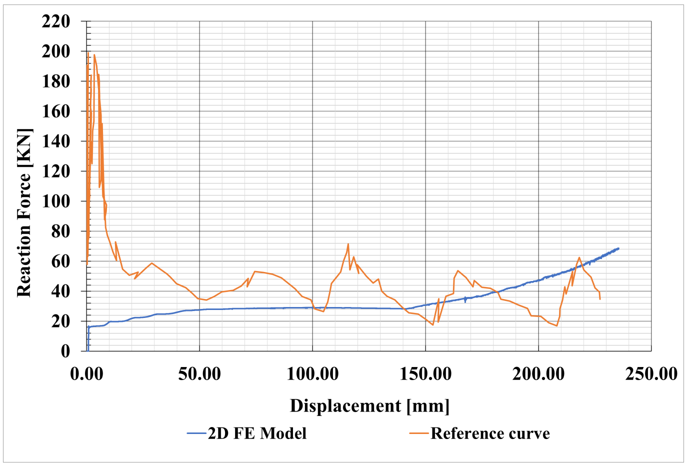

Figure 3.4: Comparison of the Force-Displacement curves for 2D model validation.

After having validated the model, the boundary conditions were adapted, since those applied in the reference study resulted in excessive deformation in the two-dimensional model. This high level of deformation adds complexity to the already unstable nature of the non-linear optimisation procedure to be performed next. This is undesirable and justifies the adjustment. Table 3.4 offers a comparison between the parameters introduced in the two-dimensional model with those from the model that served of reference.

Table 3.4: Parameter comparison between reference and applied 3D finite element model.

	Impactor	
	Mass [kg]	**Velocity [m/s]**
Reference Model	90	15
Applied Model	100	5

The time step for the dynamic simulation was adapted accordingly to account for the reduction in the velocity of the impactor. Most specifically, it had to be increased to t = 0.035 s to ensure that the impactor stops.

Running the explicit simulation for the selected model parameters, the first set of results for the 2D axial crushing simulation were obtained. Figure 3.5 shows the displacement contour in the design domain generated by the impact of the rigid body. In this step, it is important to generate the input file which stores all the necessary information about the model. This file will be read and modified by the Matlab program as part of the optimisation procedure.

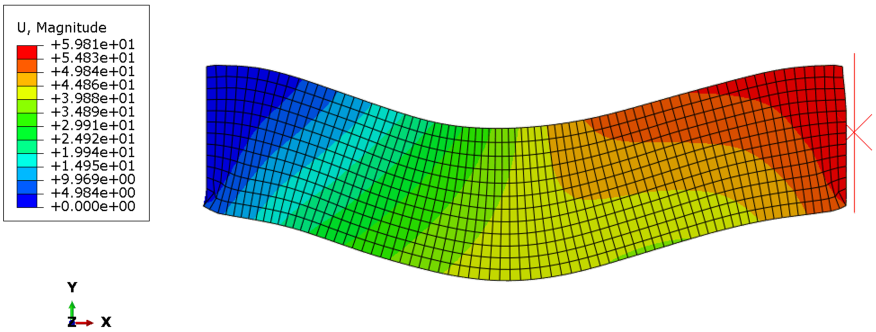

Figure 3.5: Displacement results, in mm, obtained in the direction of axial crushing.

3.2 ABAQUS-MATLAB Interface

The finite element model described in the previous section constitutes the design domain on which the optimisation algorithms will be applied. The algorithms of the various methods being studied in this work are embedded into Matlab where the optimisation takes place. In combination, the capabilities of Abaqus are utilized for conducting explicit dynamic crash simulations. If so, there is a need to link both programs, as the optimisation in MATLAB relies on information extracted from the Abaqus crash simulation. This section presents the fundamentals of the interface that enables the fulfilment of this requirement.

There has been work done in the past where ABAQUS was linked with MATLAB for structural optimisation purposes. However, prior to the development of these methods, topology optimisation was primarily conducted using Matlab codes. In fact, many freely available codes have been developed and made accessible to the public over the years [58].

As a matter of example, Sigmund was among the first researchers to propose a Matlab implementation of a topology optimisation code in [59]. The author proposed a 99-line code devised for the specific case of compliance minimization of statically loaded structures. The code incorporated an optimiser based on the optimality criteria method, a mesh-independency filter, and a subroutine for the finite element analysis. As an extension to the code, the author highlighted the possibility of replacing the default optimiser with an MMA optimiser, enabling the solution of problems with multiple constraints.

The code was intended for educational purposes and it is of public domain. In fact, the original code was extended by Andreassen et al. in [60], maintaining the same objectives but adding a density filter while reducing the length of the code to only 88 lines. According to the authors, the 88-line code is more efficient than its predecessor, being two orders of magnitude faster when compared on the same benchmark problem.

Lastly, Liu and Tovar [61] contributed by presenting a 169-line program, referred to as *top3d*. It incorporates efficient strategies for three-dimensional topology optimisation and its scope was extended to other problems, besides minimum compliance, by employing three gradient-based optimisation algorithms, namely, MMA, OC and SQP (Sequential Quadratic Programming). Although this implementation is restricted to linear topology optimisation problems with a linear constraint, it offers valuable insights into the analytical and numerical challenges associated with addressing three-dimensional structural topology optimisation problems.

In recent years, the appearance of software architecture that facilitates the integration between Abaqus and Matlab became widespread. In 2016, a group of researchers developed an interface called *Abaqus2Matlab*, connecting these two widely used packages in finite element modelling and mathematical analysis. The details and functionalities of this interface are described in [58], along with several engineering examples that demonstrate its capabilities and relevance. Its main advantage is the overall benefit obtained from combining the capabilities of both software tools. It enables the direct execution of Abaqus simulations from within Matlab and facilitates post-processing of the results, effectively bridging the gap between these two powerful tools.

3.2.1 Application to Topology Optimisation

The previous concept of a software that links Abaqus and Matlab has been widely utilized in various applications. In spite of that, the initial tools developed based on this link were meant mainly for finite element post-processing and were not adequate for conducting topology optimisation procedures. To effectively do so, the algorithm requires information on the neighbourhood of the elements, enabling the appropriate implementation of optimisation techniques such as the SIMP approach for material property penalization, or the hard-kill method for element elimination/reactivation.

In light of that information, some authors focused on enhancing this methodology for topology optimisation. For instance, Alen in [62] developed an interface designed for implementing BESO and HCA-based topology optimisation. Regarding the most specific case of crashworthiness optimisation, a similar approach was followed by Bahramian and Khalkhali in [53]. The authors employed a modified BESO algorithm written in Matlab and linked with Abaqus to run a nonlinear quasi-static crushing analysis and optimise a thin-walled square tube with the objective of enhancing its crashworthiness.

3.2.2 Optimisation Problem Formulation

During the theoretical review presented in Chapter 2, the general formulation for topology optimisation problems was presented. For this specific application, the optimisation problem is presented as a compliance minimization problem with a volume constraint. Additionally, the parameter used to decide which elements would be penalized or eliminated was the energy dissipated due to plastic deformation in the elements.

By minimizing the compliance, the intention is to obtain a less deformable structure which will experience smaller displacements, thus tackling the objective of minimizing intrusion in practical terms. Additionally, by targeting the elements that dissipate the least amount of energy by plastic deformation, insight is gained into the overall energy absorption capacity of the component. This way, it is intended to address two objectives that are conflictive, to derive a compliant component that has good energy absorption behaviour as well.

Data was extracted from Abaqus in order to materialize the problem formulation. The following definitions were retrieved from the Abaqus user manual [57]. *EPDDEN* was selected as the parameter for energy dissipation, specifically it represents the total energy dissipated per unit volume in the element by plastic deformation.

As for the compliance, it can be assessed in terms of the strain energy of the component. Moreover, the internal energy was considered which sums up the contribution of all forms of internal energy, the corresponding output is *ALLIE*.

Also, the volume of the elements was extracted since it is necessary for the volume constraint.

3.2.3 Interface Implementation

Similar to the research studies cited above, this dissertation work will implement an Abaqus-Matlab interface to test the reach of three topology optimisation algorithms in deriving an optimal topology, at the component level, under conditions that simulate a crash event. This section provides an overview of the features offered by the interface that are transversal to all the algorithms applied. In subsequent sections, the specific details of each algorithm will be discussed, along with the corresponding results.

- **Data acquisition and modification**

  For all techniques, the topology optimisation procedure is done iteratively. At each iteration, it is necessary to read and write optimisation data back into the Abaqus input file, which contains all the information of the CAE model. Matlab tools are used to easily read and modify the Abaqus files. This capability plays a crucial role in the interfacing approach, in fact, it is the key to operate on the material properties effectively.

  Prior to making any modifications, it is essential to read and store the model information in Matlab. This is achieved by creating a database containing all relevant information extracted from the Abaqus input file. The database encompasses information about the elements and their corresponding nodes, material properties, and boundary conditions defined, among others. During each iteration, the element database is refreshed with the updated information obtained from the crash simulation. In this phase, Abaqus generates a new input file, incorporating the modified data, which will be utilized in the subsequent iteration.

  In this approach, each element is treated as having individual material properties. This enables to target each element individually and iteratively modify its properties by readily implementing the material penalization and hard-kill methods that are the basis for the optimisation algorithms being investigated.

  A final aspect that was taken into account when working with modified input files was to ensure that the predefined structure of the file is maintained, as outlined in the Abaqus user's manual [57]. While it is possible to make changes to Abaqus files using Matlab, it is essential to adhere to the predefined structure; otherwise, the simulation will not run properly.

On a side note, the .odb file that contains the results of an Abaqus job can be read by Matlab as well, and in this implementation, it is read to extract the outputs of the simulation that are relevant to advance with the optimisation.

- **Write results of the Finite Element Analysis**

  A specific case of data acquisition is the retrieval of results from the crash simulation, which is required to obtain the necessary data for optimisation. As it was mentioned when the optimisation problem was defined, the necessary outputs include information such as internal energy, volume, and energy dissipation through plastic deformation. The desired outputs can be obtained from Abaqus by specifying them as requirements on a dedicated field output. *Python* scripts are employed to extract the values from the final simulation step and transfer them to Matlab for further analysis.

  Additionally, some History Outputs were requested for further analysis of the results. In order to access this information for each iteration, it is necessary to force Abaqus to write it by requesting it on the input file of each iteration.

- **Definition of frozen elements**

  As mentioned previously, manipulation of the material properties is important for the synthesis of the optimised structure. Still, not all elements in the design domain shall undergo changes promoted by the optimisation algorithms. The reason behind this is to maintain unchanged the group of elements affected by the boundary conditions originally defined in the CAE model. To achieve this, a group of, so-called, frozen elements is created. These elements are excluded from the optimisation process, meaning their properties remain unaltered. However, their contribution to the neighbouring elements will be accounted for, particularly when applying filtering techniques.

- **Image processing features**

  In addition to its tools for result post-processing and mathematical optimisation, Matlab also counts with image processing and integrated graph-plotting features. These tools can be exploited in the optimisation procedure to generate a visual representation of the density distribution in the design domain for each iteration of the topology optimisation loop. By utilizing these features, it is possible to visually monitor the preliminary results of the optimisation procedure, providing a graphical perspective on the progress and changes occurring in the density distribution throughout the iterations. This feature is extensively exploited in this optimisation procedure, especially when applied to the 2D model.

- **Introduction of geometric imperfection on the mesh**

Geometric imperfections were introduced in the initial mesh of the model, aiming to trigger buckling in the structure by avoiding artificial stiffness produced by a perfect geometrical pattern like the one in the initial mesh.

Modelling geometric imperfections can be done on Abaqus by exporting a mesh perturbed by the buckling modes after performing a quick buckle analysis of the model. Instead, this functionality was easily implemented in Matlab by introducing random increments on the coordinates of each node in the mesh. By doing so, a small perturbation is introduced in the original mesh, achieving the desired effect. The lines of code added in Matlab can be seen in Figure 3.6.

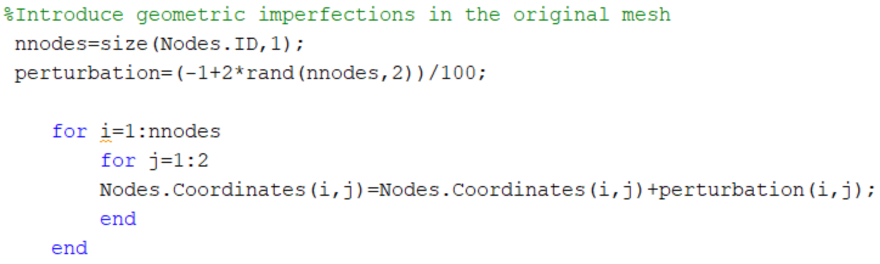

```
%Introduce geometric imperfections in the original mesh
 nnodes=size(Nodes.ID,1);
 perturbation=(-1+2*rand(nnodes,2))/100;

    for i=1:nnodes
        for j=1:2
        Nodes.Coordinates(i,j)=Nodes.Coordinates(i,j)+perturbation(i,j);
        end
    end
```

Figure 3.6: Matlab code to introduce geometric imperfections on the initial mesh.

Upon presenting the various features that can be implemented through the interface procedure, the appeal of this approach becomes evident, mainly in regard to the flexibility that this approach gives to the user. As a counterpart, approaches that use the topology optimisation environment offered by some of the commercially available finite element codes are readily implemented for users to exploit, but are much more restrictive in terms of parameter tuning. Other approaches, like those that perform the optimisation procedures exclusively within the context of a programming software, like Matlab, provide flexibility in the choice of optimisation methods. However, the user is responsible for developing the finite element analysis routine, so this flexibility comes at the expense of the robust analysis capabilities offered by commercial FEA tools.

Then, it can be said that the type of approach followed in this work constitutes a positive compromise between flexibility in the optimisation and robustness of the simulation. Allowing to define parameters for the optimisation algorithms with more freedom and, at the same time, conduct the finite element analysis with all the precision offered by the state-of-the-art programs.

Figure 3.7 shows a flowchart of the process followed by the interface on Matlab to materialize the topology optimisation procedure. The process starts with the user definition of the optimisation method and its parameters. Out of the general parameters that can be defined, it is relevant to define the target volume fraction for the final topology, as well as the maximum number of iterations for the optimisation process. Additionally, the option to apply a filter can also be activated. Inside the optimisation loop, convergence is checked and the filtering technique is applied for each iteration.

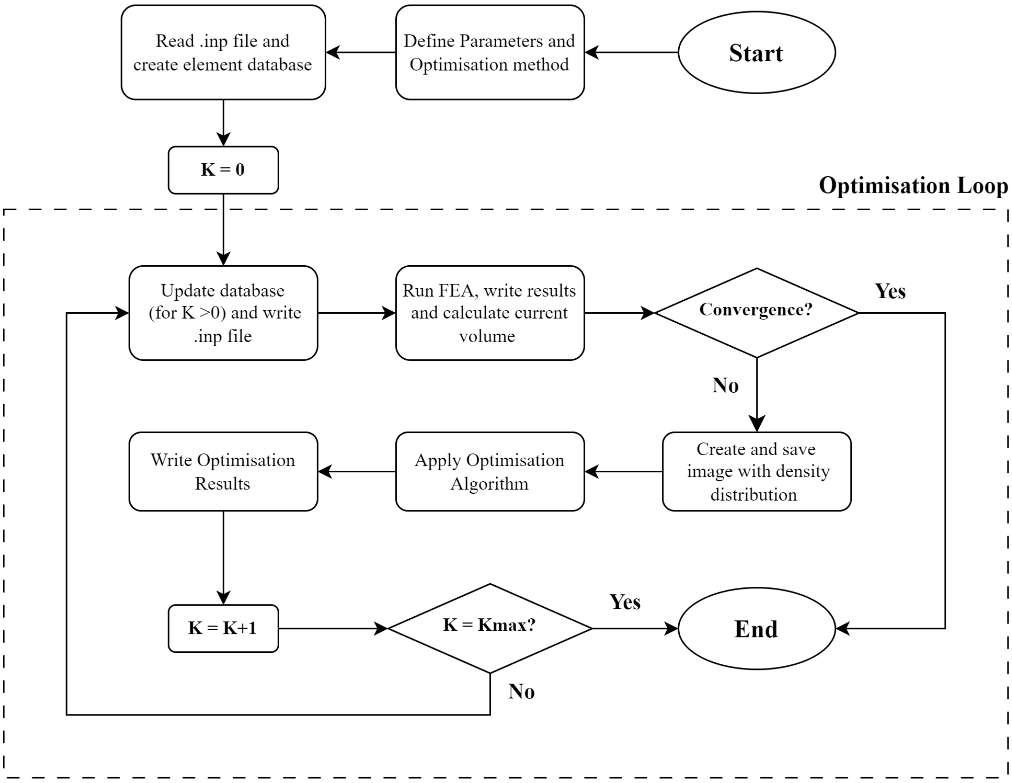
Start
Define Parameters and Optimisation method
Read .inp file and create element database
K = 0
Optimisation Loop
Update database (for K >0) and write .inp file
Run FEA, write results and calculate current volume
Convergence?
Yes
No
Create and save image with density distribution
Apply Optimisation Algorithm
Write Optimisation Results
K = K+1
K = Kmax?
Yes
No
End

Figure 3.7: Flowchart of the topology optimisation procedure on Matlab.

The filtering technique applied involves considering the weighted contribution of neighbouring elements to achieve a smoother distribution of energy results in the model. The filtering process is divided into two stages, implemented as two separate scripts in Matlab.

In the first stage, the filter is prepared by creating a list that includes information about the neighbouring nodes of each element. The neighbouring nodes are identified as those located within a specified radius measured from the element centroid. Additionally, the weighted contribution of each neighbouring node is computed based on its distance to the element centroid.

In the second stage of the filtering process, the energy absorbed by each element, obtained from the FEA results, is extrapolated to its corresponding nodes. By doing this, an energy value is allocated to each node in the model. Subsequently, the energy values are extrapolated back to the elements, taking into account the weighted contribution of all neighbouring nodes, as determined in the first stage. This ensures that each element receives a filtered energy absorption value. The filtered energy absorption values are then stored in a vector, to be used in the remainder of the optimisation iteration. In addition to that, the optimisation process is further stabilized by using historical information. In other words, the energy values are averaged with those obtained in the previous iteration. This idea was proposed by Xie and Steven in [63].

3.3 ESO Method

Before exploring the specifics of the application of each studied method, it is relevant to highlight some final details about the crash model that serves as the basis for the optimisation procedure. For the two-dimensional model, the optimisation will be performed on two different mesh discretizations, and their parameters are presented in Table 3.5.

Table 3.5: Geometric parameters of the two meshes used on the optimisation process for the 2D model (element type CPS4R).

	Element Size [mm]	**Nº of Elements**	**Nº of Nodes**
Mesh 1	4	900	988
Mesh 2	2.5	2400	2541

Additionally, to verify if the Abaqus-Matlab interface is properly storing the input data, a visual comparison of the results for the first iteration (referred to as iteration zero) can be conducted. Figure 3.8a shows the Von Mises stress distribution obtained when submitting the 2D model for simulation. In turn, Figure 3.8b depicts the same result but for the input file generated by Matlab on iteration zero. A difference that can be commented is that the output produced by Matlab exhibits slightly less smooth contours compared to the original simulation. However, it accurately captures the dynamic behaviour of the initial simulation, suggesting that the process of extracting and modifying Abaqus data was executed correctly, providing confidence to proceed with the iterations.

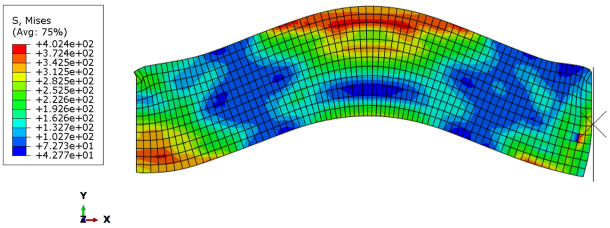

(a) From original job submitted on Abaqus

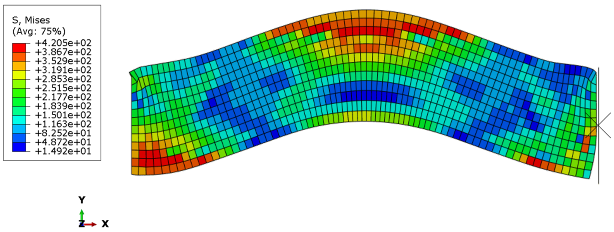

(b) From .inp file generated on Matlab for iteration zero

Figure 3.8: Von Mises Stress distribution, in MPa, obtained after running the 2D model.

3.3.1 ESO Algorithm definition

The first algorithm to be defined is the evolutionary method based on energy. Besides the general parameters that need to be specified for all algorithms, the ESO method requires the definition of the element rejection ratio (RR). This parameter was set to a default value of $RR = 0.01$ and it is used to compute the number of elements to be removed by the algorithm at each iteration. Specifically, the parameter gives the number of rejected elements as a ratio of the total volume of the structure. For the chosen rejection ratio, 1% of the volume of the structure is removed at each iteration, by setting a higher value, more elements are removed from the component.

The ESO algorithm is relatively straightforward to apply. It involves determining the number of elements to be deleted per iteration and then targeting those with the lowest energy absorption value. The algorithm ranks the elements according to their energy absorption values, from lowest to highest, and proceeds to eliminate the number of elements as calculated according to the rejection ratio. The deletion of the elements is based on the elemental density and is accomplished with a *for loop* in Matlab. This portion of the code can be seen in Figure 3.9.

The elements that are meant to be removed according to the ESO algorithm have their density updated to a "void density" value, set to $1.0e-4$. This effectively converts the solid elements into void elements. It can be noted that only active elements can be deleted, respecting the frozen element set. For the next iteration, the elements that have void density are excluded from the finite element model and simulation by not being written to the .inp file. The cycle of element deletion continues until the desired number of elements to be eliminated is reached.

It is also relevant to point out that it was decided not to apply filtering techniques to the implementation of this algorithm, but to do it only for the bi-directional method to be analysed subsequently. The intention was to define two distinct methodologies for the comparison of both evolutionary approaches. In any case, the implications of this decision on the optimisation process will be discussed upon the analysis of the results for the ESO algorithm.

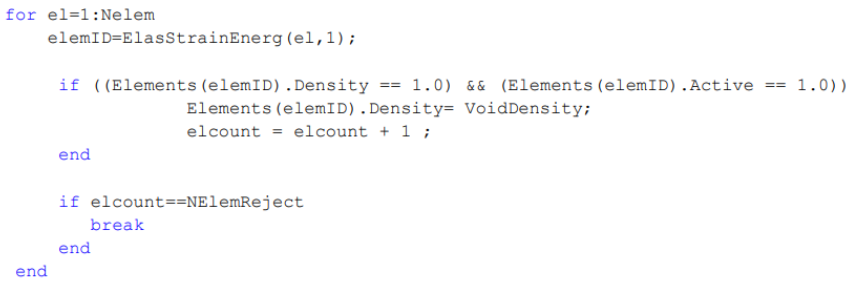

```
for el=1:Nelem
    elemID=ElasStrainEnerg(el,1);

     if ((Elements(elemID).Density == 1.0) && (Elements(elemID).Active == 1.0))
                 Elements(elemID).Density= VoidDensity;
                 elcount = elcount + 1 ;
     end

     if elcount==NElemReject
        break
     end
 end
```

Figure 3.9: Element deletion with the ESO algorithm.

3.3.2 ESO Optimisation Results

Before presenting the optimisation results for this first method, a final verification will be performed, to guarantee that the algorithm is targeting the correct elements. The contour tool on the visualization environment of Abaqus allows to limit the areas shown on the plot according to a user-defined maximum or minimum value. This tool can be exploited to highlight the areas with the least amount of dissipated energy by plastic deformation, and subsequently get an idea of the elements that the optimisation process should target on the next iteration.

This procedure can be seen in Figure 3.10. On the left (Figure 3.10a), the contour plot obtained from iteration zero can be seen. On it, the elements inside the areas in black are among the ones with the lowest value of energy absorption. On the right (Figure 3.10b), the optimisation results for the subsequent iteration can be seen. According to what was desired, the deleted elements belonged to areas highlighted before. This type of inspection will be replicated for the remaining methods as well.

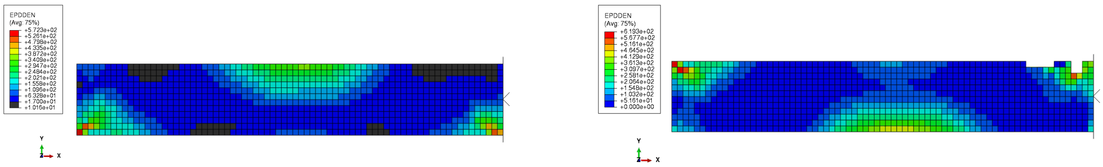

(a) Highlighted areas with the lowest value of energy absorption (Iteration zero).

(b) Deleted elements on the first iteration.

Figure 3.10: Verification of the ESO algorithm for the first iterations of the 2D model.

Starting the analysis of the optimisation results with the evolution of the constraint and objective function of the optimisation problem that can be seen in Figures 3.11a and 3.11b, respectively. It can be seen that the ESO algorithm was able to derive, with some minor oscillation of the objective function, a geometry with half the material and lower compliance. Regarding the influence of the mesh refinement in the results, the method converged in both cases, at iteration 48 for mesh 1 and only necessitating an extra iteration for the finer mesh.

As for the geometry of the synthesized topology, it is presented in Figure 3.12a for mesh 1, and in Figure 3.12b for mesh 2. Most specifically, these figures show the density distribution throughout the design domain obtained with the image processing capabilities of Matlab. The "surviving" elements are those that can be seen in black.

Upon comparing the geometries obtained with the finer and coarser meshes, the geometry generated with the finer mesh exhibits greater geometric intricacy, potentially suggesting a variation in the results due to mesh dependency. Also, the effect of checkerboards is more prominent. However, it is worth noting that the removal of material appears to occur in similar regions, but in different elements, which can be attributed to the finer discretization. All in all, this result was expected since no filtering techniques were applied to the implementation of the ESO algorithm. Consequently, the method became susceptible to numerical instabilities.

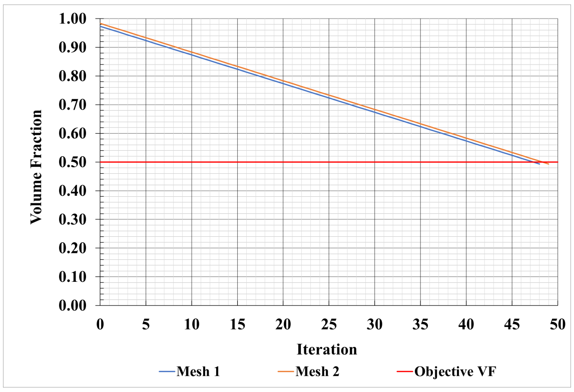

(a) Constraint

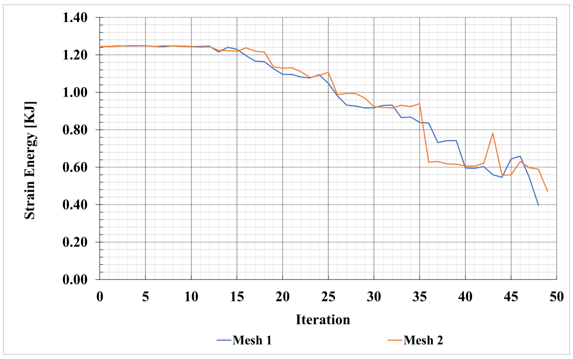

(b) Objective Function

Figure 3.11: Evolution of the optimisation problem for the ESO method applied to the 2D model.

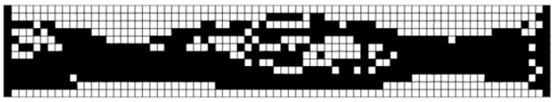

(a) Mesh 1

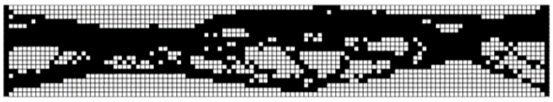

(b) Mesh 2

Figure 3.12: Resultant 2D Topologies obtained with the ESO method for a volume fraction of 50%.

3.4 BESO Method

In Chapter 2, the bi-directional evolutionary structural optimisation (BESO) method was briefly introduced, which not only allows for the deletion of poorly performing elements but also provides the option to reactivate elements if necessary. For this implementation, filtering techniques are applied to address the numerical instabilities that affected the optimisation results obtained with the ESO method.

3.4.1 BESO Algorithm definition

In order to materialize the bi-directional behaviour of the BESO algorithm, an additional parameter called the addition ratio (AR) is introduced alongside the rejection ratio (RR). The functioning of the addition ratio is analogue to that of the rejection ratio as explained for the ESO method, and it is used to calculate the number of elements to be added to the design domain. In this application, the chosen values are $RR = 0.02$ and $AR = 0.01$. As presented by Huang and Xie in [47], a criterion based on the variation of the objective function is used for checking the convergence of the optimisation process with the BESO method.

The implementation of the BESO algorithm begins by sorting the elements in descending order based on their energy absorption results. This ranking is the opposite of what was done in the ESO method. Next, the target volume is determined, which represents the desired volume of the structure after the topology optimisation process. This target volume is calculated by multiplying the design volume by the specified volume fraction.

The target volume is a constant of the optimisation process. However, at each iteration, the expected volume change is calculated according to the element rejection ratio previously defined. Depending on the current volume of the structure, which is updated at each iteration, the volume change can be either added or subtracted. If the current volume exceeds the target volume, which is the case for most iterations, material will be removed. Otherwise, elements will be reactivated and material will be added to increase the volume.

Independently, the process of eliminating and reactivating elements in the BESO algorithm can be performed simultaneously at any iteration. This is achieved by sorting the elements in descending order based on their energy absorption values. Then a reverse search is performed, starting from the elements with the highest energy absorption. During the search, the algorithm keeps the best-performing elements and adds their volume contribution until the target volume defined for the iteration is reached. If any elements with void density are encountered during the search, these will be activated as long as the addition ratio defined is not surpassed. Once the target volume is reached, the remaining elements coincide with those with the lowest energy absorption. These elements contribute the least to the overall energy absorption capacity of the structure and are effectively eliminated.

3.4.2 BESO Optimisation Results

Beginning with the verification of the first optimisation iteration, the contour tool of Abaqus is used once again and the comparison is presented in Figure 3.13. Already a difference between the evolutionary methods becomes noticeable from these images. It is possible to note that the BESO method eliminates more material, at least for the first iteration. This observation aligns with the expectation since a higher rejection ratio was defined among the parameters of the BESO algorithm. This choice is reasonable considering there is also element reactivation materialized with the addition ratio.

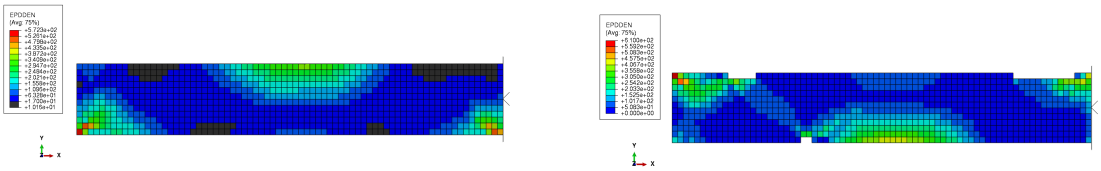
EPDDEN
(Avg: 75%)
+5.723e+02
+5.261e+02
+4.798e+02
+4.335e+02
+3.872e+02
+3.409e+02
+2.947e+02
+2.484e+02
+2.021e+02
+1.558e+02
+1.096e+02
+6.328e+01
+1.700e+01
+1.016e+01
Y
Z
X
EPDDEN
(Avg: 75%)
+6.100e+02
+5.592e+02
+5.083e+02
+4.575e+02
+4.067e+02
+3.558e+02
+3.050e+02
+2.542e+02
+2.033e+02
+1.525e+02
+1.017e+02
+5.083e+01
+0.000e+00
Y
Z
X

(a) Highlighted areas with the lowest value of energy absorption (Iteration zero).

(b) Deleted elements on the first iteration.

Figure 3.13: Verification of the BESO algorithm for the first iterations.

Another difference between these first two methods is that the BESO algorithm continues to iterate despite having achieved the desired volume fraction. In fact, it does so until reaching the maximum number of iterations defined by the user, which for this work was set to 200. These details can be seen in Figure 3.14 which contains the graphs with the evolution of the constraint and objective function of the optimisation problem.

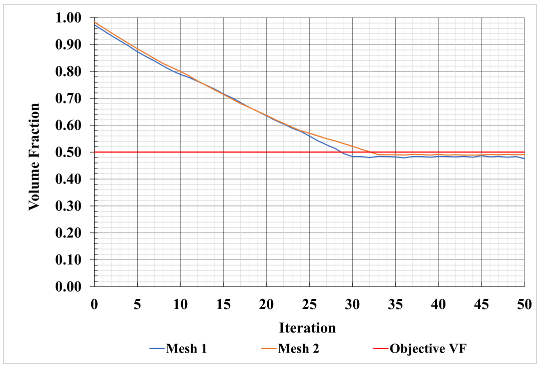

(a) Constraint

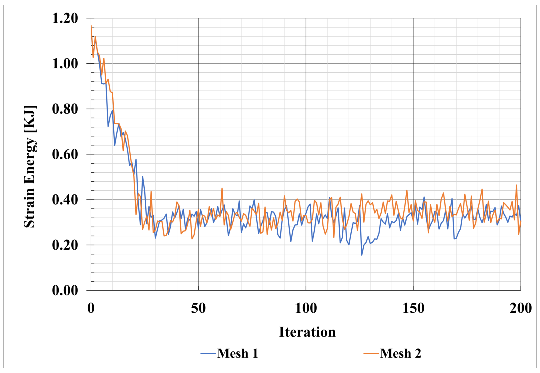

(b) Objective Function

Figure 3.14: Evolution of the optimisation problem for the BESO method applied to the 2D model.

The next set of figures displays the topologies obtained for mesh 1 (Figure 3.15) and mesh 2 (Figure 3.16). They intend to highlight the geometrical differences between the initial satisfaction of the volume constraint and the final iteration. It can be seen that the contour for the final iteration is noticeably better defined, particularly for mesh 2, exhibiting a smooth geometry with all elements adequately connected. However, analysing the area near the frozen elements, despite these elements remaining unaffected, it can be observed that their connection to the rest of the structure appears unconventional.

All in all, the fact that the algorithm continues to iterate can be regarded as positive. By doing so, the objective function continues to be minimized, resulting on a further optimised topology. All this was possible by activating and deactivating different elements, leading to diverse outcomes while maintaining the volume constraint close to the desired value. It should be noted that this capability was not feasible with the ESO method.

A relevant comment can be made in regard to the effect of setting an arbitrary limit for the number of iterations in the optimisation process. By doing so, it is not guaranteed that an optimal solution is reached for the final iteration defined since the convergence of the objective function might not be verified. Still, the intention of these preliminary approaches is to evaluate the performance of the selected algorithms for the crashworthiness conditions that are relevant to the application under study. By limiting the number of iterations, it is possible to gain insight into the performance of each algorithm without having to compromise to higher computational costs resulting from further iterations.

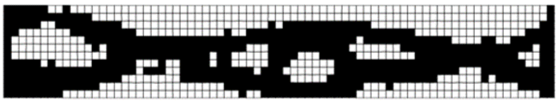

(a) Iteration 29

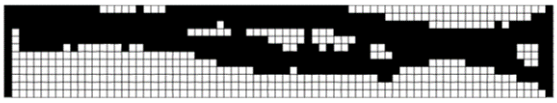

(b) Iteration 200

Figure 3.15: Resultant Topologies obtained with the BESO method for a volume fraction of 50% (Mesh 1).

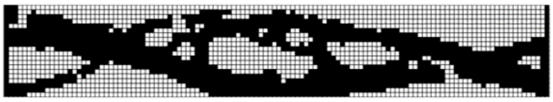

(a) Iteration 34

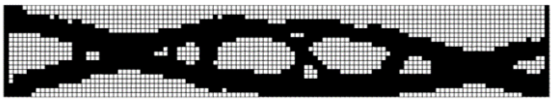

(b) Iteration 200

Figure 3.16: Resultant Topologies obtained with the BESO method for a volume fraction of 50% (Mesh 2).

One final comment that can be given regards the significant impact that the filtering of the energy values has on the resultant topologies, particularly in mitigating the presence of checkerboard patterns. Indeed the obtained geometries exhibited a much smoother appearance compared to those obtained with the ESO method.

3.5 Optimality Criteria Method

In contrast to the evolutionary methods presented thus far, the Optimality Criteria (OC) method uses continuous design variables. If so, the implementation of this method requires different features that are presented in this section. Despite the differences, a common detail is that the filtering techniques as defined above are also applied in this case.

3.5.1 Optimality Criteria Algorithm definition

For the implementation of the OC method, the Solid Isotropic Material with Penalization (SIMP) model is used for material parametrization, specifically for dealing with the intermediate material properties resulting from the continuous design variables used.

The key parameter to be defined for the SIMP model is the penalization factor, initially set to $p = 3$. However, among the possible features within the Matlab implementation is the option to incorporate an exponent update strategy, which can be enabled or disabled as desired.

This strategy consists in gradually increasing the penalization exponent between an initial and final iteration until reaching a maximum value. To implement this strategy, the above parameters must be defined by the user. The Matlab code portion that enables the exponent update strategy is illustrated in Figure 3.17. The intention behind updating the exponent to higher values is that of driving the optimisation results towards black-and-white configurations.

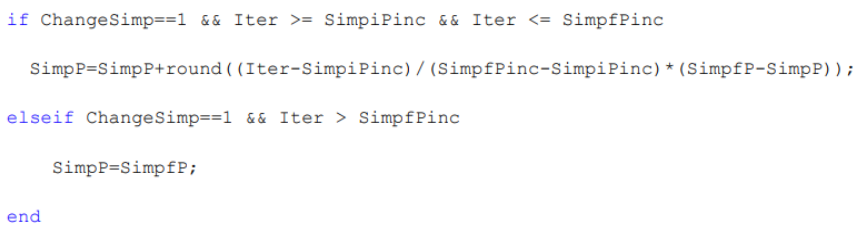

```
if ChangeSimp==1 && Iter >= SimpiPinc && Iter <= SimpfPinc

  SimpP=SimpP+round((Iter-SimpiPinc)/(SimpfPinc-SimpiPinc)*(SimpfP-SimpP));

elseif ChangeSimp==1 && Iter > SimpfPinc

    SimpP=SimpfP;

end
```

Figure 3.17: Exponent update strategy implemented in Matlab.

As stated before, the SIMP method is based on penalizing the material properties through the use of the design variables and the penalization factor. For each element, the design variable represents the elemental density and its value is updated at each iteration by considering the energy distribution within the elements and a Lagrange multiplier, denoted as λ, that is related to the volume constraint. Part of the algorithm process consists in finding the value of λ. This is done through a rough bracketing of its value and a subsequent dichotomy process until the correct density value that satisfies the volume constraint is obtained [64]. After having the updated values of the elemental densities, the material properties are penalized and the topology optimisation problem is solved.

The outputs of the optimisation process with the Optimality Criteria method are presented next.

3.5.2 Optimality Criteria Optimisation Results

The results obtained by means of the Optimality Criteria method were significantly different than those presented previously for the evolutionary methods. This distinction arises from the nature of the OC method, which is a continuous approach. Consequently, the density distribution obtained with the optimisation process exhibits more grey areas, indicating a different pattern compared to the previous methods.

The SIMP model used for material parametrization allows for a wider range of tunable parameters. In the first run, the method was applied to the model with coarser mesh, the volume fraction was set to 50% and the SIMP parameters were kept at their default values. The obtained geometries from this run can be seen in Figure 3.18.

During the first iterations, the algorithm is able to derive a relatively well-defined contour, up until iteration 30. However, after this point, the evolution of the contour becomes less noticeable. In fact, the density distribution in the final iteration (Iteration 200) closely resembles the one obtained in Iteration 30.

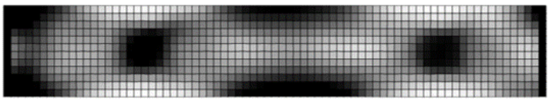

(a) Iteration 15

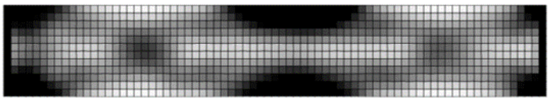

(b) Iteration 30

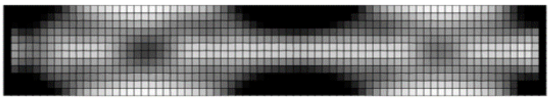

(c) Iteration 200

Figure 3.18: Resultant Topologies obtained with the OC method (First run).

Even though the final iteration of the OC algorithm does not yield a well-defined contour, it still provides a good indication of how the optimised geometry would be by following this approach.

As it was done for the previous methods, the results can be visually verified by highlighting the areas with lower energy absorption using the contour tool of Abaqus (Figure 3.19). In this case, the technique was applied to the .odb file of iteration 29 so the results obtained at iteration 30 could be verified. Indeed, it can be seen that the contour obtained aligns with what was expected, as the algorithm allocates material outside of the black areas as much as possible.

Another notable observation is that the results obtained with the OC method exhibit a distinctive symmetry, which was not observed in the results obtained from the evolutionary methods.

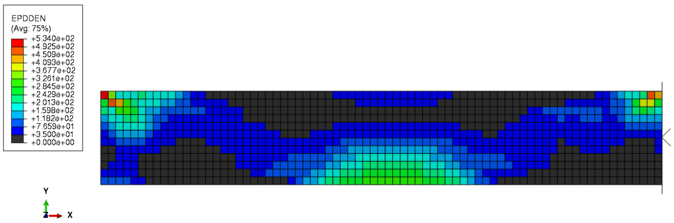

Figure 3.19: Areas with lower energy absorption, highlighted in black, for iteration 29.

To try and improve the results obtained, the parameters of the optimisation process can be adjusted. Most specifically, it was decided to rerun the simulation for the same mesh, but setting the desired final volume fraction to 70%. The rationale behind this adjustment was to retain more material, with the intention of obtaining a better-defined contour.

In addition to that, another modification was made by activating the change of exponent feature of the SIMP model. The idea behind this adjustment was to increase the penalization factor with the goal of driving the geometry towards a black-and-white configuration and, thus, a better-defined contour. The penalization exponent was initially set to $p = 3$ and was incremented up to the maximum value of 6 over a defined period of iterations.

Figure 3.20 depicts the results for the new run. Indeed the adjustment in the parameters led to a more defined contour, until the simulation in Abaqus started to encounter convergence problems due to excessive deformation in some elements, causing the analysis to abort. The Abaqus job corresponding to iteration 68 that generated the geometry in Figure 3.20a was the last one to complete successfully. Afterwards, the algorithm continued to iterate and produce unsatisfactory results, like the one in Figure 3.20b.

The deformation errors encountered are primarily caused by elements that have an extremely low elastic modulus value, which is a consequence of the penalization applied by the SIMP material model. While the algorithm attempts to address this issue by increasing the stiffness of the problematic elements, it remains a recurring problem that ultimately leads to the termination of the Abaqus analysis.

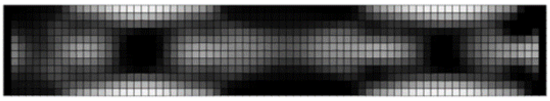

(a) Iteration 68

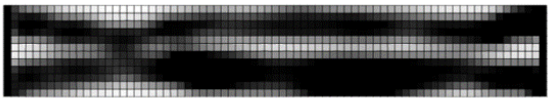

(b) Iteration 178

Figure 3.20: Resultant Topologies obtained with the OC method (Second run).

The overall instability in the optimisation procedure when applying the SIMP method is reflected in the evolution of the objective function, as depicted in Figure 3.21. Considering these results, it was decided not to proceed with the application of this method on a finer mesh.

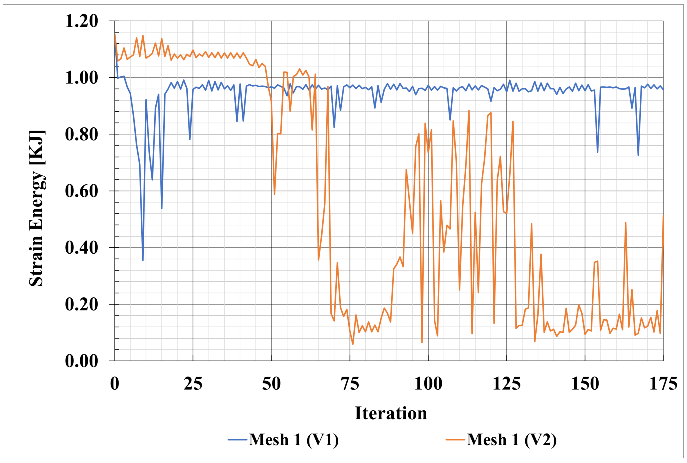

Figure 3.21: Evolution of the objective function for the OC method applied to the 2D model.

3.6 Discussion of the applied methods

After having explained the implementation of the algorithms and presented the results obtained with the topology optimisation procedure applied to the two-dimensional crash simulation, a brief discussion to determine the best-performing methods for this particular application is in order.

By comparing the evolutionary methods first, it is evident that the BESO method represents an improvement over ESO. Indeed, the topologies derived with the first method exhibit better-defined contours and are less susceptible to numerical instabilities, specially checkerboards, owed to the application of filtering techniques. However, the real advantage lies in the bi-directional nature of the BESO method, which enables continued refining of the optimisation results. This is in contrast to ESO, which considers the optimisation complete once the volume constraint is satisfied.

Another evident conclusion that can be discussed from the results, is that both evolutionary methods outperformed the Optimality Criteria method in terms of achieving better topologies. One of the main issues that affected the implementation of the OC method was the convergence problems verified, mainly due to the Abaqus simulation aborting as a result of excessive deformation in certain elements.

The elements that were penalized with low elastic modulus values by the SIMP material model were precisely the ones that experienced excessive deformation. This behaviour is expected for those material properties, especially on a crash simulation that is already characterized by its non-linearities and large deformations. On the other hand, these issues were not encountered for the implementation of evolutionary methods, since low-performing elements are eliminated from the numerical simulation with these approaches.

To try and bypass the convergence problems in the OC method, a similar approach as in the evolutionary methods could have been devised. This could involve, for example, the definition of a minimum value for the material properties, specifically the elastic modulus, to avoid the large deformation in the elements that lead to the termination of the numerical simulation.

Considering the unsatisfactory results obtained in this two-dimensional application, the Optimality Criteria method will not be further studied on a more complicated model. Rather it was opted to continue with the implementation of the evolutionary methods considering the geometries obtained and their computational effectiveness which is an advantage for this crashworthiness application.

In any case, having studied a continuous method added comparison value to the discussion and could be an approach to consider if the numerical problems found are eventually bypassed.

Chapter 4

3D Application

After successfully applying the interface approach to a two-dimensional model in Chapter 3 and determining the most effective methods, it was decided to move forward with the implementation of the optimisation process on a three-dimensional model. The first step for this implementation was to adapt the Matlab code for the purpose since it was initially built to be applied to 2D problems.

Minor adjustments were made to the code to account for the increased dimensionality of the problem. The Matlab scripts responsible for reading and writing data into the Abaqus input file were updated to handle data acquisition and modification for three-dimensional models. As a result, the database created by Matlab was able to correctly store information for elements with corresponding nodes containing three coordinates instead of two.

This was a straightforward process, however, the generation of images with the density distribution for each iteration was not included in the three-dimensional implementation. This feature proved to be convenient in the 2D application due to the possibility of readily monitoring the optimisation results. However, this constitutes no problem moving forward, since the results can be visualized directly in Abaqus by opening the .odb file for the desired iteration. By doing so, a broader range of results is accessible in the visualization environment, and the dynamics of the optimised geometry during the numerical impactor strike can be analysed as well. Still, it is worth noting that the image processing feature could also be implemented for 3D problems with appropriate modifications to the dedicated Matlab scripts. While it was not included in this particular implementation, the author acknowledges the potential for extending this functionality to three-dimensional scenarios.

This chapter starts with the introduction of the 3D finite element model to simulate the conditions of axial impact for the thin-walled component. Subsequently, the obtained results with the evolutionary methods are presented and discussed.

4.1 3D Finite Element Model

Having a 3D model as the subsequent step for this research was the logical choice since it can better capture the dynamics of a crash event simulated by an axial crushing test. In addition to that, working with a 3D model means walking towards a high-fidelity model of the crash box component to be incorporated into the coach structure, which is the goal of the research.

4.1.1 3D Model Definition

For the three-dimensional model, once again the conditions applied by Nagel and Thambiratnam in [56] were taken as reference. This includes the geometry, boundary conditions and contact interactions. Starting with the part module, the crash box part was created as a 3D deformable shell with a section of 100x50 mm, a length of 300 mm, and a wall thickness of 1.5 mm. The selected material was a mild steel, with the properties as defined in Chapter 3. Analogically to the 2D model, the impactor is defined as an analytical rigid body with mass M = 90 kg and speed V= 15 m/s. Figure 4.1 shows the assemble of the three-dimensional bodies and highlights the mesh and geometrical dimensions given to the crash box.

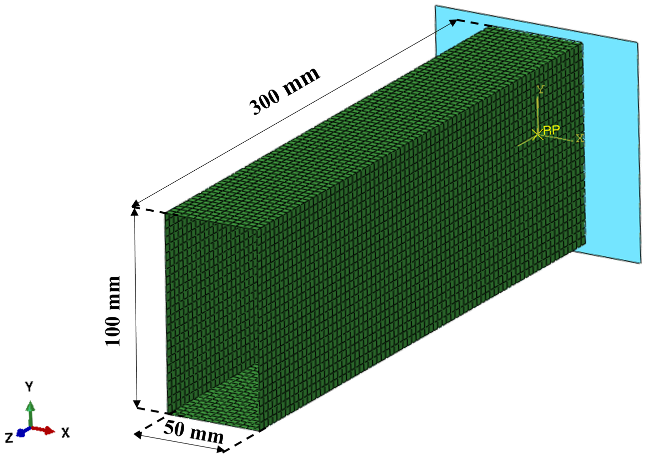

Figure 4.1: 3D finite element axial crash model.

For the three-dimensional approach, the material properties were assigned using a shell section. As such, the element type selected for meshing changed accordingly. The thin-walled component was meshed with an element size of 4 mm, which generated a mesh with 5776 nodes and 5700 linear quadrilateral elements of type S4R. These elements are quadrilateral shell elements with four nodes, suitable for large strain analyses [57].

4.1.2 3D Model Validation

After defining the model, a job was created and submitted for simulation. In this section, some simulation results will be presented in order to validate the model according to the results retrieved from the literature. The displacement field obtained from the axial impact simulation can be seen in Figure 4.2. A first comment that can be made pertains to the fact that the result reflects a proper buckling behaviour, with formation of plastic hinges, characteristic of axial crushing. This observation is a good indication that the model was properly defined and is able to capture the details of real-world conditions.

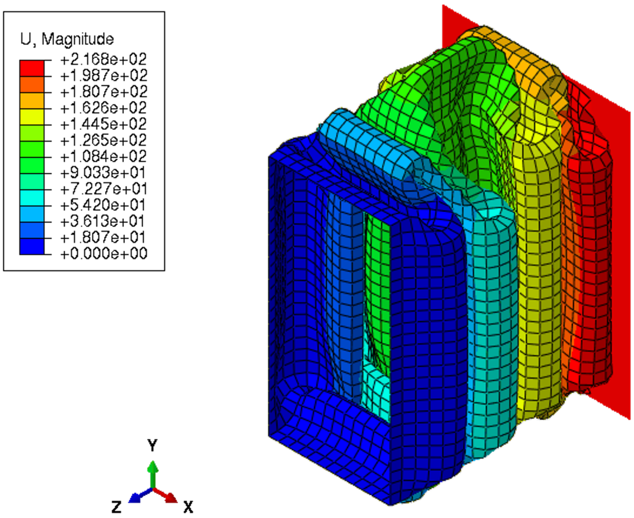
U, Magnitude
+2.168e+02
+1.987e+02
+1.807e+02
+1.626e+02
+1.445e+02
+1.265e+02
+1.084e+02
+9.033e+01
+7.227e+01
+5.420e+01
+3.613e+01
+1.807e+01
+0.000e+00
Y
Z
X

Figure 4.2: Displacement field, in mm, obtained for the 3D crash simulation.

Analogically to what was done for the two-dimensional model in Chapter 3, the 3D model will also be validated according to the reference study. Once again, the force-displacement curves for both cases are plotted and displayed in Figure 4.3. It is evident that the behaviour captured by the 3D model can be considered a good fit to the reference values. This provides a higher level of certainty to the model validation and allows to advance towards the 3D implementation of the optimisation process with confidence.

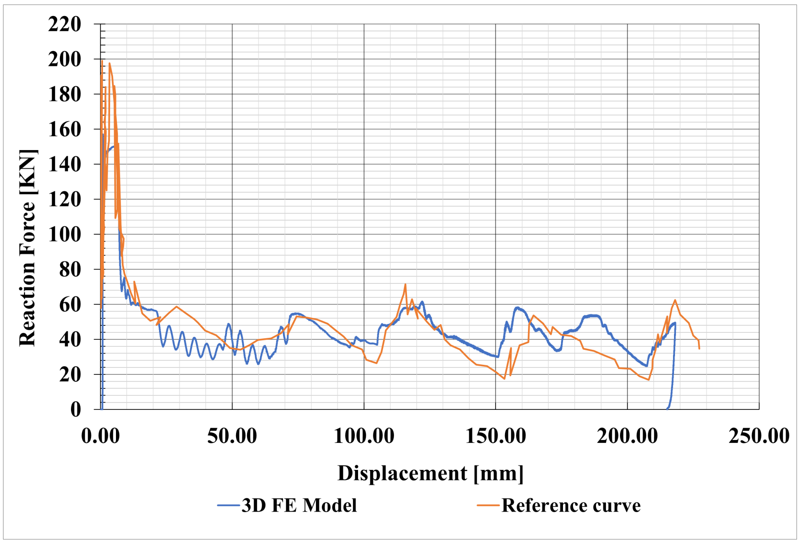

Figure 4.3: Comparison of the Force-Displacement curves for 3D model validation [56].

Before presenting the optimisation results, it is worth noting that certain modifications were made to the conditions outlined in the reference study. Specifically, the dimensions of the final model were scaled down with the intention of saving computational resources during the optimisation procedure. The resulting geometry is illustrated in Figure 4.4, and the corresponding parameters are summarized in Table 4.1.

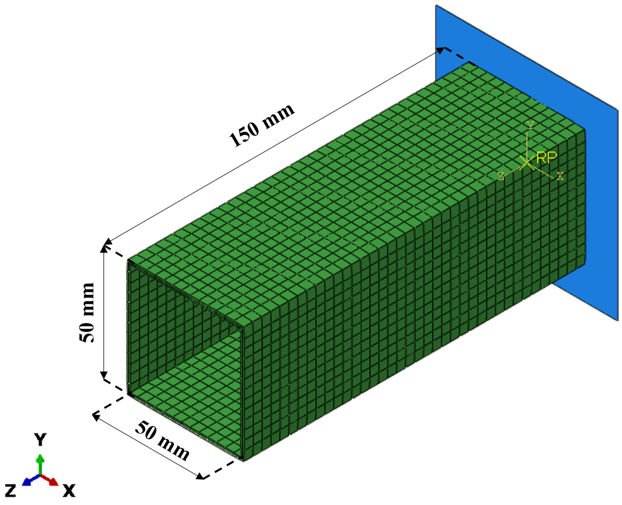

Figure 4.4: Final geometry defined for the 3D crash model.

Table 4.1: Parameter comparison between reference and applied 3D finite element model.

	Crash Box				**Impactor**	
	Length [mm]	**Width [mm]**	**Height [mm]**	**Wall Thickness [mm]**	**Mass [kg]**	**Velocity [m/s]**
Reference Model	300	50	100	1.5	90	15
Applied Model	150	50	50	2	50	15

By reducing the impactor mass while keeping the velocity constant, the amount of energy transferred to the crash box during the simulation was decreased. This effect is reflected in the results, particularly in the displacement field, where the component deformation is reduced, accordingly to the reduction in impact energy. This can be seen on Figure 4.5.

The decision to reduce the impact energy was made in anticipation of the subsequent optimisation process. As material is removed from the design domain during optimisation, higher deformations are expected. By reducing the initial energy input, the objective is to prevent the introduction of excessive deformations that could potentially impact the accuracy and convergence of the simulation.

Another aspect that had not been addressed until now is the effect of the geometric imperfections introduced on the mesh in accordance with the procedure presented in Chapter 3. The displacement contour in Figure 4.6 is retrieved from iteration zero of Matlab, where the mesh is affected by geometric imperfections. Comparing it with Figure 4.5, it is evident that the presence of imperfections triggered a different buckling behaviour on the part.

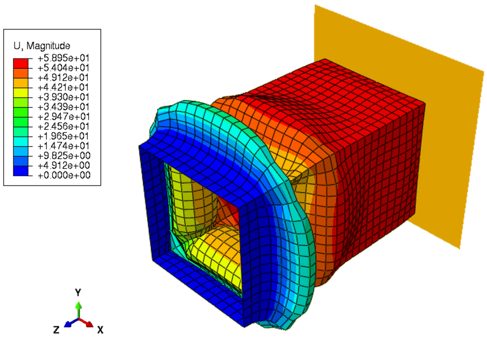
U, Magnitude
+5.895e+01
+5.404e+01
+4.912e+01
+4.421e+01
+3.930e+01
+3.439e+01
+2.947e+01
+2.456e+01
+1.965e+01
+1.474e+01
+9.825e+00
+4.912e+00
+0.000e+00
Y
Z
X

Figure 4.5: Displacement field, in mm, obtained for the 3D crash simulation with final geometry.

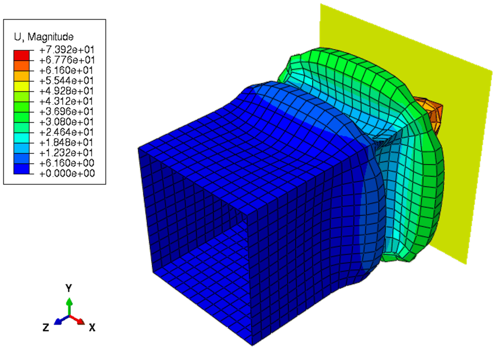
U, Magnitude
+7.392e+01
+6.776e+01
+6.160e+01
+5.544e+01
+4.928e+01
+4.312e+01
+3.696e+01
+3.080e+01
+2.464e+01
+1.848e+01
+1.232e+01
+6.160e+00
+0.000e+00
Y
Z
X

Figure 4.6: Displacement field, in mm, obtained with introduction of geometric imperfections on the mesh.

The next two figures are meant to compare the results of the simulation with the output of iteration zero from Matlab, as it was done for the two-dimensional model. As a matter of example, the Von Mises stress contour for both cases is shown in Figure 4.7, for the case without introduction of geometric imperfections. As previously concluded for the 2D application, the contour obtained on Matlab and read with Abaqus is in good agreement with the simulation results.

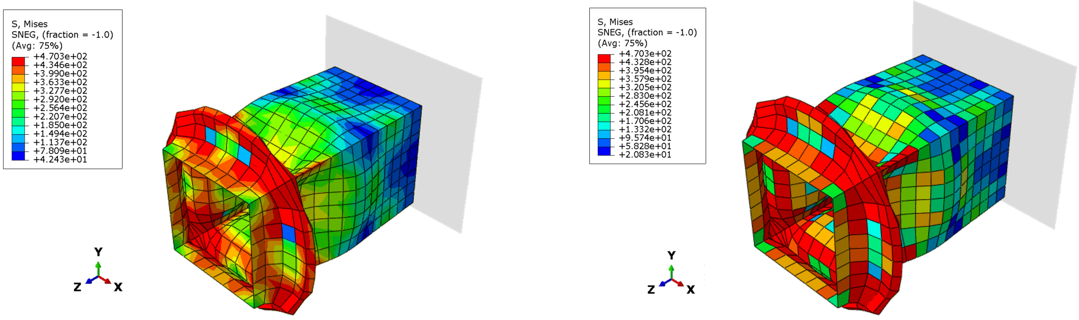
S, Mises
SNEG, (fraction = -1.0)
(Avg: 75%)
+4.703e+02
+4.346e+02
+3.990e+02
+3.633e+02
+3.277e+02
+2.920e+02
+2.564e+02
+2.207e+02
+1.850e+02
+1.494e+02
+1.137e+02
+7.809e+01
+4.243e+01
Y
Z
X
S, Mises
SNEG, (fraction = -1.0)
(Avg: 75%)
+4.703e+02
+4.328e+02
+3.954e+02
+3.579e+02
+3.205e+02
+2.830e+02
+2.456e+02
+2.081e+02
+1.706e+02
+1.332e+02
+9.574e+01
+5.828e+01
+2.083e+01
Y
Z
X

(a) From original job submitted on Abaqus

(b) From .inp file generated on Matlab for iteration zero

Figure 4.7: Von Mises Stress distribution, in MPa, obtained after running the 3D model.

The three-dimensional optimisation procedure will be carried out with the evolutionary algorithms, ESO and BESO, for three mesh discretizations that are summarized in Table 4.2.

Table 4.2: Geometric parameters of the meshes used on the optimisation process for the 3D model (element type S4R).

	Element Size [mm]	**Nº of Elements**	**Nº of Nodes**
Mesh 1	6	800	832
Mesh 2	4	1976	2028
Mesh 3	2.5	4800	4880

4.2 ESO Method

All the details of the ESO algorithm explained in Chapter 3 apply to three-dimensional implementation. As it was done in that chapter, the application of the algorithm will be quickly verified following the contour approach. Figure 4.8 shows the areas to target and, effectively, the elements removed during the first iteration belonged to them.

Moreover, it is relevant to point out that this area includes some of the frozen elements defined, specifically, those that represent the encastre constraint. Despite having a low value of energy dissipation, these elements were correctly identified and kept by the optimisation algorithm.

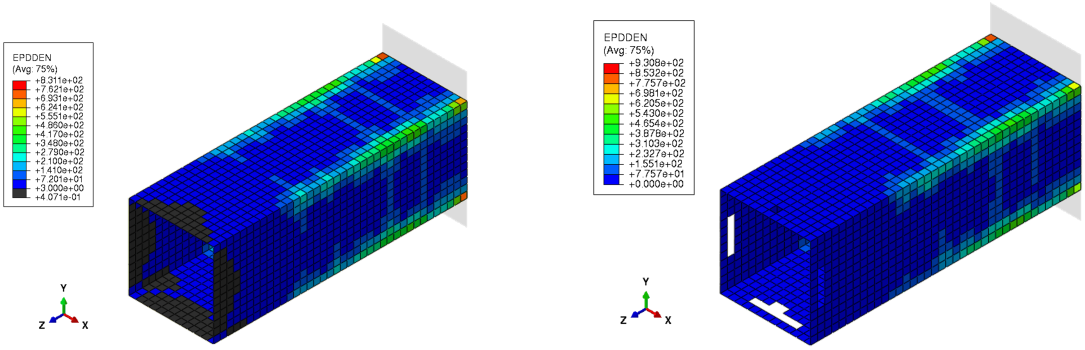
EPDDEN
(Avg: 75%)
+8.311e+02
+7.621e+02
+6.931e+02
+6.241e+02
+5.551e+02
+4.860e+02
+4.170e+02
+3.480e+02
+2.790e+02
+2.100e+02
+1.410e+02
+7.201e+01
+3.000e+00
+4.071e-01
Y
Z
X
EPDDEN
(Avg: 75%)
+9.308e+02
+8.532e+02
+7.757e+02
+6.981e+02
+6.205e+02
+5.430e+02
+4.654e+02
+3.878e+02
+3.103e+02
+2.327e+02
+1.551e+02
+7.757e+01
+0.000e+00
Y
Z
X

(a) Highlighted areas with the lowest value of energy absorption (Iteration zero)

(b) Deleted elements on the first iteration

Figure 4.8: Verification of the BESO algorithm for the first iterations of the 3D model.

After doing this visual verification, the first set of results of the optimisation process can be presented. Figure 4.9a show the evolution of the volume fraction constraint, while 4.9b gives the same information but for the objective function. Some comments regarding the way the optimisation process evolved can be made. It can be seen that, as the mesh is refined, the algorithm necessitates more iterations to satisfy the volume fraction defined. However, the increase in the number of iterations is not dramatic.

Another apparent effect of running the optimisation with a finer mesh is the higher fluctuations in the objective function values, being more critical for Mesh 3. In fact, it was needed to post-process the data to eliminate some outliers that were impeding the proper visualization of data on the plot. The objective of minimizing the strain energy was achieved, except for this last discretization. This will be further discussed when analysing the derived geometries.

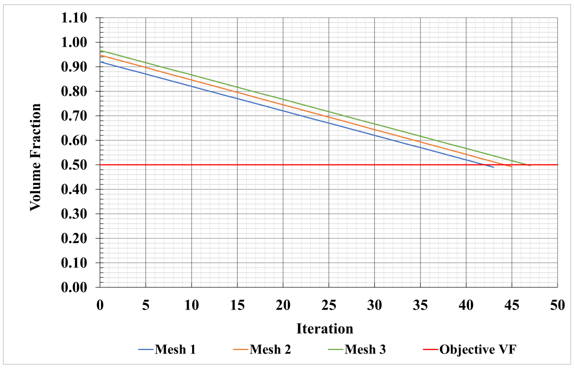

(a) Constraint

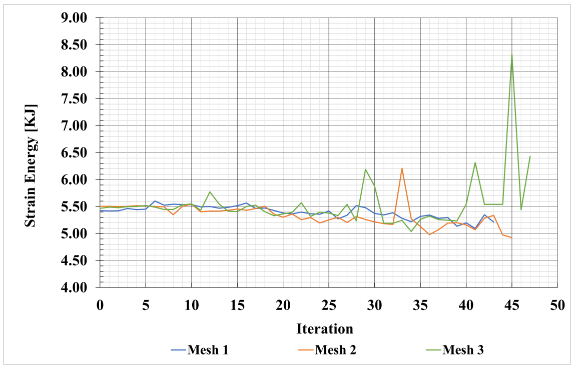

(b) Objective Function

Figure 4.9: Evolution of the optimisation problem for the ESO method applied to the 3D model.

Regarding the final geometries synthesized by this topology optimisation procedure, let us first analyse the final iteration, which represents the removal of approximately half the elemental volume in the design domain. Figure 4.10 contains the outputs obtained for each of the meshes analysed.

As it was discussed for the results of this method when applied to the 2D model, the checkerboarding effect becomes more noticeable when optimising with finer meshes. Once again, this issue will be accounted for in the BESO implementation, by applying a proper filter. All in all, it can be considered that the geometries obtained were similar, in the sense that the elements deleted by the algorithm were from the same areas, with more or less detail as the mesh is changed.

Another aspect to discuss is the fact that the amount of disconnected elements increases with the mesh refinement. This might be one of the reasons behind the instabilities in the simulation verified for Mesh 3.

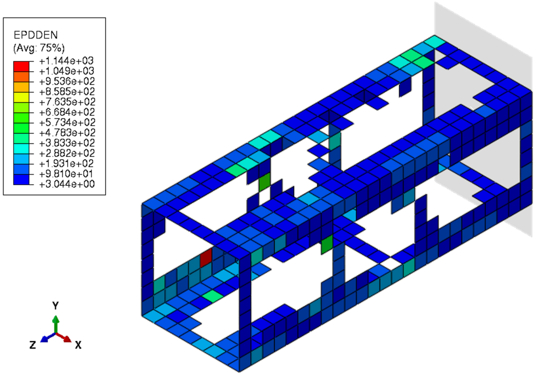
EPDDEN
(Avg: 75%)
+1.144e+03
+1.049e+03
+9.536e+02
+8.585e+02
+7.635e+02
+6.684e+02
+5.734e+02
+4.783e+02
+3.833e+02
+2.882e+02
+1.931e+02
+9.810e+01
+3.044e+00
Y
Z
X

(a) Iteration 43 - Mesh 1

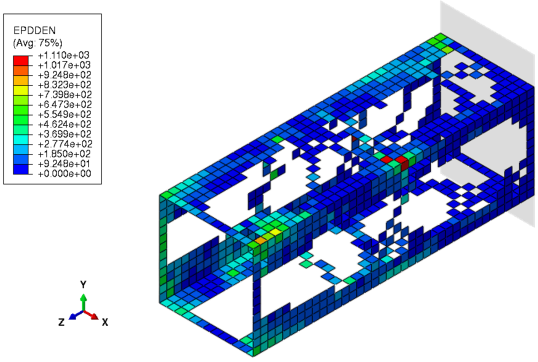
EPDDEN
(Avg: 75%)
+1.110e+03
+1.017e+03
+9.248e+02
+8.323e+02
+7.398e+02
+6.473e+02
+5.549e+02
+4.624e+02
+3.699e+02
+2.774e+02
+1.850e+02
+9.248e+01
+0.000e+00
Y
Z
X

(b) Iteration 44 - Mesh 2

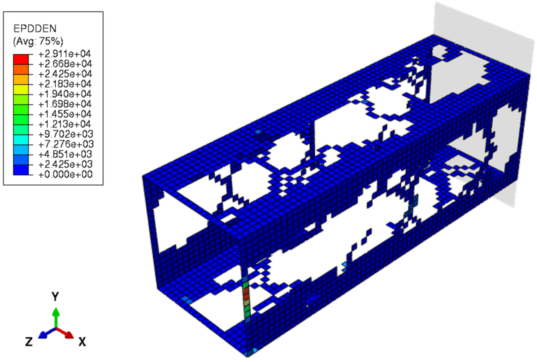
EPDDEN
(Avg: 75%)
+2.911e+04
+2.668e+04
+2.425e+04
+2.183e+04
+1.940e+04
+1.698e+04
+1.455e+04
+1.213e+04
+9.702e+03
+7.276e+03
+4.851e+03
+2.425e+03
+0.000e+00
Y
Z
X

(c) Iteration 47 - Mesh 3

Figure 4.10: Resultant 3D topologies obtained with the ESO method for a volume fraction of 50%.

Before moving forward let us analyse the optimisation results for a more conservative design, namely the geometries obtained if only 30% of the volume is removed. Said geometries are shown on Figure 4.11. Since less elements are being removed, it is expected that the dynamic simulation will run more smoothly, due to lower deformations being verified. In fact, by isolating the evolution of the objective function for Mesh 3 after post-processing the outliers (Figure 4.12), a smooth progression can be seen until approximately iteration 30, where the first peak value is observed. At around this iteration, the volume of the optimised geometry reaches approximately 70% of the initial value.

If so, the verified fluctuation in the objective function for Mesh 3 might be attributed to the excessive deformation promoted by removing half of the material available, while maintaining the same impact energy. This might lead to believe that optimising for a volume fraction of 50% is not a favourable design choice, at least for the defined conditions for this model. In addition to that, the topologies of Figure 4.11 are much more coherent.

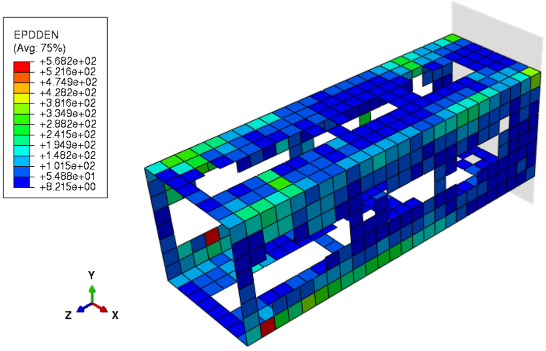
EPDDEN
(Avg: 75%)
+5.682e+02
+5.216e+02
+4.749e+02
+4.282e+02
+3.816e+02
+3.349e+02
+2.882e+02
+2.415e+02
+1.949e+02
+1.482e+02
+1.015e+02
+5.488e+01
+8.215e+00
Y
Z
X

(a) Iteration 22 - Mesh 1

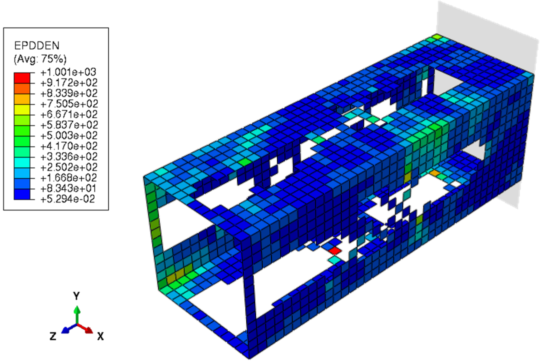
EPDDEN
(Avg: 75%)
+1.001e+03
+9.172e+02
+8.339e+02
+7.505e+02
+6.671e+02
+5.837e+02
+5.003e+02
+4.170e+02
+3.336e+02
+2.502e+02
+1.668e+02
+8.343e+01
+5.294e-02
Y
Z
X

(b) Iteration 24 - Mesh 2

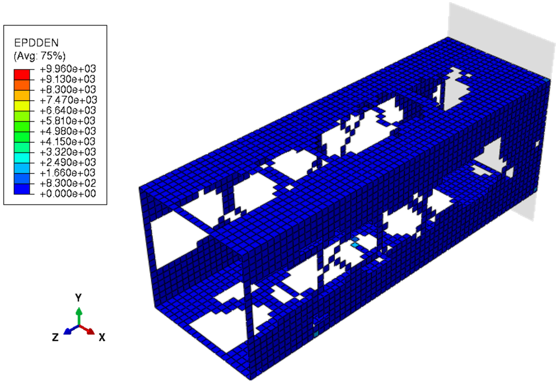
EPDDEN
(Avg: 75%)
+9.960e+03
+9.130e+03
+8.300e+03
+7.470e+03
+6.640e+03
+5.810e+03
+4.980e+03
+4.150e+03
+3.320e+03
+2.490e+03
+1.660e+03
+8.300e+02
+0.000e+00
Y
Z
X

(c) Iteration 26 - Mesh 3

Figure 4.11: Resultant 3D topologies obtained with the ESO method for a volume fraction of 70%.

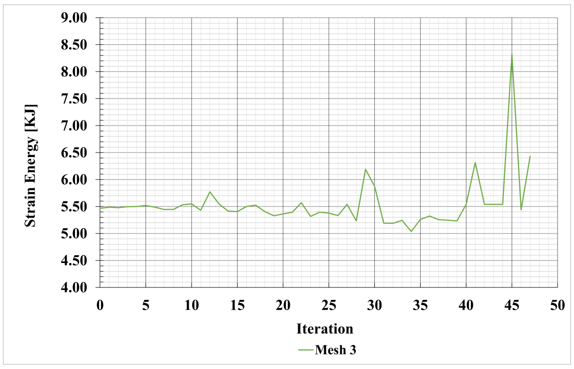

Figure 4.12: Evolution of the objective function for the ESO method applied to the 3D model (Mesh 3).

4.3 BESO Method

As for the results obtained with the bi-directional evolutionary method, beginning with the progress of the optimisation problem that can be seen in Figure 4.13, many fluctuations in the objective function are verified once again. Moreover, only the model discretized with the intermediate-sized mesh was able to converge to a topology with minimization of the strain energy on the last iteration.

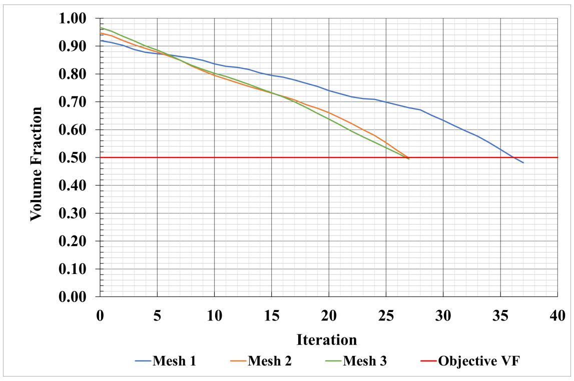

(a) Constraint

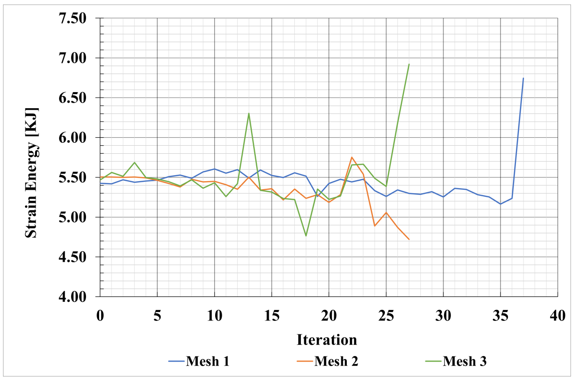

(b) Objective Function

Figure 4.13: Evolution of the optimisation problem for the BESO method applied to the 3D model.

When comparing the optimised geometries obtained with the evolutionary methods, the conclusions reached in the 2D implementation are transposed to the three-dimensional case as well. The BESO method continues to produce better-defined geometries that are less prone to the appearance of checkerboard patterns.

This last affirmation was expected, since filtering techniques were applied only for the BESO method, in accordance with the selected procedure for the two-dimensional application. Figure 4.14 showcases the optimised geometries for a volume fraction of 50%.

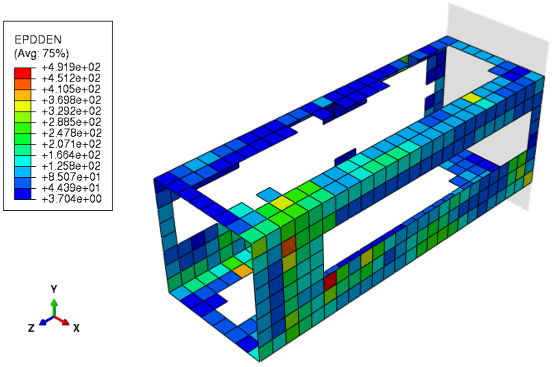
EPDDEN
(Avg: 75%)
+4.919e+02
+4.512e+02
+4.105e+02
+3.698e+02
+3.292e+02
+2.885e+02
+2.478e+02
+2.071e+02
+1.664e+02
+1.258e+02
+8.507e+01
+4.439e+01
+3.704e+00
Y
Z
X

(a) Iteration 35 - Mesh 1

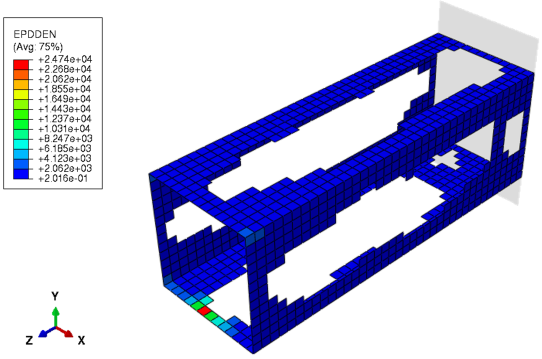
EPDDEN
(Avg: 75%)
+2.474e+04
+2.268e+04
+2.062e+04
+1.855e+04
+1.649e+04
+1.443e+04
+1.237e+04
+1.031e+04
+8.247e+03
+6.185e+03
+4.123e+03
+2.062e+03
+2.016e-01
Y
Z
X

(b) Iteration 27 - Mesh 2

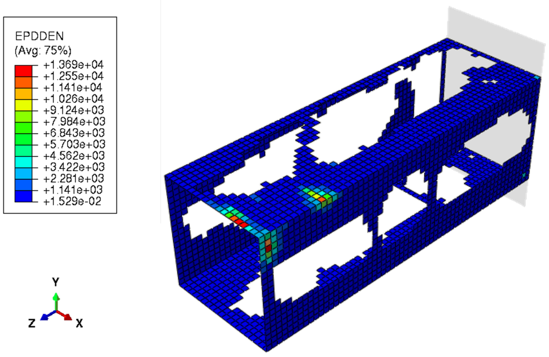
EPDDEN
(Avg: 75%)
+1.369e+04
+1.255e+04
+1.141e+04
+1.026e+04
+9.124e+03
+7.984e+03
+6.843e+03
+5.703e+03
+4.562e+03
+3.422e+03
+2.281e+03
+1.141e+03
+1.529e-02
Y
Z
X

(c) Iteration 26 - Mesh 3

Figure 4.14: Resultant 3D topologies obtained with the BESO method for a volume fraction of 50%.

Still, the instability observed towards the end of the optimisation process is concerning and confirms the suspicion that eliminating half of the material is excessive, at least for the crash conditions defined, especially the amount of crash energy transferred to the thin-walled component. A possible solution to avoid this type of situation could be that of incorporating a criteria that stops the optimisation process when instability in the evolution of the objective function is verified, independently of the volume fraction initially set.

Despite not having explored this possibility, results for a more conservative volume fraction objective of 70% were retrieved and are presented in Figure 4.15. This matches the approach followed when presenting the geometries obtained for the ESO method.

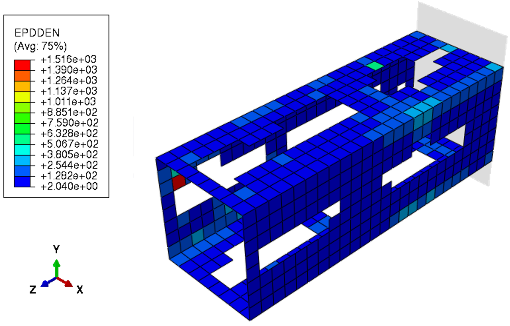
EPDDEN
(Avg: 75%)
+1.516e+03
+1.390e+03
+1.264e+03
+1.137e+03
+1.011e+03
+8.851e+02
+7.590e+02
+6.328e+02
+5.067e+02
+3.805e+02
+2.544e+02
+1.282e+02
+2.040e+00
Y
Z
X

(a) Iteration 24 - Mesh 1

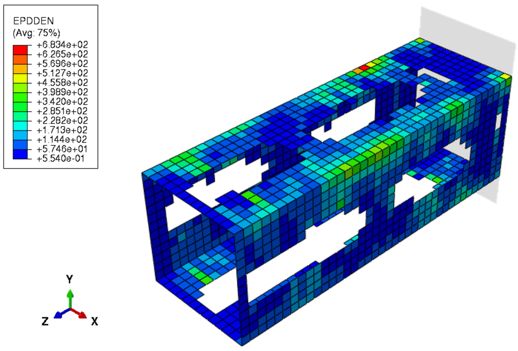
EPDDEN
(Avg: 75%)
+6.834e+02
+6.265e+02
+5.696e+02
+5.127e+02
+4.558e+02
+3.989e+02
+3.420e+02
+2.851e+02
+2.282e+02
+1.713e+02
+1.144e+02
+5.746e+01
+5.540e-01
Y
Z
X

(b) Iteration 17 - Mesh 2

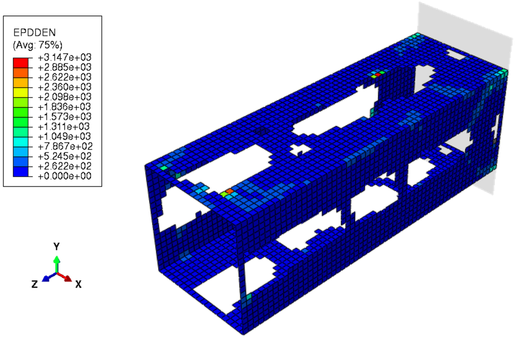
EPDDEN
(Avg: 75%)
+3.147e+03
+2.885e+03
+2.622e+03
+2.360e+03
+2.098e+03
+1.836e+03
+1.573e+03
+1.311e+03
+1.049e+03
+7.867e+02
+5.245e+02
+2.622e+02
+0.000e+00
Y
Z
X

(c) Iteration 17 - Mesh 3

Figure 4.15: Resultant 3D topologies obtained with the BESO method for a volume fraction of 70%.

By reducing the amount of material to be removed by the algorithm, a pattern of material removal is visible when the mesh is refined, and all elements appear to be properly connected. Overall the increase in the volume fraction parameter affects the results positively, producing a more structurally sound topology.

4.4 Final Remarks of the 3D Application

In summary, the best optimisation results were obtained with the BESO method, consistent with the findings from the 2D application of Chapter 3. This is not surprising considering that the bi-directional approach is a natural progression of the ESO method.

The results were specially improved in what pertains the final geometries derived, with well-defined contours and reduced numerical instabilities, particularly the occurrence of checkerboard patterns due to the filter applied, as discussed previously. Still, some difficulties were encountered during the 3D implementation as well. The main challenge was the instabilities in the optimisation process, reflected by fluctuations in the objective function, particularly for the case of the most refined meshes. It was observed, however, that the encountered fluctuations can be attributed to an excessive material removal for the crash conditions defined, leaving the structure weakened and susceptible to large deformations that lead to optimisation instabilities.

Overall, it can be remarked that the BESO method proved to be the most suitable algorithm for this application among the ones studied. In spite of the possibility of the derived topologies not being globally optimal, the results are acceptable for the application of a topology optimisation algorithm in the crashworthiness context. If so, this method will be applied during the industrial application presented in the next chapter and will result in an optimised geometry for a crash box component to be integrated into the structure of a coach for energy absorption purposes.

Despite having obtained decent contours, it is expected that the topology obtained with the BESO algorithm applied to the final crash box component will have to pass for a final post-processing step to smooth the contour given by the optimisation process. This comes as an advantage for eventual manufacturing purposes.

Chapter 5

Industrial Application

After having validated the Abaqus-Matlab interface with both 2D and 3D approaches, it was possible to apply the optimisation procedure to a component with proper dimensions to be incorporated into the frontal structure of a coach which can be considered as the industrial application of the theoretical and numerical background presented thus far on this dissertation work.

This chapter presents, first, the final geometry chosen for the crash box with some theoretical background to justify its selection. Subsequently, the optimisation results obtained with the BESO algorithm will be presented. Most specifically, three different optimised geometries, retrieved after setting the volume fraction objective for values of 50, 60 and 70%.

The finite element model of the coach is also presented. It constitutes the baseline structure to be optimised, with the goal of improving its crashworthiness under frontal impact. The optimised components are to be inserted into the coach frontal structure, to be submitted for a frontal impact simulation on the software VPS/PamCrash® under the conditions of regulation ECE R-29. A total of five simulations were performed, including simulations of the coach baseline structure and with the crash box component before undergoing any topology optimisation. This allowed to retrieve a good amount of data to be confronted and discussed at the end of this chapter.

5.1 Crash Box Development

The final geometry chosen is a double-chambered thin-walled structure, these types of structures have better energy absorption potential than the single-cell structures that had been analysed thus far in this dissertation. This conclusion is retrieved from the comparative research performed by Chen et al. in [65]. The authors studied the axial crushing of hollow multi-cell columns, Figure 5.1 shows one of the results in regard to crushing behaviour and subsequent energy absorption.

This figure shows the superior capabilities of multi-cell structures when compared to single-cell, which justifies the change in geometry for this work. Moreover, when comparing the triple-cell and double-cell columns, the latter exhibit a comparable behaviour with the added advantage of having a lower mass and being easier to manufacture.

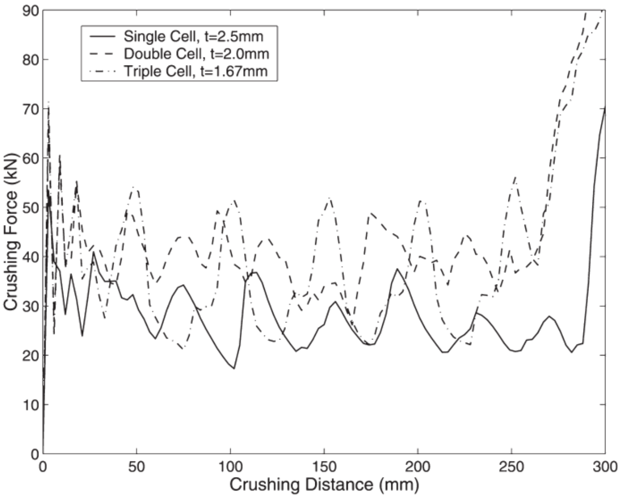

Figure 5.1: Crushing force (KN) and distance (mm) responses of single-cell, double-cell and triple-cell columns [65].

Figure 5.2 represents the final geometry with indication of its main dimensions. The interactions between crash box and impactor defined for the 2D and 3D approaches were replicated for the final model as well.

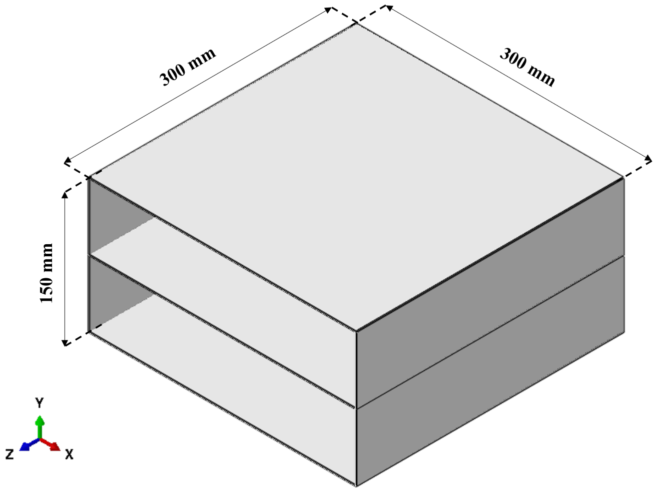

Figure 5.2: Final Geometry chosen for the crash box component.

One relevant change, however, has to do with the material properties assigned to the crash box component for this final model. As it had been presented thus far, the component was initially modelled and optimised with a mild steel as the material. However, when the crash box was coupled into the coach structure and simulated for frontal impact, the results were not as intended for the industrial application. The steel crash box did not undergo plastic deformation, leading to limited absorption of impact energy. Instead, it acted as a component to transfer the impact kinetic energy, resulting on higher intrusion into the driver's survival space.

To address this issue, a more ductile material was chosen for the industrial application. Aluminium was opted as the new material, which has also been extensively explored in applications of energy-absorbing components in the automotive industry. For instance, Segade et al. in [66] studied the influence of different materials on the energy absorption, and compared the performance of steel and aluminium crash boxes. The aluminium mechanical properties were retrieved from MatWeb [67], and can be seen in Tables 5.1 and 5.2. The latter contains the strain data used to define the plasticity of aluminium. Specifically, it depicts the tensile yield stress, similar to the properties of the mild steel defined for the previous models.

Table 5.1: Density and elastic properties for aluminium [67].

Density (ρ) [Ton/mm^3]	**Young's Modulus (E) [MPa]**	**Poisson's Ratio (ν)**
2.50E-09	70,000	0.33

Table 5.2: True stress-plastic strain data points to define plasticity properties of aluminium [67].

Yield Stress (σ_t) [MPa]	80	250	251
Plastic Strain (ε_p)	0	0.18	1

In addition to that, the attributes of the rigid body that simulates the impactor were also changed. Specifically, its mass and velocity were updated according to regulation ECE R-29. Given that the final model is intended for industrial application, and the crash test simulation for the coach structure will be subject to regulation R29, it makes all sense to undergo the optimisation process with boundary conditions that replicate those presented in the regulation, especially in terms of the amount of energy with which the crash box component is impacted.

According to the followed regulation, and as it was presented in Chapter 2, the impactor should have a mass of 1,500 kg and strike the structure with an impacting energy of 55 KJ. If so, the required velocity can be easily calculated from the kinetic energy formulation (Eq. 5.1), resulting in an impactor velocity of 8.56 m/s.

$$E_k = \frac{1}{2} \cdot m \cdot v^2 \ = \ 55 \ KJ \tag{5.1}$$

The regulation stipulates an impactor mass equal to 1,500 kg. Still, it is important to note that for the optimisation procedure, the crash box component is being struck directly by the impactor, thus receiving all the impact energy. In the real-world structure, however, there are other intervening components that absorb energy as well, thereby reducing the amount solely received by the crash box. Considering that the crash box will be mounted approximately in front of the steering wheel, it can be assumed that its area of application is half of the total area of the coach frontal structure, refer to Figure 5.3. If so, the assumption made is to perform the optimisation process with half the mass for the impactor, namely 750 kg.

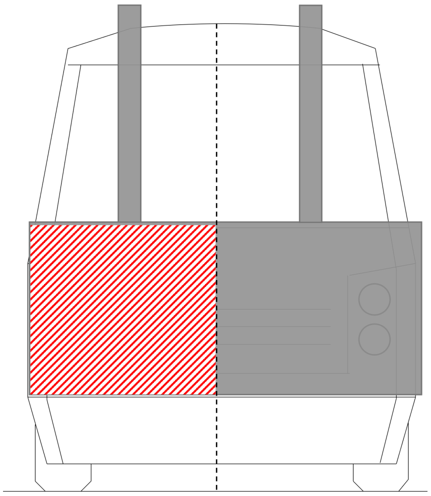

Figure 5.3: Area of application assumed for the crash box component.

Regarding the mesh of the final model, once again the meshing was done using element type S4R with a seed size of 6 mm, which resulted in 10,100 elements and 10,251 nodes. The decision of using a coarser mesh was influenced by the conclusions retrieved from the optimisation results of Chapters 3 and 4. As it was verified, the results were satisfactory, with little to no convergence issues, and considering the scale of the final model, the selection of a coarser mesh is justified. This information, along with other relevant details of the final FE model, is summarized in Table 5.3.

Table 5.3: Summary of the final crash box finite element model.

Crash Box				**Impactor**		**Mesh (Element Type S4R)**		
Length [mm]	**Width [mm]**	**Height [mm]**	**Wall Thickness [mm]**	**Mass [kg]**	**Velocity [m/s]**	**Element Size [mm]**	**Nº of Elements**	**Nº of Nodes**
300	300	150	2	750	8.56	6	10,100	10,251

5.2 Optimised Crash Box

After having analysed three different topology optimisation algorithms and streamlined them until the BESO method was chosen as the best performing for the analysed conditions, this bi-directional approach was applied to the final crash box model described in the precedent section, and the optimisation results are presented below, for the three cases of defined volume fractions.

Beginning the analysis of the results by commenting the evolution of the volume constraint. Figure 5.4a demonstrates that the desired objective volume fraction is achieved in the early iterations and that the iterations needed to do so increase together with the amount of volume that the algorithm is meant to exclude. In addition to that, it is noted that the optimisation process continues iterating despite having met the volume constraint, as the primary objective of the optimisation process is to further minimize the strain energy. Indeed, the process continues to iterate until reaching the maximum number of iterations defined in the algorithm. During this iterative process, the progression in the objective function is characterized by an oscillating behaviour, as it is evident from Figure 5.4b. Still, there are no significant peak values, in contrast to what was verified in the optimisation results of Chapter 4.

In light of the aforementioned oscillations in the objective function, it is not guaranteed that the solution obtained at the last iteration is the optimal one. In other words, a precedent iteration might have a lower value of the objective function while also satisfying the volume fraction. The approach of assessing the convergence of the solution according to the value of the objective function is meant to solve this issue since it checks if the strain energy values are stable during a defined number of successive iterations. In this case, the limit of iterations defined is reached before said convergence criterion is verified. Still, considering that convergence is not guaranteed for this crashworthiness application, the results of the last iteration are a good compromise between computational effectiveness and a lower value of the objective function as commented for the results of the three-dimensional approach.

Table 5.4 presents the strain energy values of the original component and of the resulting geometry at the final iteration. A reduction in strain energy was accomplished for all cases. In general, as more material is removed, a greater reduction in strain energy is achieved.

Table 5.4: Reduction achieved in the strain energy for the optimised geometries.

Volume Fraction (%)	**Initial value**	**Final value**	**Reduction (%)**
50	18.45	16.78	9.05
60	18.45	15.58	15.52
70	18.45	18.15	1.58

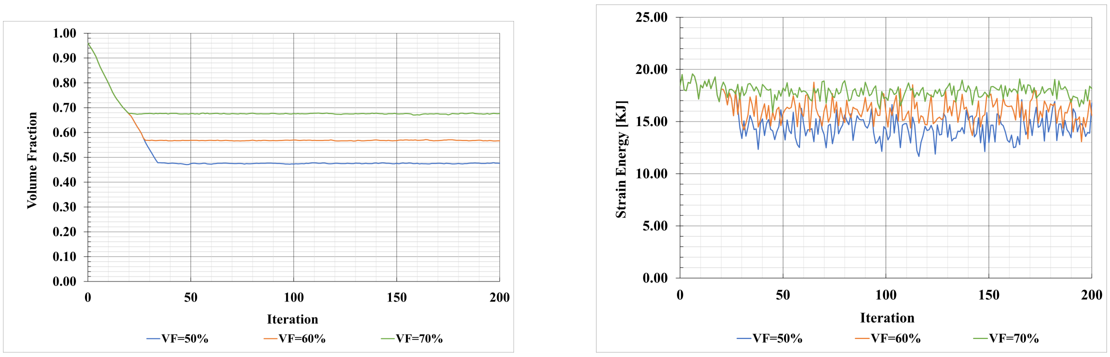

(a) Volume Fraction (b) Objective Function

Figure 5.4: Evolution of the optimisation problem for the BESO method applied to the final model.

Next, the final geometries obtained as outputs of the optimisation process can be analysed as well. The geometries are presented in Figure 5.5, on an undeformed configuration with the EPDDEN contour. When examining Figure 5.5a, which showcases the obtained topology for a volume fraction of 70%, it is visible that no elements were deleted on the lateral walls, and only a few elements were extracted from the middle cell. In contrast, as the volume to be eliminated increases, the algorithm starts targeting elements on both the lateral walls and the middle cell of the component, as it was the case of Figures 5.5b and 5.5c. This outcome suggests that the middle cell is a significant geometric feature for addressing the specific problem under investigation.

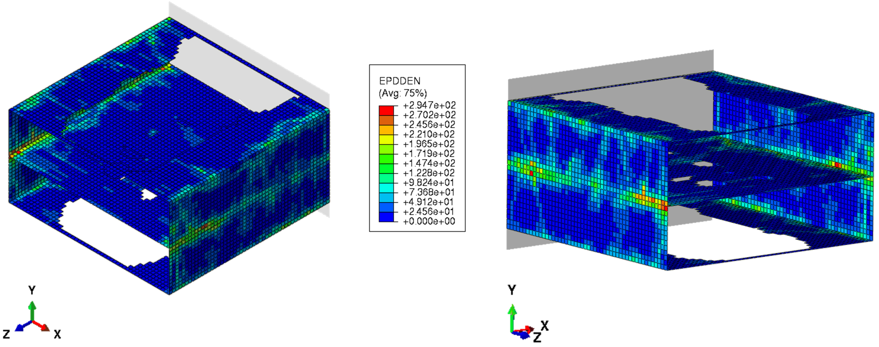
EPDDEN
(Avg: 75%)
+2.947e+02
+2.702e+02
+2.456e+02
+2.210e+02
+1.965e+02
+1.719e+02
+1.474e+02
+1.228e+02
+9.824e+01
+7.368e+01
+4.912e+01
+2.456e+01
+0.000e+00
Y
Z
X
Y
X
Z

(a) Volume Fraction of 70 %

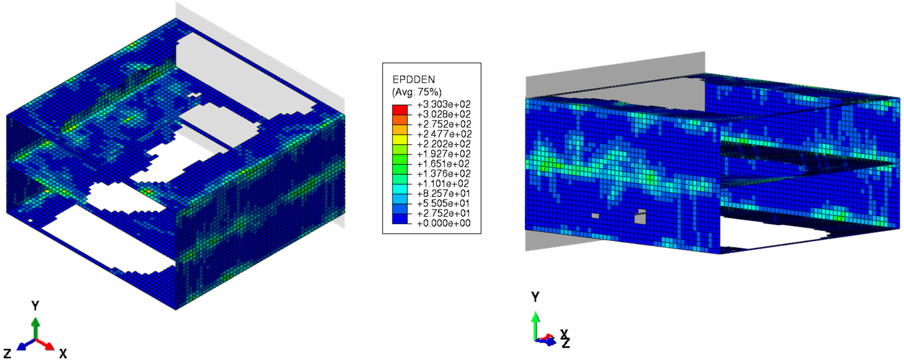
EPDDEN
(Avg: 75%)
+3.303e+02
+3.028e+02
+2.752e+02
+2.477e+02
+2.202e+02
+1.927e+02
+1.651e+02
+1.376e+02
+1.101e+02
+8.257e+01
+5.505e+01
+2.752e+01
+0.000e+00
Y
Z
X
Y
X
Z

(b) Volume Fraction of 60 %

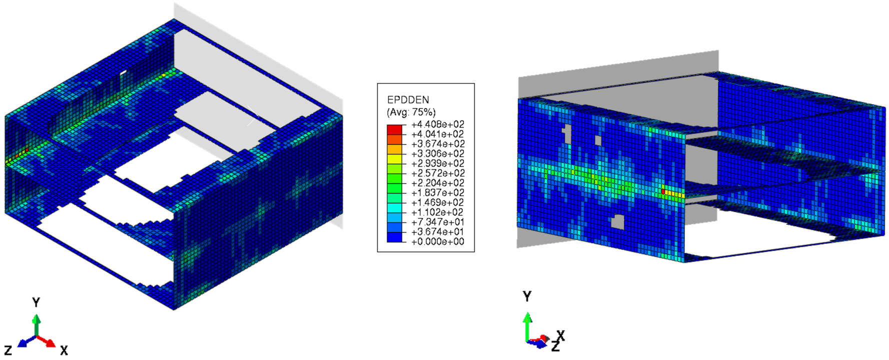
EPDDEN
(Avg: 75%)
+4.408e+02
+4.041e+02
+3.674e+02
+3.306e+02
+2.939e+02
+2.572e+02
+2.204e+02
+1.837e+02
+1.469e+02
+1.102e+02
+7.347e+01
+3.674e+01
+0.000e+00
Y
Z
X
Y
X
Z

(c) Volume Fraction of 50 %

Figure 5.5: Final Geometries obtained with the optimisation algorithm.

In this stage, the energy absorption capabilities of the obtained structures can also be assessed. This has not been done thus far in the dissertation work but it is indeed an important parameter for the industrial application. As it was defined in the theoretical review of Chapter 2, the energy absorption can be calculated by computing the area under the force-displacement curve (Equation 2.1). Figure 5.6 shows the plotted curves for all derived topologies, including the full crash box component (VF = 100%) for comparison. A script on Matlab was used to calculate the areas.

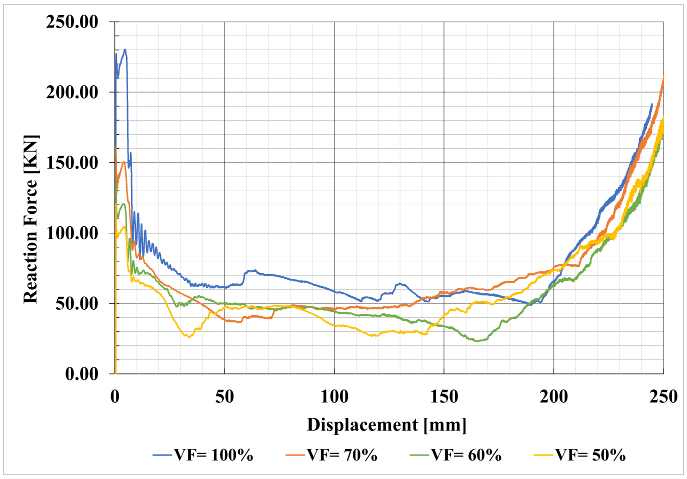

Figure 5.6: Force-Displacement curves for the crash box component with different volume fractions.

Table 5.5 displays the energy absorption values calculated for each component. It can be seen that the amount of energy absorbed decreases as more material is removed from the crash box. Nevertheless, if these results are analysed considering the efficiency in utilizing the mass of the structure, the output of the optimisation process turns out to be more favourable. If so, by presenting the results for the specific energy absorption (SEA) metric, an increase in the specific energy is verified for all cases, as indicated in the table. In fact, the highest value was obtained in the structure derived with half the initial volume.

The specific energy absorption was calculated as defined in Equation 2.2, and the mass of the component was computed considering the total volume of active elements (disregarding the frozen elements) and the density of Aluminium, as shown in Table 5.6. For each case, the mass value was affected by the corresponding volume fraction.

Table 5.5: Energy Absorption for the crash box component with different volume fractions.

	Volume Fraction	**Final Mass [kg]**	**EA [KJ]**	**SEA [KJ/kg]**
VF = 100%	0.96	0.83	18.87	22.75
VF = 70%	0.68	0.58	16.34	27.96
VF = 60%	0.57	0.49	13.72	28.03
VF = 50%	0.48	0.41	13.79	33.51

Unlike the geometries presented in Chapters 3 and 4 for the 2D and 3D applications, respectively, the final geometries underwent an additional post-processing step. This involved manually

Table 5.6: Mass of the full crash box considering the volume of active elements and the density of Aluminium.

Volume [mm^3]	Density [kg/mm^3]	Mass [kg]
345,600	2.50E-06	0.86

smoothing the surface using the CAD software *FUSION360*. The purpose of this step was to generate a geometry that would be easier to manufacture. As a matter of example, Figure 5.7 shows a before and after comparison of the top view contour of the crash box obtained for VF = 50%. The process of manually smoothing the surface involved making decisions about the appropriate sketches for each geometry. This task was challenging as it aimed to simplify the contour without compromising the overall geometry generated by the topology optimisation algorithm.

After completing the smoothing process, the crash box components were deemed ready for the final frontal impact simulation. This simulation involved integrating the crash box into the existing finite element model of the coach, in which it will interact with other components. The following section presents the specifics of the coach finite element model and outlines how the optimised crash box component was integrated into it.

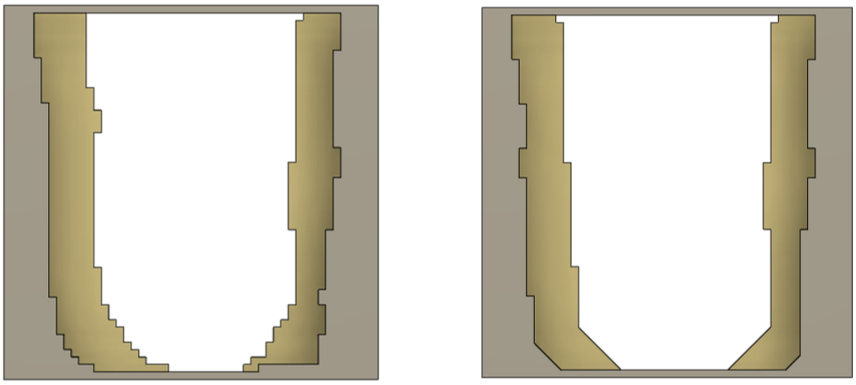
(a) Non-smooth surface

(b) Smoothed surface

Figure 5.7: Comparison of the component contour before and after manual smoothing.

5.3 Coach finite element model definition

The aim of this dissertation work is to incorporate an optimised crash box component, produced by means of topology optimisation techniques, and investigate its influence on the crashworthiness of a coach model tested under frontal conditions.

The crashworthiness of the baseline structure in a frontal impact scenario has been previously investigated by Lopes et al. in [12, 68]. The work presented in this document represents a continuation of the research that has been carried out by the previous authors, who performed experimental and numerical tests on the coach structure in accordance with regulation ECE R29.

To be more specific, the coach structure examined belongs to class M3 and, as part of the experimental procedure, a prototype of its frontal section was built. Said prototype was a simplification of the complete coach structure, maintaining the areas of interest for a frontal crash. It included the driver's cab, frontal passenger entrance and the front wheel axle. By simplifying the coach structure in this way, greater emphasis is placed on the critical areas during frontal impacts. Additionally, computational resources are saved by removing non-essential components from the analysis.

Figure 5.8 depicts the selected section of the coach structure that encompasses the critical areas of interest. It also showcases the prototype developed by the authors for experimental testing purposes. The prototype was constructed using a combination of various components made from different materials, aiming to built a high-fidelity model that closely represents the actual structure.

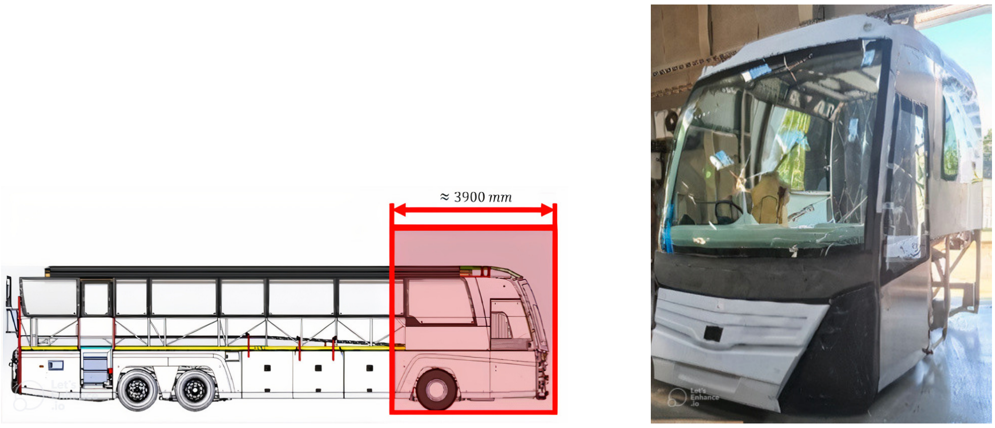

(a) Coach section

(b) Section prototype

Figure 5.8: Selected section and its corresponding prototype that was tested according to ECE R-29 [68].

Besides the coach prototype, a pendular structure was constructed to simulate the impact in accordance with the ECE R29 test setup. To assess the response of the coach structure after impact, various structural monitoring techniques were employed. A total of 15 strain gauges and two triaxial accelerometers were strategically distributed throughout the structure to measure the chassis strain and transmitted accelerations. Additionally, Digital Image Correlation (DIC) techniques were used to monitor the driver's lateral side for strain and displacement measurements.

Some of the numerical data obtained in this study corresponds to the same points where the strain gauges and accelerometers were positioned in the experimental setup. This facilitates the eventual comparison with the experimental results obtained in previous studies. Table 5.7 provides the nomenclature assigned by Lopes et al. in [68], the same nomenclature will be used when presenting the results of this study.

Table 5.7: Nomenclature given to the strain gauges used on the experimental procedure [68].

Component	**Reference**	**Designation**	**Reference**	**Designation**
Unidirectional Strain Gauges	TD	Right ceiling	FDD	Right front Inside
	TE	Left ceiling	FDC	Right front up
	LDF	Right front side	FDM	Right front medium
	LEF	Left front side	FDI	Right front interior
	LDT	Right rear side	FEC	Left front up
	LET	Left rear side	FEM	Left front medium place
	BTD	Right rear low	FEI	Left front Interior
	BTE	Left rear low		

As for the numerical analysis performed by the authors, it was conducted using the Pam-Crash® software to simulate the frontal test of the coach in accordance with the ECE R-29 regulation. The numerical model was properly defined taking into account connections, boundary conditions, contact interactions and material characterization. The simulation employed a dynamic approach with an explicit formulation. Figure 5.9 depicts the coach FE model submitted for simulation. It includes the numerical impactor and a variety of components including glass, panels, the dashboard, and others. To accurately represent the behaviour of these components involved in the simulation, a range of material constitutive models available in the software had to be used.

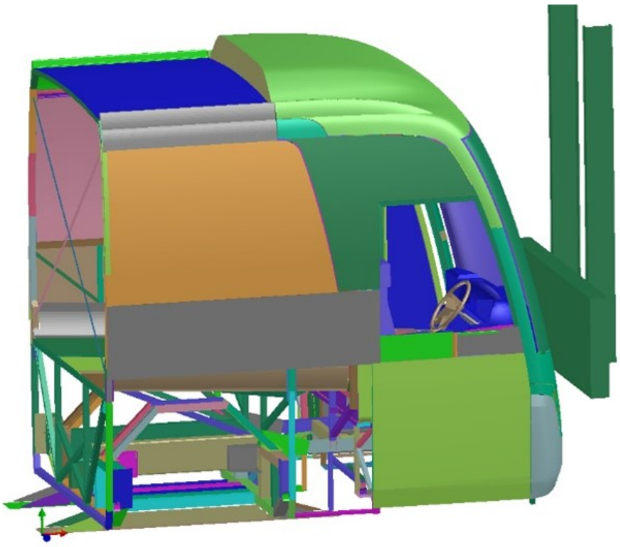

Figure 5.9: Finite element coach model simulated in [68].

Based on the simulation and experimental results, the authors elaborated some final conclusions in regard to the crashworthiness of the structure. It was found that, in its current configuration, the coach section does not meet the requirements set by the ECE R29 standard. After the experimental impact test, the conformity of the structure was verified by positioning a dummy according to the regulation to evaluate the residual space for the driver. It was found that the residual space was insufficient to accommodate the right leg, which was enough to deem the test invalid and conclude the no compliance of the studied section with regulation R29.

5.3.1 Crash box assembly into the coach structure

Based on the previous conclusion that the current structure of the coach requires reinforcement to ensure the driver's survival, this dissertation work serves as a continuation of previous investigations in the effort of improving the crashworthiness behaviour of the structure that has been verified experimentally. This section provides details about the coach finite element model used in this study. It includes additional simplifications made to the model and, more importantly, explains how the optimised crash box components were integrated into the structure.

In this dissertation work, the coach model used for numerical simulations retained the overall conditions mentioned in the previous section. However, further simplifications were made by removing the exterior panels and the dashboard. The resulting model consisted, mainly, of the metallic frame of the coach, as depicted in Figure 5.10.

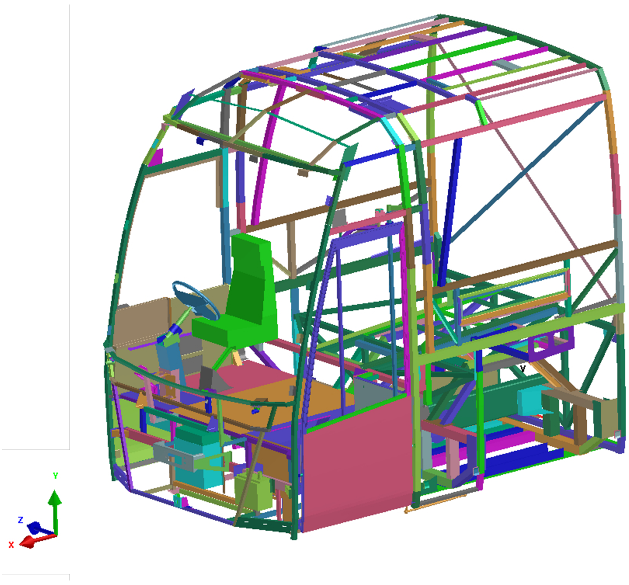

Figure 5.10: Simplified coach structure in the FE model used in this research.

Regarding the way the component is mounted in the coach structure, in order to reinforce the driver's zone and enhance the crashworthiness of the structure, it was decided to incorporate the crash box in front of the steering wheel. This was strategically done to harness its energy-absorbing properties for the intended purposes. Specifically, the crash box was placed between the steering column and the main frontal transversal bar of the chassis, constraining all its degrees of freedom. The component can be seen in Figure 5.11, highlighted in red.

Once the crash box was assembled onto the frontal structure of the coach, everything was set to submit the finite element model for dynamic explicit simulation on PamCrash® as it was done in [68].

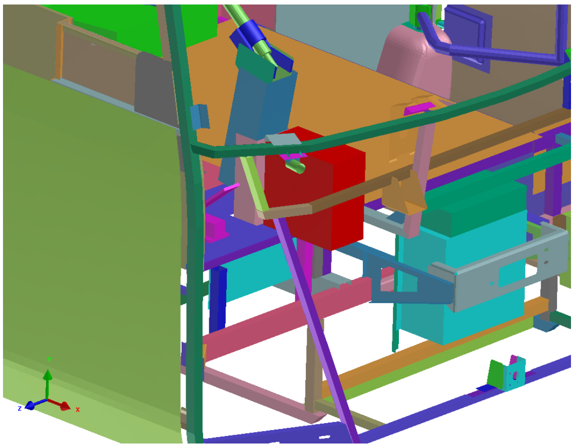

Figure 5.11: Position of the crash box component, highlighted in red, in the coach structure.

5.4 Discussion of the Results

In a precedent section of this chapter, preliminary results were presented in which the behaviour of the individual optimised crash box components was analysed. The set of results to be presented in this section shifts to the overall behaviour of the coach structure, including the integrated energy-absorbing component.

The data obtained from the crash event simulation is used to analyse several parameters, including the translational velocity of the impactor, internal energy absorbed by the structure, displacement of some analytical points, as well as strain and accelerations experienced by the structure. Towards the end of the chapter, concluding remarks are made regarding the obtained results, offering insights into the crashworthiness behaviour of the optimised structure. It is important to point out that, for better comprehension of the figures, the results obtained for the crash box with VF = 60% will not be presented. Still, it can be said that its behaviour was intermediate, in relation to the components obtained with volume fractions of 50 and 70%.

5.4.1 Impactor velocity results

The first set of results presented focuses on the evolution of the impactor translational velocity during the crash simulation. The importance of analysing this parameter relies on its relation to the intrusion of the structure. Having a structure that is stiff enough to rapidly decelerate the impactor is a desired behaviour to minimize the intrusion. This is in fact verified in the structures that incorporate crash box components, being able to stop the impactor movement faster, as depicted in Figure 5.12. The structure with the full-volume crash box achieves the fastest reduction in impactor velocity, making it the best performer in this regard. Being closely followed by the structure with the optimised crash box having a volume fraction of 70%. This observation suggests that having a larger amount of material offers greater resistance to the advancement of the impactor. Additionally, once the impactor's velocity reaches zero, it is rejected by the structure and inverts its displacement.

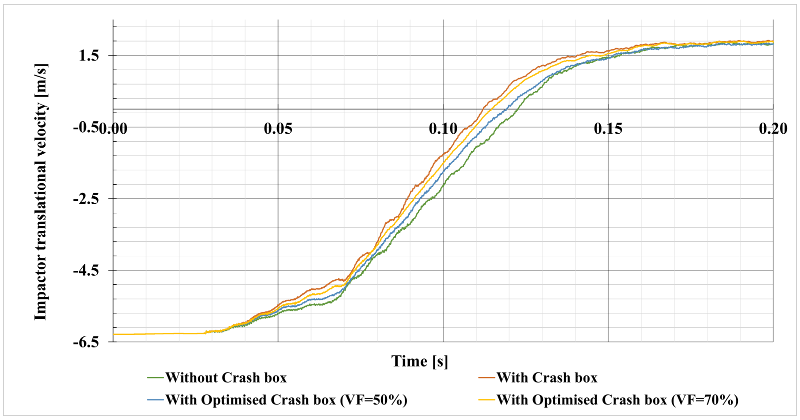

Figure 5.12: Impactor translational velocity curves (m/s) for all cases under study.

5.4.2 Displacement results

The next set of results is of significant importance for this industrial application, as they provide insights into the displacement experienced by the selected points, which translates into the intrusion verified in the structure during the frontal impact. Also, the regulation being followed in this study places particular emphasis on the intrusion parameter, which for the reference system defined on the FE model is measured in the negative *X* direction.

First, the displacement results will be presented for two specific nodes located on the coach chassis, labelled as nodes 97 and 1937. Their position and displacement results can be seen in Figures 5.13 and 5.14, respectively. A general observation from these results is that the maximum intrusion occurs at approximately the same instant when the impactor reaches zero speed, by comparing with Figure 5.12. Also, the aforementioned statement that structures able to stop the impactor earlier result in lower intrusion is confirmed. This is evident in both nodes, where the structure with the full crash box exhibits the least intrusion, while the baseline structure experiences the most. Of particular interest is the behaviour of node 1937, situated on the right-hand side of the coach structure. Due to its location, the influence of the crash box components becomes more prominent. Notably, the displacement curve for the crash box with VF = 70% closely aligns with that of the full crash box, with the lines nearly overlapping, as illustrated in Figure 5.14b. This result highlights a positive outcome for the topology optimisation process.

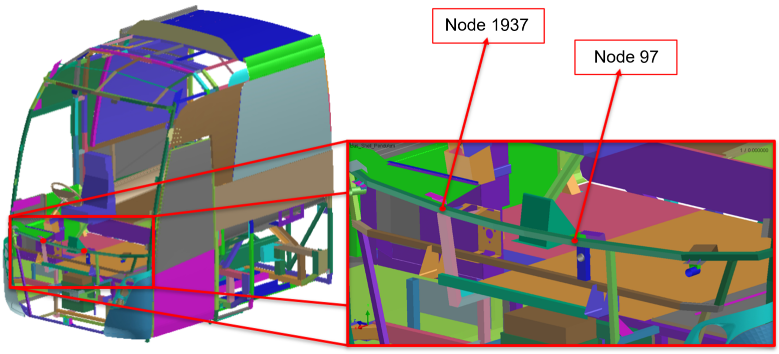

Figure 5.13: Location of nodes for displacement results.

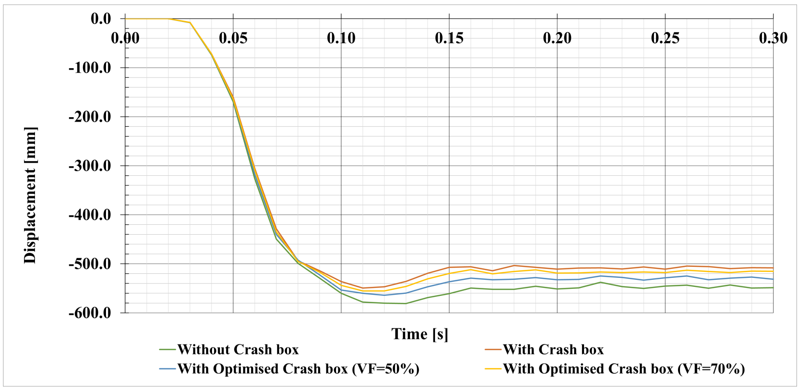

(a) Node 97

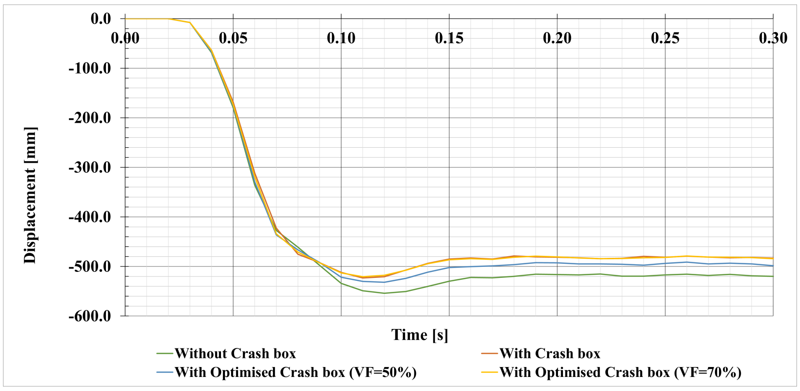

(b) Node 1937

Figure 5.14: Displacement, in mm and *X* direction, of selected nodes for all cases under study.

In addition to analysing the displacement of the nodes shown above, a point was defined in the steering wheel and displacement results were retrieved for it, the location of the created point can be seen in Figure 5.15.

According to the results obtained in [68] the dashboard revealed itself as the critical area in terms of intrusion into the driver's compartment. Despite not having the dashboard in this simulation, the steering wheel constitutes a good point of reference to assess the intrusion and thus the safety of the driver.

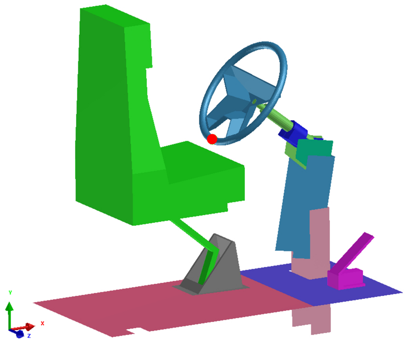

Figure 5.15: Point created on the steering wheel to monitor its displacement.

The displacement results for this reference point at the steering wheel in the X direction are presented in Figure 5.16. In general, all the optimised structures experienced a reduction in intrusion. An interesting finding in this figure is that the best-performing structure was not the one with the not-optimised crash box, as it had been verified for all the other results thus far. Instead, the lowest intrusion of the steering wheel was obtained for the structure optimised with a crash box obtained for a VF = 70%.

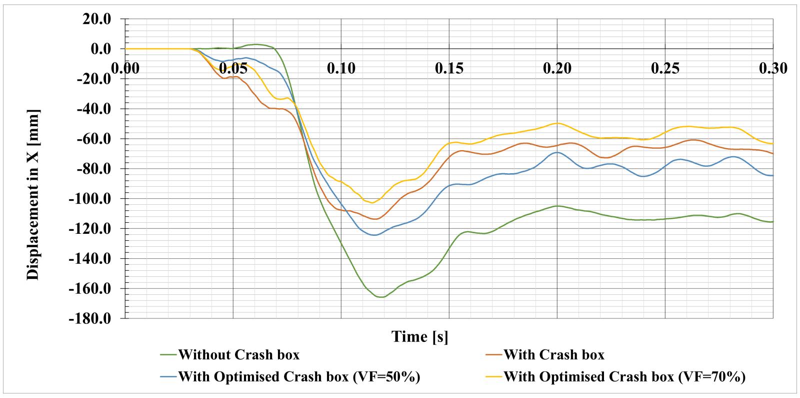

Figure 5.16: Intrusion of a point on the steering wheel, in mm, for all cases under study.

Considering the displacement of the steering wheel point in the Y direction as well, a curve that represents its trajectory on the XY plane can be traced. This was done for all the structures under study and the resulting curves are shown in Figure 5.17.

The figure offers a better visualization of the displacement and highlights the reduction in intrusion for the optimised structures. Additionally, changes in the Y-coordinate can be observed. The graph is centred around the initial position of the reference point, represented by the origin of the graph. To provide further context, a dark grey line representing the contour of the driver's seat was included. This line serves to contextualize the trajectory curves. From the figure, it can be seen that none of the trajectory curves intersects the seat contour, indicating that there would be no contact between the steering wheel and the driver during the impact. Still, it is important to note that this graph constitutes an approximation, as the driver's seat also undergoes displacement during the impact. Therefore, it should be primarily considered for visualization purposes.

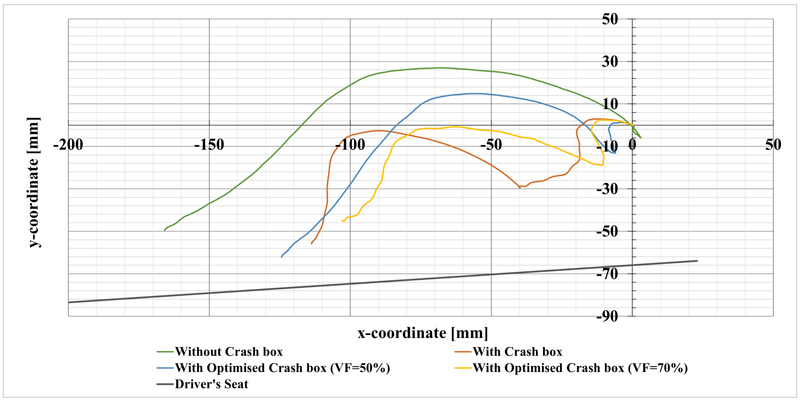

Figure 5.17: Trajectory of a point on the steering wheel on the *XY* plane for all cases under study.

5.4.3 Energy absorption results

The results of this section represent the internal energy absorbed by the structure and are presented in Figure 5.18. The first comment that can be made is in regards to the general evolution of the curves, exhibiting a lower plateau in the time range of [0.0, 0.025] seconds, as a result of the initial stiffness of the structure, indicating its elastic behavior.

Similar to what was verified for the energy absorption analysis of the isolated components presented in Table 5.5, the analysis for the coach structure demonstrate that the structures absorbing the highest values of internal energy are those that retain the most volume. It is also evident from the figure that the peak of energy absorption occurs later as the impactor is stopped later as well. Table 5.8 shows the peak value of energy absorbed for each structure and ranks them from highest to lowest value.

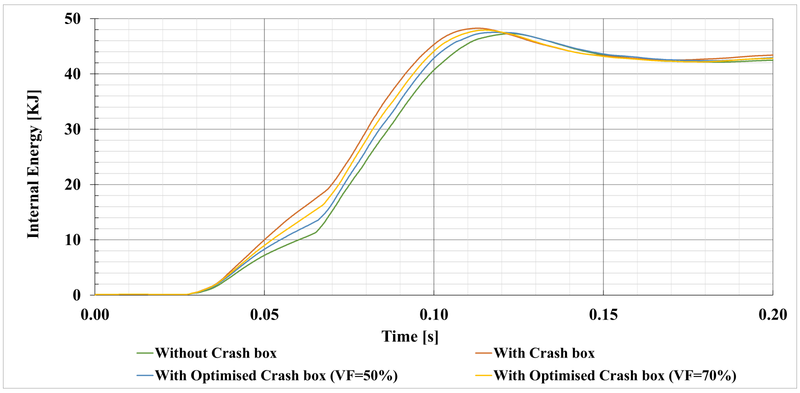

Figure 5.18: Internal Energy absorbed by the structure, in KJ, for all cases under study.

Table 5.8: Peak energy absorption values for all structures under study.

	Maximum Energy Absorbed [KJ]
With Crash box	48.25
With Optimised Crash box (VF=70%)	47.92
With Optimised Crash box (VF=50%)	47.51
Without Crash box	47.28

5.4.4 Strain and acceleration results

Starting with the acceleration results, these were retrieved from two analytical points that represent the location of the two accelerometers that were installed on the prototype of the structure built for experimental testing. As such, two graphs are presented, namely in Figures 5.19a and 5.19b, representing the results for the left-side and right-side accelerometers, respectively. It is relevant to point out that the acceleration values presented in these figures were filtered using a CFC180 filter, that removes high-frequency noise while preserving lower-frequency information that is relevant to these analyses [69]. A comment that can be given is that the accelerations felt by the accelerometer positioned on the right-hand side of the frontal structure are lower, which can be attributed to the presence of the crash box component. Still, the obtained accelerations values were generally high. These accelerations can result in sudden movements of the trunk and neck, posing a risk to the physical integrity of the driver and passengers.

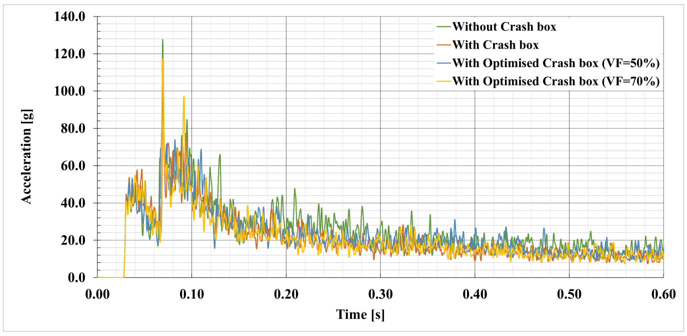

(a) Left accelerometer

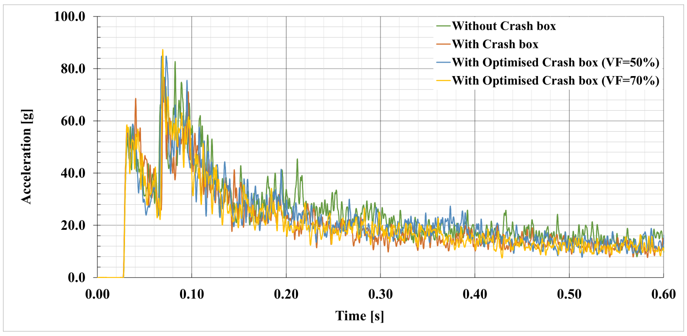

(b) Right accelerometer

Figure 5.19: Acceleration results obtained (in g).

Some justifications can be given that might explain the magnitude of these results. One possible explanation is the way certain aspects of the structure and the crash event were simulated. For instance, welding is the main manufacturing process used to join the profiles on the real model. However, the exact location of welds is not known, leading to inaccuracy in the numerical model by using excessive Tie constraints. This results in an overestimation of the structure stiffness and, consequently, the acceleration values obtained from the numerical model are also overestimated. This conclusion was drawn by Lopes et al. in [68], when comparing the acceleration results obtained from numerical simulations with experimental data.

Another aspect to consider is that, in the numerical simulation, the coach structure is perfectly fixed to the ground, meaning that no energy is transferred to the exterior as would occur in a real-world impact. In reality, part of the impact energy would be dissipated to the surrounding environment, leading to a further reduction in the acceleration values felt by the structure.

In any case, considering these results can be seen as a conservative approach to the analysis of the structure, which can be advantageous for this type of application involving safety considerations.

Continuing with the analysis, the strain results will now be presented. Since the focus of this research is the frontal impact, the deformation measurements of the areas most affected by this type of event will be provided. Specifically, the ones located towards the front of the chassis and on the A-pillars. Still, deformation plots were retrieved at other locations in the coach structure and can be seen in Appendix A.

In order to correlate with experimental results, the strain data is retrieved at the location of strain gauges positioned in the experimental setup. The numerical data was retrieved by defining a local reference system that represents each strain gauge. The nomenclature assigned to the strain gauges in Table 5.7 will be used to present the results. Figure 5.20 shows the location of these selected strain gauges on the coach structure.

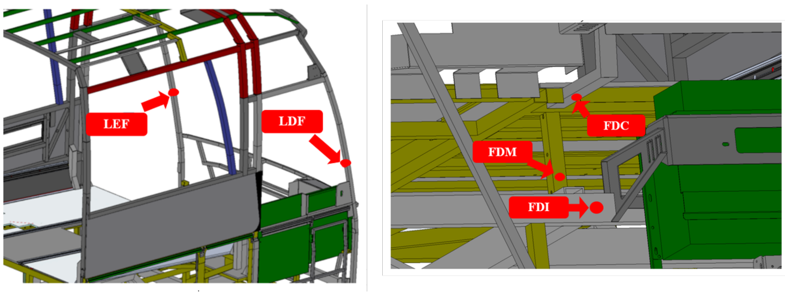

Figure 5.20: Location of some strain gauges on the coach structure [68].

Let us start by commenting the deformation results obtained at the location of strain gauges positioned in the A-pillars, which are shown in Figure 5.21. The differences between these results are a good indication of the effect the crash box component has. For instance, by observing the results for the right-hand pillar (Figure 5.21a), it can be seen that the structures optimised with the crash box component deformed less, particularly for the components with higher volume fractions.

On the other hand, the deformation observed in the left pillar (Figure 5.21b) shows similar trends for all structures.

Since the crash box has been positioned towards the right-hand side of the coach structure, it was expected to have a greater effect on the deformation results towards that side. The previous results support this expectation. Consequently, the next set of results will focus on the strain gauges located on the right-hand side of the frontal coach structure, as depicted in Figure 5.20.

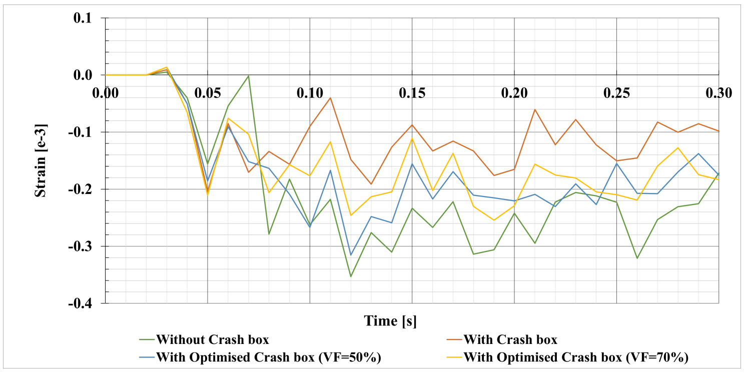

(a) LDF

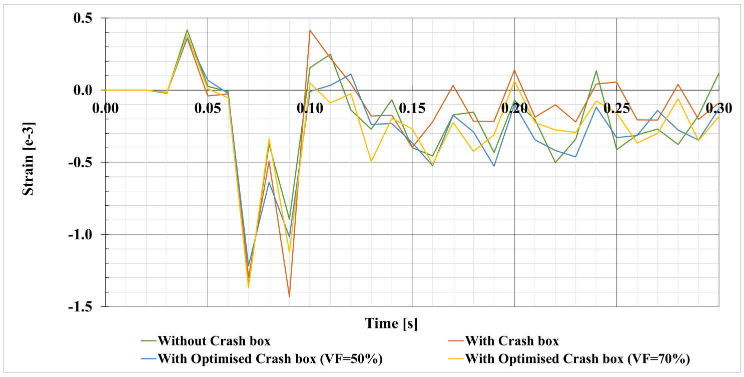

(b) LEF

Figure 5.21: Deformation results measured in the A-pillars.

The deformation curve at the location of strain gauge FDM is presented in Figure 5.22a. In contrast to the A-pillars, the structures with a crash box exhibit higher deformation in this case. The deformation is highest for the structure with the full crash box and decreases slightly as the volume eliminated from the crash box increases. However, considering the location of the strain gauge, this result can be deemed as positive. It indicates that by incorporating a crash box component in that area, the deformations were effectively directed downward toward the chassis, instead of towards the steering wheel. Similarly, higher deformations are verified at the location of strain gauge FDC (Figure 5.22b), while the deformation remained more or less the same in all structures for strain gauge FDI (Figure 5.22c).

A general conclusion that can be given after having commented on the above results is that the inclusion of a different component, such as a crash box, can significantly affect the deformation behaviour of the structure. Depending on the location, the deformation may increase or decrease with the presence of the crash box, as it was clear from the results obtained from the strain gauges positioned in various locations of the coach structure.

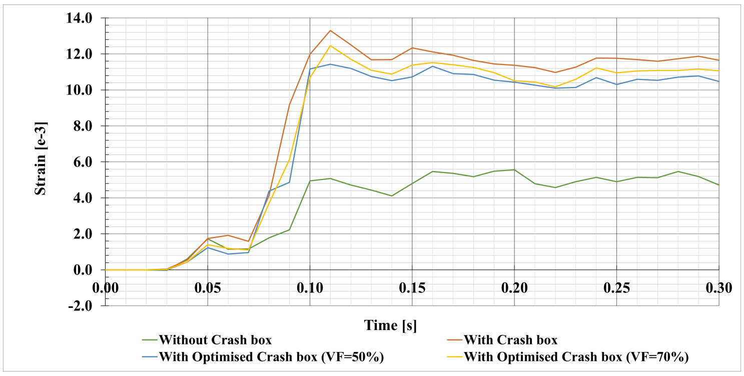

(a) FDM

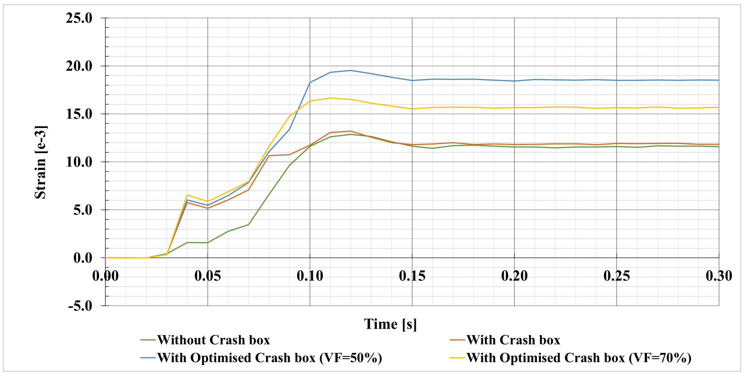

(b) FDC

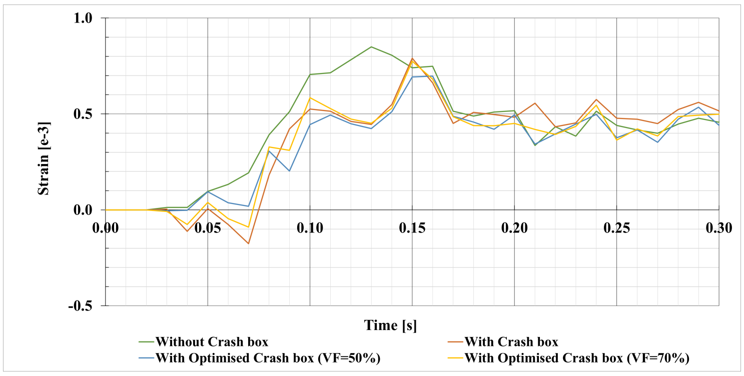

(c) FDI

Figure 5.22: Deformation results measured in the right-hand side of the frontal structure.

Some extra results that were retrieved will be presented next. They concern the deformation of the door on the driver's side for all structures under study, and can be seen in Figure 5.23. Maximum deformation of the door is verified in the structure without any crash box (Figure 5.23a), while the incorporation of the component leads to a reduction in the deformation peak of the door for all cases. Notably, the reduction is increasingly more effective as less material is removed from the crash box in the optimisation process. Indeed, the structure with the full crash box (Figure 5.23d) demonstrates the most favourable behaviour in terms of door deformation.

The analysis of these results is relevant because the door is a critical component during a crash event, and its deformation is a good indicative of the intrusion into the driver's compartment. A reduction in door deformation is accompanied by less intrusion, thus increasing the driver's survival space.

Overall, the reduction in deformation obtained for all structures with a crash box has a positive impact in the event of a crash. A less deformed door improves the probability of success of an eventual operation to rescue the driver.

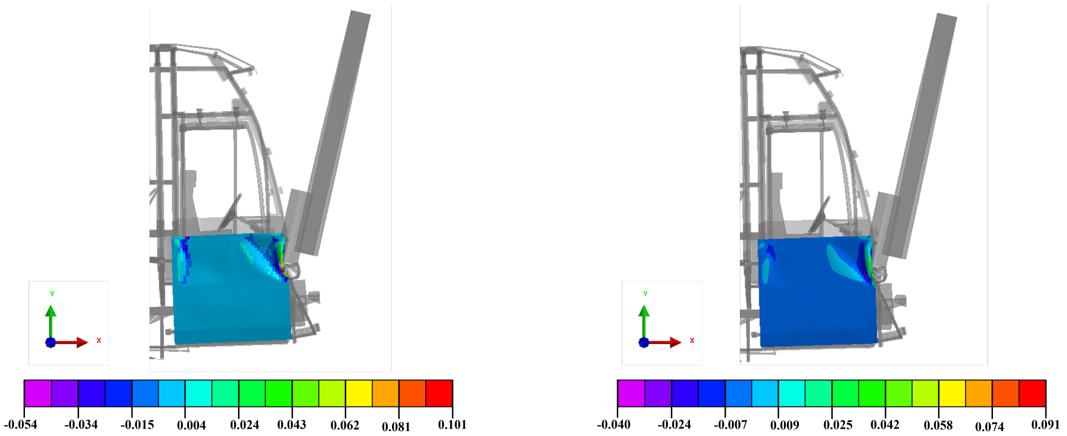

(a) Without crash box

(b) With optimised crash box (VF = 50%)

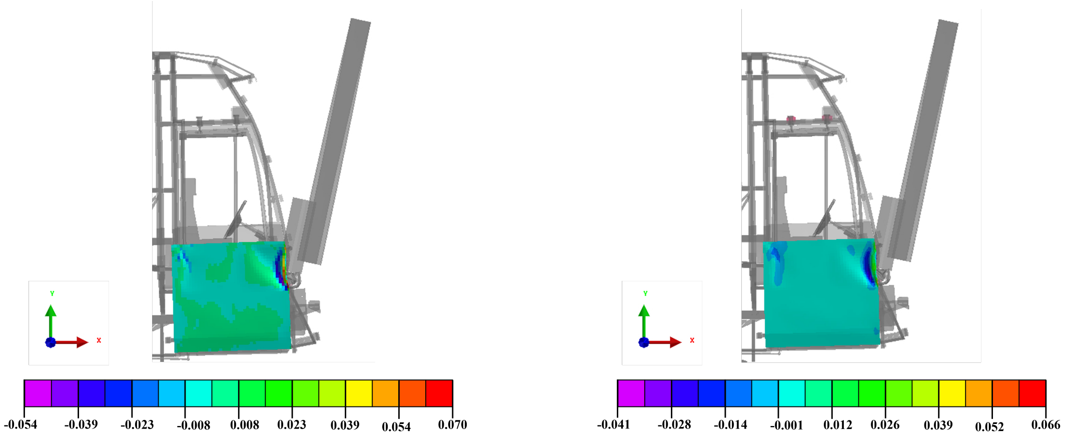

(c) With optimised crash box (VF = 70%)

(d) With crash box

Figure 5.23: Deformation in the driver's door for the studied structures.

5.5 Final Remarks of the results

After having presented and analysed the results, some final remarks can be given in regard to the performance of the different crash box components derived from the topology optimisation procedure proposed in this dissertation work. Some comments were, in fact, already offered upon the presentation of the results for the different crash parameters analysed. However, the intention of these final remarks is to try and reach a conclusion about the best-performing component, and its impact on the crashworthiness of the coach structure.

The selection of the most suitable crash box component depends on a comprehensive evaluation of various factors to ensure an optimal balance between crash performance and practical considerations. First, the energy absorption performance of the crash boxes was assessed individually. From that point of view, the full crash box demonstrated the highest energy dissipation capacity, while a decrease in this capacity was verified as the target volume fraction was reduced. However, considering the specific energy absorption, the trend was inverted, with the crash boxes having lower volume fractions exhibiting higher rates of energy absorption. This indicates a better efficiency in the usage of the material as a result of the topology optimisation performed.

This set of results was an interesting preliminary evaluation providing valuable insights into the outputs of the topology optimisation process. Still, the higher relevance comes from confronting the derived topologies in the context of an industrial application, which was done by incorporating the crash boxes into the model of the coach and simulating for frontal impact conditions. Indeed, for the majority of crash parameters analysed, the structure with the full crash box outperformed the others. Although this component did not undergo any optimisation process, its good performance is not surprising, since it retains all the inherent energy-absorbing potential expected from such a component.

As for the remaining crash boxes, the results obtained were still satisfactory. A compromise was found to generate components with lower mass and a good crashworthiness performance, that was effectively transferred when integrated into the coach structure. For all cases, structural improvement was attained in relation to the baseline structure of the coach. Specifically, there was a reduction in intrusion into the driver's compartment, decreased deformation of its door, improved structural resistance against external forces, and increased internal energy absorption within the structure. These results are promising for an increase in passive safety for the coach driver and passengers.

Special was the case of the crash box obtained with a volume fraction of 70%. It closely approached the characteristics and performance of the full crash box, and in some aspects, even outperformed it, particularly in the displacement analysis of the reference point located in the steering wheel. Out of the geometries obtained through topology optimisation, this crash box was the one that retained more material in its middle section. This section provided more resistance to the advancement of the impactor, while the upper and lower sections deformed greatly to dissipate energy. The key to the good performance of this crash box might be attributed to the way the whole component interacts with the remaining elements of the structure upon deformation.

One may wonder why to choose an optimised crash box component instead of the full crash box, given that the latter exhibited the best performance. The answer lies in the principle of achieving a structure that meets engineering requirements with the lowest possible mass. This principle was reflected in the results of this research, as the crashworthiness behaviour of the baseline structure was improved with crash box components of reduced mass. From an economic perspective, opting for an optimised component makes sense as well. By using less material while still achieving satisfactory crash performance, costs can be reduced. Therefore, choosing an optimised crash box component becomes justified both in terms of performance and cost-effectiveness.

Chapter 6

Conclusions and Future Works

6.1 Conclusions

This research aimed to apply topology optimisation techniques for a crashworthiness application with the goal of improving the passive safety measures of a coach structure in frontal impact scenarios. Through the implementation of an interface approach, it was concluded that evolutionary algorithms can effectively generate topologies at a component level in the context of crashworthiness optimisation.

The main approach followed in this dissertation work involved the utilization of an interface that links Abaqus and Matlab to perform topology optimisation, gathering data from explicit dynamic simulations. This approach was effective in combining the strengths of both software platforms. By leveraging this interface, greater flexibility was achieved in tailoring the algorithms to meet specific requirements, while also enabling accurate and precise non-linear simulations.

This study proposed a sequential methodology to identify the best optimisation algorithms for the case under investigation, starting with a simple 2D model and building up in complexity. By following this methodology, it was possible to gradually obtain insights on the functioning of the algorithms, ultimately reaching a decision on its suitability for the industrial application. Through this process, the Bi-directional Evolutionary Structural Optimisation (BESO) method was determined to be the most effective for the intended application. These findings aligned with expectations, particularly considering the theoretical background and the unique challenges associated with crashworthiness optimisation.

The objective of finding an optimised component that could improve the passive safety of a coach was successfully achieved through the topology optimisation process. A set of optimised crash box components were proposed, and their incorporation into the coach baseline structure led to significant improvements in the crashworthiness performance of the coach under frontal impact conditions. This included reduced intrusion and door deformation, and overall an increase in internal energy absorption within the structure for all cases.

Based on this conclusion, the implementation of an energy-absorbing component such as the ones presented should be considered. The proposals presented in this research provide valuable recommendations for rethinking the design of current structures for large vehicles, and potentially start developing new models with increased crashworthiness performance and enhanced passive safety. Also, the improvement of crash metrics attained with components of reduced mass makes this potential recommendation more appealing to vehicle manufacturers from an economic perspective.

Moreover, the research conducted in this dissertation constitutes a significant contribution towards bridging the existing gap in the field of topology optimisation, specifically for the case of coach structures and other large vehicles. It reinforces the understanding that many traditional algorithms lack the necessary capabilities to effectively address the challenges posed by the inherent non-linearities in crash simulations, which interrupt the application of classical topology optimisation techniques.

This research clearly illustrates the performance of evolutionary methods and the Solid Isotropic Material with Penalization (SIMP) material model for crashworthiness topology optimisation. Still, the investigation of other state-of-the-art methods like the Hybrid Cellular Automata (HCA) and Equivalent Static Loads (ESL) methods remains an open question and warrants further exploration that could potentially be addressed in future studies.

6.2 Future Works

Indeed, some future works could be performed to further explore some other aspects that could help better understand the implication of the results obtained.

For instance, the Abaqus-Matlab interface could be further improved to explore some extra features of this approach. As a matter of example, the code can be enhanced to enable image generation of the iteration results in the 3D application, similar to what is possible in the 2D case. This would allow users to track the advancement of the process without the need to open Abaqus. Furthermore, an unexplored feature in this dissertation is the possibility of presenting the results on a Graphical User Interface (GUI). In addition to showing the synthesized topology, this GUI would also showcase the evolution of the constraints and objective function of the optimisation problem. It would also allow the user to input optimisation parameters, select the desired algorithm, and specify the input file of the CAE model for the structure to be optimised in a more user-friendly way, instead of manually. Similarly, the possibility of devising a code to automatically smooth the surface generated by the topology optimisation process could be studied.

To gain further insights and validate the results obtained through numerical simulation, it would be beneficial to conduct experimental testing. For instance, an axial crashing test could be performed on a prototype of the optimised crash box to compare and validate its energy absorption capabilities. This would allow for a frontal impact test to be conducted using the experimental setup specified in regulation ECE R-29. By doing so, it would be possible to determine whether the coach structure benefits from the addition of the optimised crash box component, and if indeed is able to satisfy the requirements of the regulation. The results obtained from such experimental testing would provide a higher level of confidence in the results of the dissertation, supporting any recommendations for improvement that may be made. Also, it would be worthwhile to explore the implications of incorporating an additional crash box on the left-hand side of the frontal structure of the coach and assess its influence on the crash parameters analysed and on the overall crashworthiness performance of the coach structure.

Just as some final thoughts, it would be valuable to extend the application of this topology optimisation approach for the remaining tests that are described in the regulation, namely to assess the resistance of the structure in a rollover accident, and determining possible weak areas for different crash events. By doing so, the potential contributions of topology optimisation techniques in addressing other identified deficiencies within the structure can be evaluated.

All in all, the objectives proposed for this research were accomplished, successfully demonstrating the application of topology optimisation techniques to improve the crashworthiness of a coach structure under frontal impact conditions.

References

[1] Neal M Patel, Byung-Soo Kang, John E Renaud, and Andrés Tovar. Crashworthiness design using topology optimization. 2009.

[2] CA Soto. Structural topology optimization for crashworthiness. *International journal of crashworthiness*, 9(3):277–283, 2004.

[3] Mehmet Ali Güler, Muhammed Emin Cerit, Sinem Kocaoglan Mert, and Erdem Acar. Experimental and numerical study on the crashworthiness evaluation of an intercity coach under frontal impact conditions. *Proceedings of the Institution of Mechanical Engineers, Part D: Journal of Automobile Engineering*, 234(13):3026–3041, 2020.

[4] Pattaramon Jongpradist, Supakit Senawat, and Burawich Muangto. Improvement of crashworthiness of bus structure under frontal impact. In *The 2015 World Congress on Advances in Structural Engineering an Mechanics (ASEM15) Incheon, Korea*, 2015.

[5] Jianguang Fang, Guangyong Sun, Na Qiu, Nam H Kim, and Qing Li. On design optimization for structural crashworthiness and its state of the art. *Structural and Multidisciplinary Optimization*, 55:1091–1119, 2017.

[6] MF Horstemeyer, XC Ren, H Fang, Ethem Acar, and PT Wang. A comparative study of design optimisation methodologies for side-impact crashworthiness, using injury-based versus energy-based criterion. *International Journal of Crashworthiness*, 14(2):125–138, 2009.

[7] Mátyás Matolcsy. Análisis de colisiones frontales en autobuses–enfoque estadístico. *Securitas Vialis*, 8:15–30, 2016.

[8] European Commission. Facts and figures – buses / coaches / heavy goods vehicles. *European Road Safety Observatory. Brussels, European Commission, Directorate General for Transport.*, 2023.

[9] Erich Mayrhofer, Hermann Steffan, and Heinz Hoschopf. *Enhanced coach and bus occupant safety*. Citeseer, 2005.

[10] Pontus Albertsson and Torbjörn Falkmer. Is there a pattern in european bus and coach incidents? a literature analysis with special focus on injury causation and injury mechanisms. *Accident Analysis & Prevention*, 37(2):225–233, 2005.

[11] UNECE. Statistics of road traffic accidents in europe and north america. *United Nations Publications*, LVI, 2021.

[12] Rogério Lopes, Nuno V Ramos, Rafael Cunha, Ricardo Maia, Rui Rodrigues, MPL Parente, and Pedro MGP Moreira. Passive safety solutions on coach according ece r29: Experimental and numerical analyses. *Procedia Structural Integrity*, 42:1159–1168, 2022.

[13] ECE R-29. Regulation no 29 of the economic commission for europe of the united nations (un/ece) — uniform provisions concerning the approval of vehicles with regard to the protection of the occupants of the cab of a commercial vehicle. *Official Journal of the European Union*, 2010.

[14] Muhammed E Cerit, Mehmet A Guler, Bertan Bayram, and Uğur Yolum. Improvement of the energy absorption capacity of an intercity coach for frontal crash accidents. In *11th International LS-DYNA Users Conference*, 2010.

[15] Supakit Rooppakhun and Sarawut Bua-Ngam. Finite element analysis of high-decker bus frontal impact based on ece-regulation no. 29. 658:464–470, 2013.

[16] Neal M. Patel. *Crashworthiness Design Using Topology Optimization*. PhD thesis, Graduate School of the University of Notre Dame, Notre Dame, Indiana, 2007.

[17] Stephan Hunkeler. *Topology Optimisation in Crashworthiness Design via Hybrid Cellular Automata for Thin Walled Structures*. PhD thesis, School of Engineering and Materials Science, Queen Mary University of London, 2009.

[18] CH Chuang and RJ Yang. Benchmark of topology optimization methods for crashworthiness design. In *12th International LS-DYNA Users Conference, Dearborn, Michigan, USA*, pages 1–2, 2012.

[19] Prasad Tapkir. Topology design of vehicle structures for crashworthiness using variable design time. Master's thesis, Purdue University, Indianapolis, Indiana, 2017.

[20] Rogério Lopes, Francisco Barros, Francisco Q de Melo, Nuno V Ramos, Rafael Cunha, Ricardo Maia, Rui Rodrigues, MPL Parente, and PMG Moreira. Evaluation of a coach door under a frontal impact. *International journal of structural integrity*, 14(1):2–18, 2023.

[21] Hesham Kamel Ibrahim. *Design Optimization of Vehicle Structures for Crashworthiness Improvement*. PhD thesis, Concordia University, Montreal, Quebec, Canada, 2009.

[22] Lucien A Schmit. Structural synthesis-its genesis and development. *AIAA Journal*, 19(10):1249–1263, 1981.

[23] Neal M Patel, Donald Tillotson, John E Renaud, Andrés Tovar, and Kazuhiro Izui. Comparative study of topology optimization techniques. *AIAA journal*, 46(8):1963–1975, 2008.

[24] Xingtao Liao, Qing Li, Xujing Yang, Weigang Zhang, and Wei Li. Multiobjective optimization for crash safety design of vehicles using stepwise regression model. *Structural and multidisciplinary optimization*, 35:561–569, 2008.

[25] Martin Philip Bendsøe and Ole Sigmund. *Topology optimization: theory, methods, and applications*. Springer Science & Business Media, 2003.

[26] Raphael T Haftka and Ramana V Grandhi. Structural shape optimization—a survey. *Computer methods in applied mechanics and engineering*, 57(1):91–106, 1986.

[27] M Zhou, N Pagaldipti, HL Thomas, and YK Shyy. An integrated approach to topology, sizing, and shape optimization. *Structural and Multidisciplinary Optimization*, 26:308–317, 2004.

[28] Ole Sigmund. On the usefulness of non-gradient approaches in topology optimization. *Structural and Multidisciplinary Optimization*, 43:589–596, 2011.

[29] Rodolphe Le Riche and Raphael T Haftka. On global optimization articles in smo. *Structural and Multidisciplinary Optimization*, 46:627–629, 2012.

[30] Shubham Bhutada and MD Goel. Crashworthiness parameters and their improvement using tubes as an energy absorbing structure: an overview. *International Journal of Crashworthiness*, 27(6):1569–1600, 2022.

[31] Fabian Duddeck, Stephan Hunkeler, Pablo Lozano, Erich Wehrle, and Duo Zeng. Topology optimization for crashworthiness of thin-walled structures under axial impact using hybrid cellular automata. *Structural and Multidisciplinary Optimization*, 54:415–428, 2016.

[32] Martin Philip Bendsøe and Noburu Kikuchi. Generating optimal topologies in structural design using a homogenization method. *Computer methods in applied mechanics and engineering*, 71:197–224, 1988.

[33] Andrés Tovar, Neal M Patel, Glen L Niebur, Mihir Sen, and John E Renaud. Topology optimization using a hybrid cellular automaton method with local control rules. 2006.

[34] Martin P Bendsøe. Optimal shape design as a material distribution problem. *Structural optimization*, 1:193–202, 1989.

[35] SF Rahmatalla and CC Swan. A q4/q4 continuum structural topology optimization implementation. *Structural and Multidisciplinary Optimization*, 27(1-2):130–135, 2004.

[36] Ole Sigmund and Joakim Petersson. Numerical instabilities in topology optimization: a survey on procedures dealing with checkerboards, mesh-dependencies and local minima. *Structural optimization*, 16:68–75, 1998.

[37] Robert Rosario Mayer, Noboru Kikuchi, and Richard A Scott. Application of topological optimization techniques to structural crashworthiness. *International Journal for Numerical Methods in Engineering*, 39(8):1383–1403, 1996.

[38] Claus BW Pedersen. Topology optimization design of crushed 2d-frames for desired energy absorption history. *Structural and Multidisciplinary Optimization*, 25:368–382, 2003.

[39] Livermore Software Technology Coorporation. *The LS-TaSCTM Tool: Topology and Shape Computations, User's Manual, Version 4.2*. Livermore Software Corporation, Livermore, CA, 2020.

[40] H. Müllerschön, N. Lazarov, and K. Witowski. Application of topology optimization for crash with ls-opt/topology. *11th International LS-DYNA Users Conference*, 2010.

[41] Moon-Kyun Shin, Ki-Jong Park, and Gyung-Jin Park. Optimization of structures with nonlinear behavior using equivalent loads. *Computer Methods in Applied Mechanics and Engineering*, 196(4-6):1154–1167, 2007.

[42] Marco Cavazzuti, Andrea Baldini, Enrico Bertocchi, Dario Costi, Enrico Torricelli, and Patrizio Moruzzi. High performance automotive chassis design: a topology optimization based approach. *Structural and Multidisciplinary Optimization*, 44:45–56, 2011.

[43] Mohammadmahdi Davoudi and Cheol Kim. Topology optimization for crashworthiness of thin-walled structures under axial crash considering nonlinear plastic buckling and locations of plastic hinges. *Engineering Optimization*, 51(5):775–795, 2019.

[44] Chun Ren, Haitao Min, Tianfei Ma, and Fangquan Wang. An effective topology optimization method for crashworthiness of thin-walled structures using the equivalent linear static loads. *Proceedings of the Institution of Mechanical Engineers, Part D: Journal of Automobile Engineering*, 234(14):3239–3255, 2020.

[45] Yi Min Xie and Grant P Steven. A simple evolutionary procedure for structural optimization. *Computers & structures*, 49(5):885–896, 1993.

[46] Osvaldo M Querin, Grant P Steven, and Yi Min Xie. Evolutionary structural optimisation (eso) using a bidirectional algorithm. *Engineering computations*, 15(8):1031–1048, 1998.

[47] Xiaodong Huang and YM Xie. Convergent and mesh-independent solutions for the bi-directional evolutionary structural optimization method. *Finite elements in analysis and design*, 43(14):1039–1049, 2007.

[48] Xiaodong Huang and Yi Min Xie. Bi-directional evolutionary topology optimization of continuum structures with one or multiple materials. *Computational Mechanics*, 43:393–401, 2009.

[49] Q Li, GP Steven, and YM Xie. A simple checkerboard suppression algorithm for evolutionary structural optimization. *Structural and Multidisciplinary Optimization*, 22:230–239, 2001.

[50] Xiao-Ying Yang, Yi-Min Xie, Jin-Shen Liu, GT Parks, and PJ Clarkson. Perimeter control in the bidirectional evolutionary optimization method. *Structural and Multidisciplinary Optimization*, 24:430–440, 2002.

[51] Xiaodong Huang and YM Xie. A new look at eso and beso optimization methods. *Structural and Multidisciplinary Optimization*, 35(1):89–92, 2008.

[52] Xinyan Huang, Yi Min Xie, and Guoxing Lu. Topology optimization of energy-absorbing structures. *International Journal of Crashworthiness*, 12(6):663–675, 2007.

[53] Nasim Bahramian and Abolfazl Khalkhali. Crashworthiness topology optimization of thin-walled square tubes, using modified bidirectional evolutionary structural optimization approach. *Thin-Walled Structures*, 147:106524, 2020.

[54] Ciro A Soto and Alejandro R Diaz. Basic models for topology design optimization in crashworthiness problems. In *International Design Engineering Technical Conferences and Computers and Information in Engineering Conference*, volume 19715, pages 1055–1064. American Society of Mechanical Engineers, 1999.

[55] Christopher Ortmann and Axel Schumacher. Graph and heuristic based topology optimization of crash loaded structures. *Structural and Multidisciplinary Optimization*, 47:839–854, 2013.

[56] GM Nagel and DP Thambiratnam. Dynamic simulation and energy absorption of tapered tubes under impact loading. *International Journal of Crashworthiness*, 9(4):389–399, 2004.

[57] Michael Smith. *ABAQUS/Standard User's Manual, Version 6.9*. Dassault Systèmes Simulia Corp, United States, 2009.

[58] George Papazafeiropoulos, Miguel Muñiz-Calvente, and Emilio Martínez-Pañeda. Abaqus2matlab: A suitable tool for finite element post-processing. *Advances in Engineering Software*, 105:9–16, 2017.

[59] Ole Sigmund. A 99 line topology optimization code written in matlab. *Structural and multidisciplinary optimization*, 21:120–127, 2001.

[60] Erik Andreassen, Anders Clausen, Mattias Schevenels, Boyan S Lazarov, and Ole Sigmund. Efficient topology optimization in matlab using 88 lines of code. *Structural and Multidisciplinary Optimization*, 43:1–16, 2011.

[61] Kai Liu and Andrés Tovar. An efficient 3d topology optimization code written in matlab. *Structural and Multidisciplinary Optimization*, 50:1175–1196, 2014.

[62] Alen Anthony. Development of abaqus-matlab interface for design optimization using hybrid cellular automata and comparison with bidirectional evolutionary structural optimization. Master's thesis, Purdue University, Indianapolis, Indiana, 2021.

[63] Y. M. Xie and G. P. Steven. *Basic Evolutionary Structural Optimization*, pages 12–29. Springer London, London, 1997.

[64] Jeremy Bleyer. Topology optimization using the SIMP method. `https://comet-fenics.readthedocs.io/`, 2016. Online; accessed June 2023.

[65] Weigang Chen and Tomasz Wierzbicki. Relative merits of single-cell, multi-cell and foam-filled thin-walled structures in energy absorption. *Thin-Walled Structures*, 39(4):287–306, 2001.

[66] A Segade, A Bolaño, JA López-Campos, E Casarejos, JR Fernandez, and JA Vilán. Study of a crash box design optimized for a uniform load profile. In *6th International Conference Integrity-Reliability-Failure*, 2018.

[67] MatWeb. Material property data. `http://www.matweb.com/`, 2023. Online; accessed May 2023.

[68] Rogério Lopes, Nuno V. Ramos, Rafael Cunha, Ricardo Maia, Rui Rodrigues, M.P.L. Parente, and Pedro M.G.P. Moreira. Coach crashworthiness and failure analysis during a frontal impact. *Engineering Failure Analysis*, page 107369, 2023.

[69] Group, E. Virtual Performance Solution 2019.0. Solver Reference Manual. 2019.

Appendix A

Deformation results in the coach structure

A.1 Ceiling

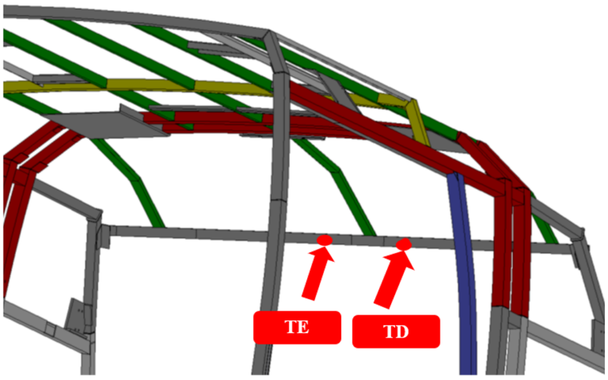

Figure A.1: Location of strain gauges in the ceiling of the coach structure [68].

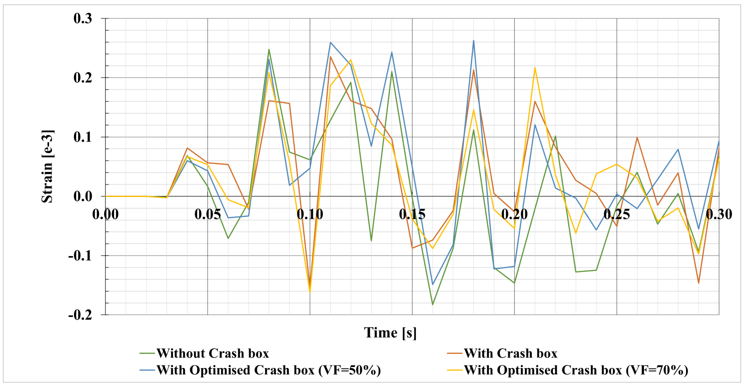

(a) TD

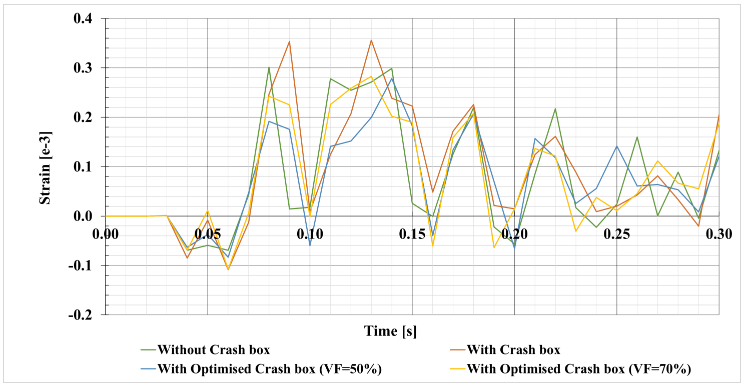

(b) TE

Figure A.2: Deformation results measured in the ceiling of the coach structure.

A.2 Frontal structure (Left-hand side)

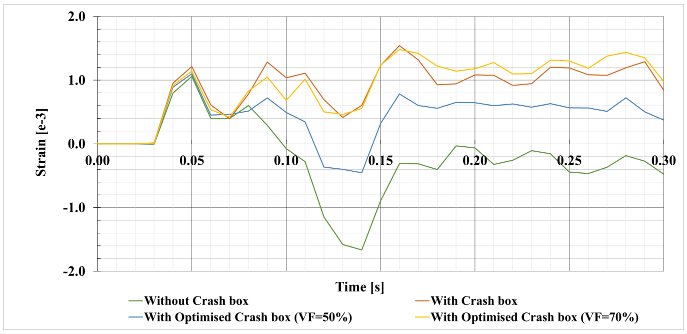

(a) FEM

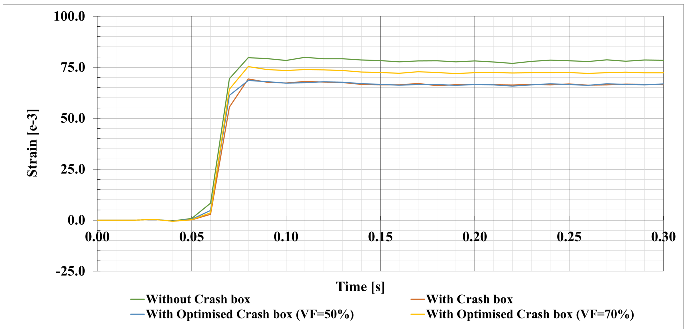

(b) FEC

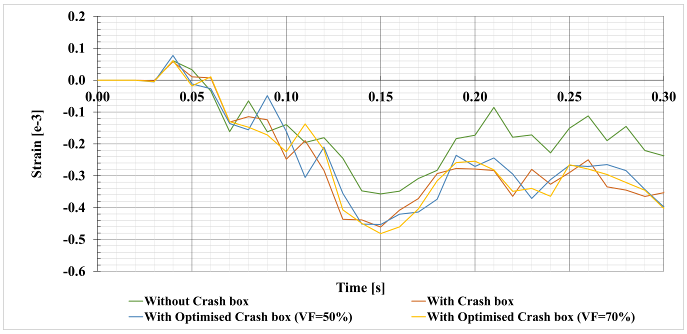

(c) FEI

Figure A.3: Deformation results measured in the left-hand side of the frontal structure.

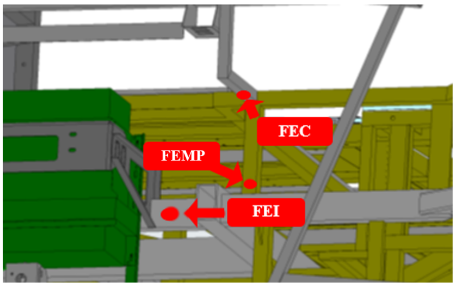

Figure A.4: Location of strain gauges in the left-hand side of the coach structure [68].

A.3 Rear structure

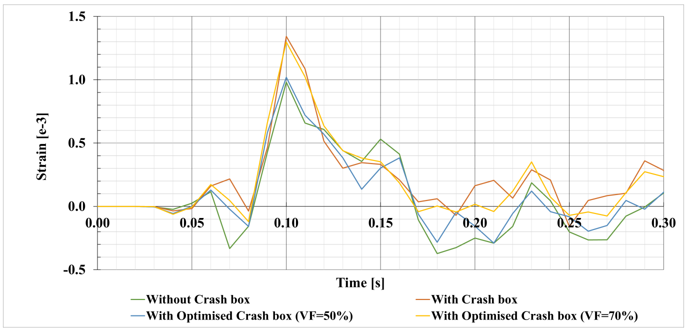

(a) LDT

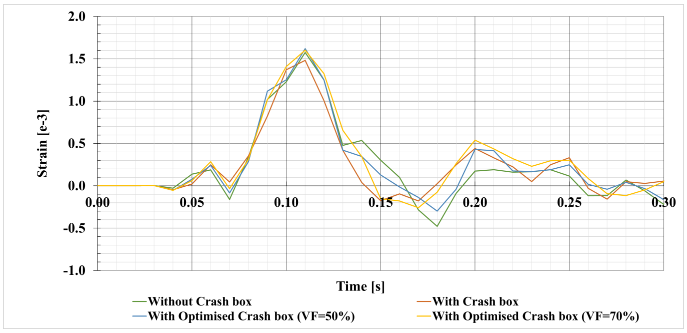

(b) LET

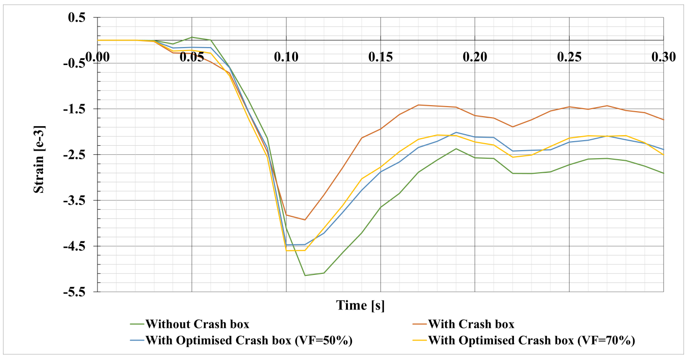

(c) BTD

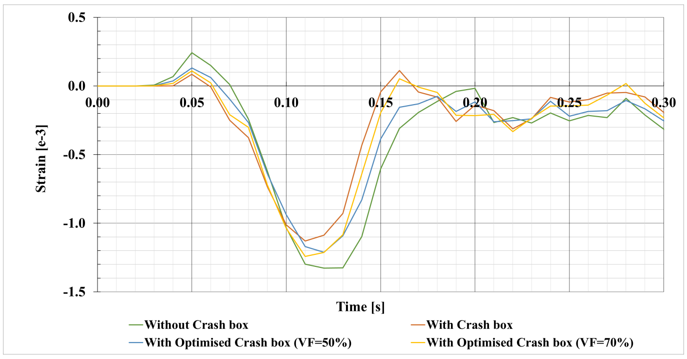

(d) BTE

Figure A.5: Deformation results measured in the rear of the coach structure.

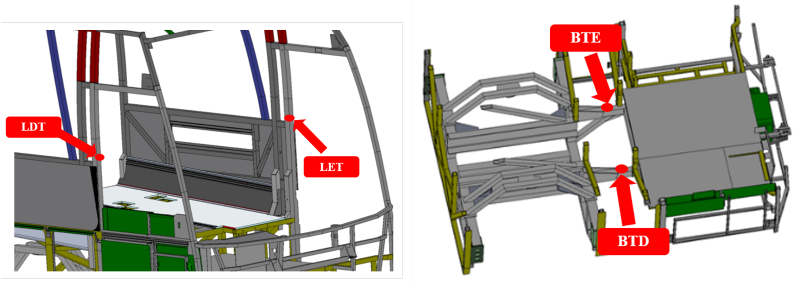

Figure A.6: Location of strain gauges in the rear of the coach structure [68].

A.4 Internal frontal structure

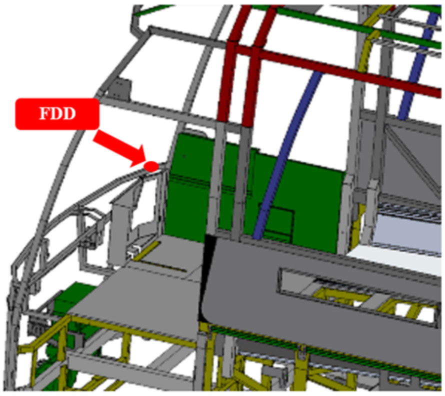

Figure A.7: Location of strain gauges in the internal frontal structure of the coach [68].

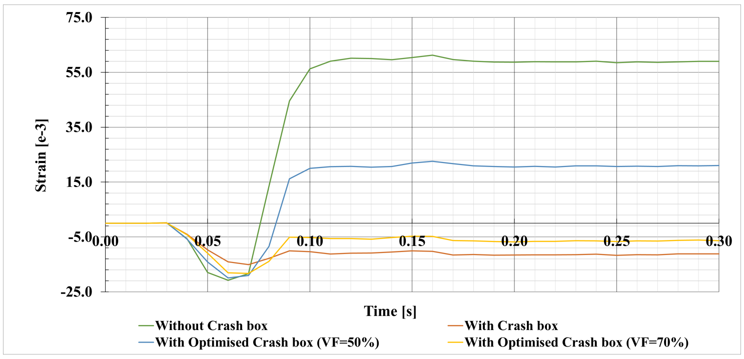

Figure A.8: Deformation results measured in the internal frontal structure of the coach.